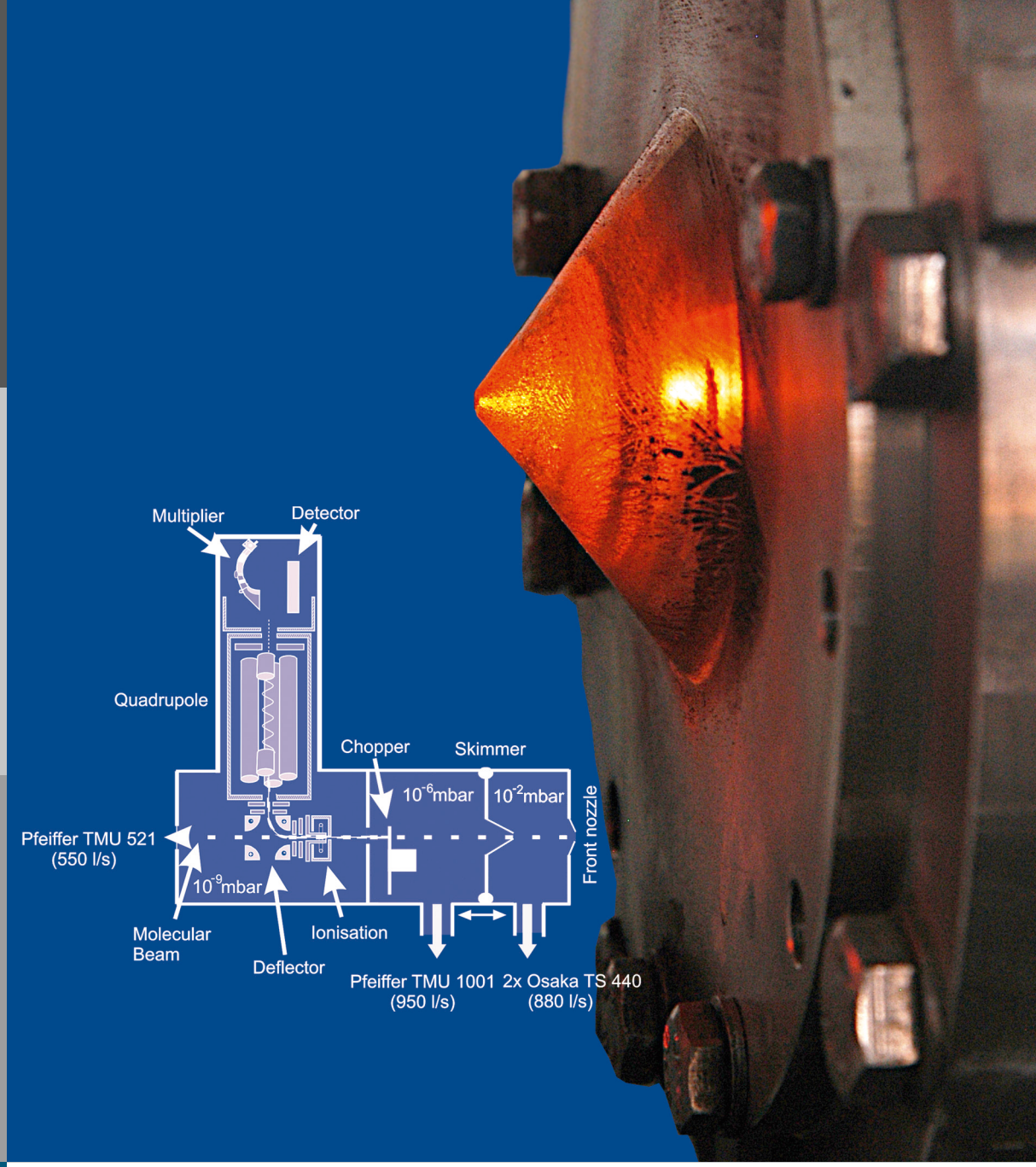

Release of Inorganic Trace Elements from High-Temperature Gasification of Coal

Marc Bläsing

Mitglied der Helmholtz-Gemeinschaft

JÜLICH
FORSCHUNGSZENTRUM

Schriften des Forschungszentrums Jülich
Reihe Energie & Umwelt / Energy & Environment Band / Volume 131

Forschungszentrum Jülich GmbH
Institute for Energy and Climate Research (IEK)
Microstructure and Properties of Materials (IEK-2)

Release of Inorganic Trace Elements from High-Temperature Gasification of Coal

Marc Bläsing

Schriften des Forschungszentrums Jülich
Reihe Energie & Umwelt / Energy & Environment Band / Volume 131

ISSN 1866-1793 ISBN 978-3-89336-772-6

Bibliographic information published by the Deutsche Nationalbibliothek.
The Deutsche Nationalbibliothek lists this publication in the Deutsche Nationalbibliografie; detailed bibliographic data are available in the Internet at http://dnb.d-nb.de.

Publisher and Distributor:	Forschungszentrum Jülich GmbH Zentralbibliothek 52425 Jülich Phone +49 (0) 24 61 61-53 68 · Fax +49 (0) 24 61 61-61 03 e-mail: zb-publikation@fz-juelich.de Internet: http://www.fz-juelich.de/zb
Cover Design:	Grafische Medien, Forschungszentrum Jülich GmbH
Printer:	Grafische Medien, Forschungszentrum Jülich GmbH
Copyright:	Forschungszentrum Jülich 2012

Schriften des Forschungszentrums Jülich
Reihe Energie & Umwelt / Energy & Environment Band / Volume 131

D 82 (Diss., RWTH Aachen University, 2011)

ISSN 1866-1793
ISBN 978-3-89336-772-6

The complete volume is freely available on the Internet on the Jülicher Open Access Server (JUWEL) at http://www.fz-juelich.de/zb/juwel

„In the structure of the earth the element carbon is hardly more than a trace element, its share in the total bulk being as small as 0.04 per cent. ... Yet, carbon may be called the most important element; not only is it an indispensable necessity of life, but also the main source of energy."

Clarke and Washington, 1924; Van Krevelen,1993

Parts of this thesis have been published:

Journals

M. Bläsing, M. Müller, Mass spectrometric investigations on the release of inorganic species during gasification and combustion of Rhenish lignite, Fuel 89 (2010), 2417-2424.

M. Bläsing, M. Müller, Mass spectrometric investigations on the release of inorganic species during gasification and combustion of German hard coals, Combustion and Flame 157 (2010), 1374-1381.

M. Bläsing, T. Melchior, M. Müller, Influence of the temperature on the release of inorganic species during high-temperature gasification of hard coal, Energy & Fuels 24 (2010), 4153-4160.

M. Bläsing, T. Melchior, M. Müller, Influence of temperature on the release of inorganic species during high-temperature gasification of Rhenish lignite, Fuel Proc. Techn., 92 (2011), 511-516.

M. Bläsing, M. Müller, Influence of pressure on the release of inorganic species during high temperature gasification of coal, Fuel 90 (2011), 90, 280-287.

Conferences

M. Bläsing, M. Müller, Mass spectrometric investigations on the release of inorganic species during gasification of lignite, 4. International Conference on Clean Coal Technologies, Dresden 2009.

M. Bläsing, M. Müller, Freisetzung von Spurstoffen bei der Verbrennung und Vergasung von Braunkohle, 24. Deutscher Flammentag, Bochum 2009.

M. Bläsing, M. Müller, Influence of steam on the release of alkali metal, chlorine, and sulphur species during high temperature gasification of lignite, 27. International Pittsburgh Coal Conference, Istanbul 2010.

Abstract

The development of cleaner, more efficient techniques in next-generation coal power plants is becoming increasingly important, especially regarding to the discussion of the influence of CO_2 emissions on global warming. A promising coal utilisation process is the integrated gasification combined cycle process. The direct use of the raw gas requires gas clean-up to prevent downstream parts of the gasifier from several problems. An increased efficiency and a decreased amount of harmful species can be achieved through hot fuel gas cleaning. This clean-up technique requires a comprehensive knowledge of the release characteristics of inorganic coal constituents. The aim of this thesis was to provide enhanced knowledge of the effect of key process parameters and of the chemical constitution of coal on the release of Na, K, S, and Cl species from high-temperature coal gasification. The experimental setup consisted of atmospheric flow tube furnaces and a pressurised furnace. In-situ analysis of the product gas was carried out using molecular beam mass spectrometry. A broad spectrum of different coals with assumed qualitative and quantitative differences in the release characteristics was investigated. Additionally, experiments with model substances were performed. The results of the experimental investigation were compared with thermodynamic calculations. Finally, recommendations, for the operation of a high-temperature gasifier are formulated.

Zusammenfassung

Die Entwicklung hocheffizienter Techniken zur energetischen Nutzung von Kohle gewinnt zunehmend an Bedeutung, u.a. aufgrund der Diskussion um den Beitrag der anthropogenen CO_2-Emission zum Klimawandel. Ein aussichtsreicher Prozess ist die integrierte Vergasung von Kohle und die Nutzung des Produktgases in einem GuD-Kraftwerk. Um nachfolgende Anlagenteile vor Schäden zu schützen, muss das Produktgas gereinigt werden. Der Einsatz einer Hochtemperaturreinigungsstufe kann sowohl die Effizienz des Gesamtprozesses erhöhen als auch die Menge an schädlichen Verbindungen im Gas reduzieren. Notwendige Voraussetzung für die Entwicklung der Hochtemperaturgasreinigung ist ein umfassendes Verständnis des Freisetzungsverhaltens anorganischer Kohlenbestandteile. Ziel dieser Arbeit war es eine Wissensbasis bezüglich des Einflusses verschiedener Prozessparameter und der Zusammensetzung der Kohle auf das Freisetzungsverhalten von Na-, K-, Cl- und S-haltigen Verbindungen zu schaffen. Bei den Freisetzungsversuchen wurden Kohlen verschiedenen Ranges in einem atmosphärischen Rohrofen bzw. in einem Druckofen umgesetzt. Das Produktgas wurde mittels Molekularstrahl-Massenspektrometer analysiert. Zusätzlich wurden Versuche mit Modellsubstanzen und thermodynamische Rechnungen durchgeführt. Abschließend wurden Empfehlungen für den Betrieb eines Hochtemperaturvergasers formuliert.

Contents

List of tables

List of figures

1 Introduction

1.1 Background

The world's energy demand is on the rise. In the reference scenario of the 'World Energy Outlook 2009', The International Energy Agency predicted a 76% increase in the demand for electricity in the period from 2007 to 2030, requiring 4800 gigawatts of additional capacity [IEA, 2009]. Furthermore, they report the ongoing dominant role of fossil fuels in worldwide energy production, with coal as one of the major fossil fuels, holding a 44% share of global power generation in 2030. However, the use of coal as a fuel leads to a relatively high emission of CO_2 in comparison with other fossil fuels, e.g. crude oil and especially natural gas [Wolk et al., 1992; Inaba et al., 1995]. The relation of CO_2 to climate change has recently been discussed. The consensus of the international community—e.g. the Kyoto protocol in 1997—is that CO_2 emissions must be reduced. The emission of the greenhouse gas CO_2 is a matter of growing public concern. Clean and more efficient energy production technologies are required to address both the rising demand for energy and environmental issues.

Advantage in the field of energy technology is related to several technical, economical, and ecological factors. The fossil fuels coal, crude oil, and natural gas have been central in supplying reliable, low-cost energy worldwide for more than a century. Despite efforts to substitute fossil fuel in the energy production sector with regenerative energies, fossil fuels are expected to play a major role in energy production over the mid-term future also in Germany. The expected worldwide demand will undoubtedly place increasing pressure on exploration and mining. However, in the short term, the world is not running out of coal, crude oil, and natural gas, as shown in Figure 1. On the basis of the demand for primary energy in the year 2007, the hard coal reserves can satisfy demand for 130 years, the lignite reserves for 265 years (German lignite for 227 years), the natural gas reserves for 60 years, and the crude oil reserves for 40 years. The amount of the resources is overwhelming—e.g. the unconventional oil resources can satisfy the actual demand for about 370 years. However, this data is extrapolated based on data from the year 2007 and is therefore static. It does not take into account a growing demand, the use of power generation techniques that are more efficient, or advances in the substitution of fossil energy resources. But the trend is clear: a significant shortage of fossil fuels will play an important role for the global energy supply in the short-to-mid–term future.

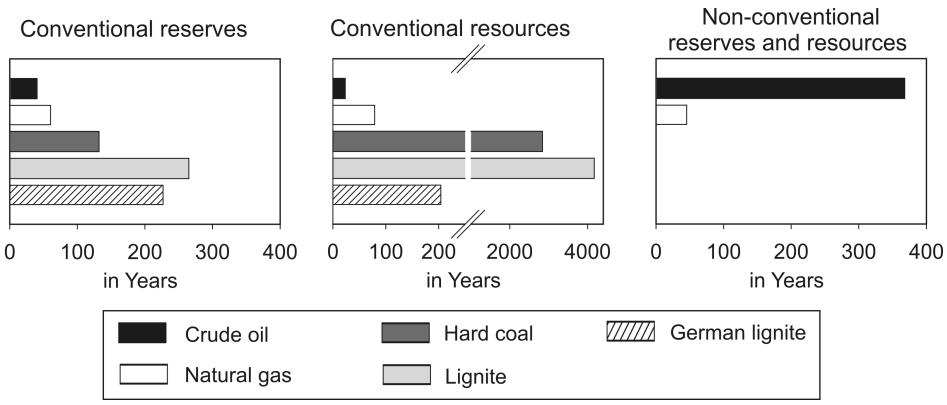

Figure 1. Statistical range of fossil fuels related to reserves and demand for the year 2007. German lignite is related to the German reserves and demand [BGR, 2009].

It is assumed that the attraction of coal for energy generation will increase in the coming decades because of its diverse locations and vast reserves compared with crude oil and natural gas. The price of imported energy resources in Germany is depicted in Figure 2.

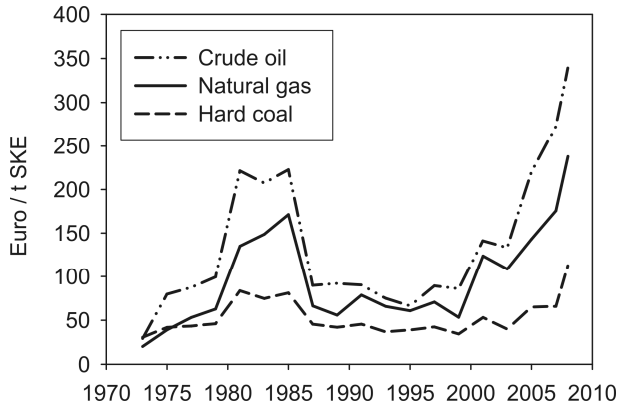

Figure 2. Development of the prices of crude oil, natural gas, and hard coal from 1973 to 2008. Taxes and duties are excluded. [Adapted from BGR, 2009].

Regarding its price, coal will remain one of the most attractive fossil fuels for the generation of electrical energy in Germany. The price increase of coal has been more moderate than the price increases of crude oil and natural gas over the last 35 years.

The change of the import price is not a direct result of a decrease of the fossil energy resources, as mentioned above. Rather, the change depends on the ratio of supply and demand. The demand, especially of emerging nations such as China and India, is assumed to increase exponentially in comparison with the demand of North American or European countries [BGR, 2009]. As a result, the pressure on the price and the dependence of Germany on crude oil, natural gas, and hard coal–exporting countries is increasing as well.

The role of coal in Germany's energy resource mix is significant, as shown in Figure 3 for electrical energy generation. The abundance and the low mining cost of low-rank coal in Germany make it a competitive fuel, especially for electricity production.

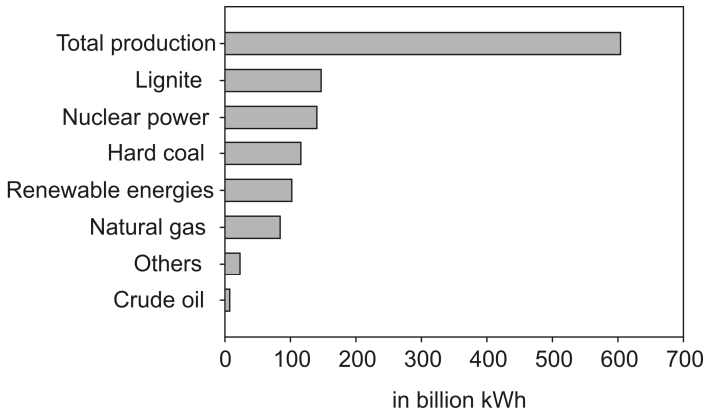

Figure 3. Electrical energy generation by energy source in Germany in 2010 [AG Energiebilanzen, 2010].

However, the vast coal reserves must be used in an environmentally acceptable way [Beer, 2007; Lior, 2008]. Research, development, demonstration, and commercialisation programmes will be critical in ensuring that coal technologies meet or exceed both economic and ecological requirements and that they are available for timely deployment.

The development of cleaner, more efficient techniques in next-generation coal power plants is becoming increasingly important. Recently, coal-based combined-cycle power generation systems (e.g. Integrated Gasification Combined Cycle) have been developed or are under development with the primary goal of increasing efficiency [Wolk et al., 1992; Higman and Van der Burgt, 2008]. A promising coal utilisation process is the integrated coal gasification combined cycle (IGCC), which is able to use a

wide variety of solid, carbogeneous fuels with high efficiency [Mondol et al., 2009]. The IGCC has a design that can facilitate CO_2 capture, making the technique more environmentally friendly [Newcomer and Jay, 2007; Beer, 2007; Wall, 2007]. Inaba et al. [1995] recommended the use of low-rank coal for advanced gasification technologies with CO_2 capture. This could allow the vast lignite reserves in Germany to be used in an economically and ecologically acceptable way.

During high-temperature coal gasification, a complex mixture of solid, liquid, and gaseous phases is formed. Of special interest are vapour species that contain Na, K, S, and Cl, which are highly volatile under the given conditions and can lead to problems when they reach cooler parts of the plant, where they form sticky and corrosive layers. This can cause several problems in the gasifier and the downstream plant components [Bakker et al., 2004]. Both an increase in efficiency and a decrease in the amount of harmful species can be achieved through hot gas cleaning, which is currently under development [Müller et al., 2009]. This clean-up strategy depends on a comprehensive knowledge of the release and hot gas chemistry of inorganic compounds. Despite research efforts during the last few decades, there are many open questions regarding the release and the underlying release mechanisms, especially for Na, K, S, and Cl species. Further investigations on the release under the conditions of the IGCC process need to be carried out.

1.2 Aim of the thesis

The aim of this thesis was to provide enhanced knowledge of the qualitative and quantitative release of several inorganic species as well as of the underlying release mechanisms under gasification conditions. The focus was on Na, K, S, and Cl species because they can cause several problems—e.g. deposition and corrosion—in downstream parts of the gasifier. The development of hot gas cleaning will benefit from a detailed knowledge of the release as well as the capture reactions of gaseous species with the remaining mineral matter. To better understand and eventually to predict the release behaviour, systematic measurements for a variety of conditions and coals are needed. Therefore, experiments were carried out under well-defined conditions, and they focused on the influence of the conditions of high-temperature coal gasification, e.g. the IGCC process, on the release. This included the oxygen partial pressure, the temperature, the steam content, the absolute pressure, and the coal rank. The setup for the batch-scale experiments consisted of atmospheric flow tube furnaces and a pressure furnace, as well as a molecular beam mass spectrometer.

Online analysis of the high-temperature product gas was carried out by molecular beam mass spectrometry. A broad range of different coals was investigated. The rank of the coals reached from lignite to anthracite and covered a wide spectrum of different fuels with release characteristics that are assumed to be qualitatively and quantitatively different. Additionally, experiments with model substances were performed in order to obtain more detailed information on the release mechanisms. The results of the experimental investigation were compared with thermodynamic calculations. The results of the thermodynamic calculations can support the discussion.

2 Fundamentals

2.1 Coal

2.1.1 Origin and nature of coal

Coal is ‘organic rock’ [Van Krevelen, 1993] that is generated over millions of years through a process commonly known as coalification. Plant matter was deposited, hermetically sealed, and placed under pressure and increasing temperature resulting from a growing sediment layer. Therefore, coal is ‘aged biomass’ [Van Krevelen, 1993] that underwent transformation and decomposition over aeons. This process includes biochemical degradation by microorganisms and fungi under the exclusion of oxygen and geochemical degradation by the heat and pressure caused by a growing sediment layer. Coal is a heterogeneous material, and it contains inorganic and organic fractions in varying proportions. Despite the differences caused by variations in the nature of the original plant material, the heterogeneity of coal is increased by the process of coalification and by the intrusion of several types of matter that are present according to the sedimentation area, e.g. ground water, sea water, or clay. Usually, coal is classified by the coal rank, which expresses the degree of coalification. Common classifications are lignite, bituminous coal, and anthracite. Lignite is a low-rank coal, and anthracite is a high-rank coal. There are also coals that do not fit into this classification [Oader, 1985]. However, all coals contain three components: organic matter, mineral matter, and moisture. Organic matter refers to the organic coal substance, which by definition consists of five elements: C, H, O, N, and S [Van Krevelen, 1993]. The amount of organic matter varies widely, usually ranging from 50 to 90 mass%. Mineral matter can have two modes of occurrence in coal. First, mineral matter can be present as discrete particles that are relatively easy to remove. Second, mineral matter can be finely divided in the coal matter, with a particle size smaller than 0.1 mm. Inherent mineral matter usually makes up less than 10 mass% [Merrick, 1984]. Moisture can be divided into free and inherent moisture. The latter cannot be removed by drying. Usually, the inherent moisture content decreases with increasing coal rank [Van Krevelen, 1993]. The amount of inherent moisture is generally less than 10 mass% [Merrick, 1984].

2.1.2 Mode of occurrence of mineral matter in coal

The release of inorganic compounds during thermal coal conversion is a complex process that is influenced by the conversion environment as well as the concentration and mode of occurrence of the inorganic matter in the coal. Owing to the importance of these compounds, their concentration and chemical forms in coals of different rank have been extensively investigated. Therefore, a summary of the mode of occurrence of mineral matter in coal is given below. The focus is on minerals that are strong correlated with the release and capture of Na, K, S, and Cl.

Raask [1985] reported that aluminosilicates and quartz are the main coal minerals. Clay minerals account on average for 60–80% of the mineral matter in coal [Groen et al., 1994]. Common species of clay minerals are illite-sericite (K-aluminosilicates), kaolinite (aluminosilicate), and mixed-layer illite-montmorillonite of variable composition. The second most abundant coal mineral is quartz. Sulphide minerals are the third most abundant mineral group in coals. Within the sulphide group, iron sulphide (pyrite) is by far the most common compound. Carbonate minerals are usually the fourth most abundant minerals found in coal. Coal can contain significant amounts of carbonate. The most common carbonates in coal are, in decreasing order of their fraction of the total carbonate content, $CaCO_3$ (54 mass%), $MgCO_3$ (24 mass%), $FeCO_3$ (20 mass%), and $MnCO_3$ (2 mass%). Additionally, Skipsey [cited in Raask, 1985] reported $CaCl_2$ as an important Ca-bearing mineral.

In addition to the major minerals, coal contains minor and trace elements in various chemical forms. Heavy metals are commonly found in coal in trace amounts. Little is known regarding the release and capture of heavy elements. However, keeping in mind that a single power-generating unit handles, on average, 1000 t of coal per day, even trace elements can become a significant problem.

On account of their relation to deposition and corrosion, the amount and the mode of Na, K, Cl, and S compounds were comprehensively investigated.

The mode of occurrence of the alkali metals Na and K is of a different nature. In general, in high-rank coal, a significant amount of Na was found in the form of soluble inorganic salts. Manzoori and Argwal [cited in Nykänen, 2002] reported that about 42% of the total Na was present as NaCl dissolved in pore water, and 30% was organically fixed (acid soluble). Only small parts were found to be weakly bound to the coal surface. The fraction of carboxylic-bound Na is limited because of the small amount of these functional groups in high-rank coals as compared to low-rank coals.

The dominant alkali metal in low-rank coals is Na. Usually, much of the Na in low-rank coal is found to be surface-bound to the coal matrix. The major fraction of Na in low-rank coals is assumed to occur in the form of cations bound to functional groups, e.g. carboxylate groups [cited in Nykänen, 2002; Howarth et al. 1987]. Smaller amounts can be found associated with Cl, and usually only small amounts exist as Na silicates such as $Na_2O*Al_2O_3*6SiO_2$ [Raask, 1985; Yudovich et al., 2006]. In addition, the authors highlighted the correlation between the Na and Cl content of coal. In general, the Cl content is an indicator of the NaCl content of the coal. This organically bound Na is finely dispersed throughout the coal [Shah et al., 1995].

K present in coal minerals is almost exclusively fixed in aluminosilicates and is therefore a common mineral in both high- and low-rank coals [Raask, 1982; Raask, 1985]. Illite is a primary K-bearing aluminosilicate. Usually, the mode of occurrence is in the form of finely divided minerals [Spiro et al., 1986]. Furthermore, Spiro et al. [1986] reported that the mode of occurrence of K in coal is dependent on the coal rank. Anthracite exhibited a fixation of K in muscovite, and lignite showed K also in the form of organic sorbates.

Tillman et al. [2009] and Yudovich et al. [2006] have recently given a comprehensive review on the topic of Cl in coal. Cl compounds are common parts of coal minerals. Yudovich et al. [2006] highlighted two broad modes of occurrence of Cl in coal. The main parts can be found to be inorganically bound in the form of discrete minerals, e.g. salt-like Cl (NaCl as a common Cl-bearing mineral, which might also be dissolved in pore water), and organic-bound Cl adsorbed to the functional groups of the organic coal matter. Also, small parts may be found in the form of Cl-containing silicates. Yudovich et al. [2006] pointed out that the majority of Cl in coal seems to be organically bound. Similar statements about the relation of Cl to the organic coal matter have been made by Shet et al. [cited in Tillman, 2009]. Tillman et al. [2009] reported that the mode of occurrence of Cl is very complex. They emphasised that the majority of Cl occurs in water soluble and ion-exchangeable forms. This amount is highly mobile/volatile and is therefore very significant for thermal coal utilisation processes.

S can be found in the form of inherent mineral matter, mainly in the form of FeS_2, or as organically bound S fixed in the coal matrix [Osborn, 1992; Maes et al., 1997]. Attar [1978] mentioned that the ratio of inorganic to organic S is in the range of 1:1 to 3:1. The inorganic forms of S are typically sulphides. Pyrite is the major inorganic S contaminant in most coals [Calkins, 1994]. The organic S structures are part of the macromolecular structure of coal [Calkins, 1994], and they can be divided into aliphatic and aromatic or heterocyclic structures. The heterocyclic S structures vary from single-ring to multi-ring structures, and they may also contain nitrogen and/or oxygen heteroa-

toms [Calkins, 1994]. However, there is a strong correlation between the mode of occurrence of organic S and the coal rank [Raask, 1982]. High-rank coals contain relatively small amounts of aromatic sulphides and disulphides as compared with heterocyclic S compounds [Calkins, 1994]. Based on an investigation of nine coals (anthracite to lignite), Maes et al. [1997] reported a decreasing amount of sulphide and an increasing amount of thiophenes in high-rank coals and a higher amount of sulphide-fixed S in low-rank coals. Additionally, they reported that thiophenes constitute the main S-containing group for high-rank coals. However, the authors also mentioned that the S structures can vary widely, even for coals of the same rank.

The correlation between the mode of occurrence of several coal minerals and the coal rank was studied by Vassilev et al. [1996]. They reported that low-rank coal ash is commonly rich in basic oxides (e.g. MgO, CaO), whereas high-rank coal ash is usually rich in acid oxides (e.g. SiO_2, Al_2O_3). The amount of organically fixed inorganic elements commonly decreases with increasing coal rank. This can be partially explained by the decreasing amount of functional groups (e.g. R_{org}–COOH) and the decreasing porosity with increasing rank. Weakly fixed, easily exchangeable ions can be removed and can form more stable compounds (e.g. ion-exchangeable fixed Ca can form calcite or water soluble alkali, and alkali earth compounds can even be leached by ground water). The extent of alteration due to various environmental influences was expressed by Groen et al. [1994]. They reported that relatively small contributions from originally carried elements other than S remain in coal during the stages of development from low rank to high rank. Additionally, Sakanishi et al. [2002] reported that organically bound Si, Al, Fe, and Ca are present in Chinese and Indonesian coals. Furthermore, they highlighted the increasing amount of organically associated minerals with decreasing coal rank. Huffman and Huggins [1984] and Huffman et al. [1989] have shown that Ca in lignites and sub-bituminous coals occurs in organically fixed form and not exclusively in the form of discrete minerals, e.g. $CaCO_3$.

2.2 Gasification

2.2.1 Principles of coal gasification

The gasification of coal is the transformation of solid matter into gaseous fuels using O_2, H_2O, H_2 or CO_2, and heat. The product of the gasification process is a mixture consisting mainly of CO, H_2, CO_2, H_2O, CH_4, and small amounts of minor compounds, e.g. H_2S and COS. The composition of the product gas depends on the gasification conditions and the feedstock, e.g. the product gas from entrained-flow gasification consists mainly of CO and H_2 without significant amounts of CH_4.

Coal gasification is carried out at temperatures of 700–1600 °C and at pressures up to 70 bar [Oader, 1985]. Several parallel and consecutive reactions take place during the gasification process. An overview of coal gasification reactions is given in Table 1. The aim of gasification is the complete conversion of the organic coal matter into gaseous products. The mineral matter of coal undergoes decomposition and secondary reactions to form ash or slag, depending on the temperature. The reactions of the mineral matter are outlined in Section 2.3.

Table 1. Reactions relevant for coal gasification [Merrick, 1984; Oader, 1985].

Reaction	Reaction	Kinetics	ΔH in kJ/mol
Devolatilisation	Coal $\longrightarrow$ CO + CO_2 + H_2 + CH_4 + H_2O + tar	Fast	Endo-therm
Combustion (C)	C + O_2 $\longrightarrow$ CO_2	Fast	-394
Combustion (H)	H_2 + 0.5 O_2 $\longrightarrow$ H_2O	Fast	-242
Partial combustion	C + 0.5 O_2 $\longrightarrow$ CO	Fast	-111
Water–gas reaction	C + H_2O $\leftrightarrow$ CO + H_2	Moderate	+134
Boudouard reaction	C + CO_2 $\leftrightarrow$ 2 CO	Rather slow	+173
Shift reaction	CO + H_2O $\leftrightarrow$ CO_2 + H_2	Moderate	-41
Methanation reaction	C + 2 H_2 $\longrightarrow$ CH_4	Slow	-75

In principle, the gasification of a coal particle can be divided into three phases: devolatilisation, char reactions, and ash reactions. When coal is heated to about 300 °C, devolatilisation begins. The devolatilisation temperature of coal is in the range of 300 to 800 °C [Merrick, 1984]. Devolatilisation corresponds to the decomposition and vola-

tilisation of coal matter, resulting in the formation of char, and it gives rise to liquid and gaseous products, e.g. hydrocarbons, H_2, CO_2, CO, and H_2O. CO_2 and CO are formed mainly from the decomposition of carboxyl, carbonyl, and ethereal groups. Hydrocarbons are formed through the dealkylation of alkyl groups. H_2 is the product of the dehydrogenation of naphthenic ring structures and the decomposition of aromates. The remaining char undergoes gasification and combustion reactions. The intensity and kinetic of devolatilisation increase with increasing temperature. The devolatilisation is instantaneous above 700 °C. Devolatilisation occurs as a result of the distillation of low-boiling compounds in coal and the cracking of macromolecular structures. The low-boiling compounds of coal leave the coal matter without the breaking of chemical bonds. As a result of cracking, reactive fragments are formed, e.g. radicals and intermediate species. Several decomposition reactions and composition reactions, e.g. polymerisation, take place. In addition, several physical changes occur: the char becomes more porous and therefore experiences an increase in its internal surface area. However, caking coal can undergo softening and the pore system can collapse [Oader, 1985] which significantly retards the mass transfer. The results of devolatilisation are a hydrogen-deficient char and hydrocarbons. The hydrocarbons are cracked and primarily converted into CO and H_2 depending on the amount of oxygen which is provided during the gasification process. The remaining char is converted into gaseous products as well. After conversion of the organic coal matter, only non-volatile mineral matter—which also underwent several transformations during the gasification process—remains.

2.2.2 Advanced coal energy conversion technique—the IGCC

Gasification is probably the most versatile of the thermal coal conversion processes. Several coal gasification technologies were invented to handle different coals effectively and to satisfy almost every sector of energy demand. The techniques cover the production of low–caloric value gas or medium–caloric value gas for industrial installations and power generation systems. Furthermore, medium–caloric value gas can be converted into liquid fuels and chemicals [Merrick, 1984]. Finally, high–caloric value gas is cost-competitive and transportable and is, therefore, suitable as a substitute for natural gas. For further details, the reader is referred to Merrick [1984], Oader [1985], and Higman and Van der Burgt [2008].

The objective of advanced coal conversion technology is to provide power generation that is highly efficient, reliable, cost-competitive, and environmentally friendly in comparison to conventional coal-fuelled power generation technology [Newby and Bannister, 1994]. One auspicious gasification process is the integrated gasification combined cycle (IGCC) process with an entrained-flow gasifier. As a result of continuous research and development, this coal-based combined cycle power generation process has made significant improvements in efficiency during the last few decades [Joshi and Sunggyu, 1996]. Demonstration plants in the Netherlands, Spain, and the United States are proving the reliability of the technique in commercial-scale applications. Some important advantages of IGCC are summarised in Table 2.

Table 2. Summary of the advantages of the IGCC process, adapted from Joshi and Sunggyu [1996] and Mondol et al. [2009].

Advantages
Reduced emissions from power generation: S species, NO_x, Hg, particulate matter
Possibility of producing synthetic fuels, chemicals, and marketable by-products
Possibility of cost-effective capture and storage of CO_2 in the future
Possibility of upgrading simple cycle plants (powered by gas turbines) to combined cycle plants by integrating a coal gasification unit and a steam cycle → stepwise upgrade with increasing competitiveness of coal in comparison with natural gas
Possibility of handling nearly all kinds of carbogeneous fuel

Many different configurations of an IGCC with integrated CO_2 removal are possible. However, all setups work under the basic principles of an IGCC. The gasification unit is an entrained-flow reactor that works in the temperature range of 1400 to 1600 °C and at pressures up to 70 atm [Merrick, 1984; Higman and Van der Burgt, 2008]. Finely ground coal with particle size less than 0.1 mm is injected with the reactant gases (O_2/H_2O) into the reaction chamber. The gasification reactions take place in a flame similar to that of a pulverised coal combustion chamber. The coal particles are heated up at about 1000 °C/s [Higman and Van der Burgt, 2008]. The residence time of the coal particle is a few seconds. The carbon is almost completely converted into gaseous products; mainly CO (about 60 mol%) and H_2 (about 30 mol%) are formed [Higman and Van der Burgt, 2008]. High-temperature gasification melts nearly all of the original mineral phases and destroys all metal–organic bonds within the coal matter, leading to exhaustive volatilisation of weakly bound species. Released Na, K, S, and Cl compounds usually end up in the form of chlorides, hydroxides, sulphides, and silicates. To protect the combustion turbines and environment from emissions generated during coal conversion, a gas clean-up system must be used [Scandrett, 1984; Newby and Bannister, 1994]. For use in a gas turbine, the raw gas from any coal gasification process must be cleaned of both particulate matter and S gases in order to prevent downstream surfaces from experiencing several problems, e.g. erosion, fouling, or corrosion of the gas turbine blades [Brown, 1982]. However, performance data for gasifiers are not available, and this makes specification of gas cleaning equipment difficult. Furthermore, there is still no common standard for gas cleaning requirements to protect advanced gas turbines in temperatures above 1000 °C. Because of a lack of data and experience in this field, problems in advanced gas turbines are anticipated based on the knowledge of gas turbines fired by residual fuel oil. Scandrett [1984] summarised several studies, and, in general, the amount of gas-phase Na and K in the flue gas entering the gas turbine should be less than 20 ppbw. In the state-of-the-art IGCC process, the clean-up involves cooling of the gasifier product gas. A heat recovery unit produces steam, which drives a steam turbine. The clean gas is heated again and combusted in a gas turbine, which generates electricity. The exhaust gas from the turbine still contains significant heat, which is used in a boiler to produce steam for a steam turbine; the steam drives generators.

The efficiency of conventional IGCC plants without CO_2 capture is reported to be 41–46% LHV (lower or net heating value), and for advanced new technologies the efficiency can even reach 55% LHV [Beer, 2007; Christou et al., 2008; GTW, 2006]. Various studies have shown that the efficiency of conventional and advanced IGCC plants with CO_2 capture is in the range of 32 to 43% [Descamps et al., 2008; Kanniche and Boual-

lou, 2007]. However, IGCC plants must reach efficiencies of 50% to produce electricity at a competitive price and to reach commercial breakthrough [Christou et al., 2008]. Furthermore, CO_2 sequestration must be commercially viable [Beer, 2007].

It follows that the IGCC process represents a promising approach to cleaner and more efficient use of coal for power generation. Advances in IGCC technology continue to increase efficiency and decrease emissions of CO_2 [FAA, 2006]. Further improvement requires several additional approaches. First, the gas turbine inlet temperature should be increased, but this increase requires the development of super-alloys or cooling techniques that allow continued operation at increased inlet temperature. Second, higher efficiency could be attained by replacing cold gas cleaning with hot gas cleaning; this technique was mentioned by Wolk et al. as early as 1992. Third, development of H_2 and CO_2 membranes can help the process to reach higher efficiencies.

Many low-temperature gas cleaning processes are currently available. State-of-the-art gas cleaning facilities employ particle separation—achieved through the use of a candle filter unit. Furthermore, a scrubber, COS-hydrolysis, and wet S removal unit are employed—to provide a gas that fits the requirements of gas turbine manufacturers. Also, the gas can be cleaned of CO_2 through the use of a CO-shift and CO_2 separation. The state of the art in CO_2 separation is the rectisol scrubber. However, it causes a significant loss in efficiency because the gas is cooled down to -70 °C and afterwards heated up again for the following processes. Advanced CO_2 removal could employ a membrane separation technique. Depending on the type of membrane, hot S removal may be necessary to prevent poisoning or corrosion of the membrane material [Müller et al., 2009].

A schematic of an advanced IGCC power plant that includes hot gas cleaning and CO_2 removal is presented in Figure 4. The IGCC concept with integrated hot gas cleaning and CO_2 removal consists of the following units: air separation unit, liquid slag separator, alkali removal, heat recovery, S removal, catalytic (shift) membrane, combustion chamber, gas turbine, heat recovery steam generator, steam turbine, and generator [Müller et al. 2009].

Hot gas cleaning reduces the efficiency loss caused by ordinary cleaning systems, such as the wet scrubber. The energy benefit to a combined cycle plant obtained through the use of a high-temperature gas cleaning process is variously reported between 2 and 8% [Brown, 1982]. Hot gas cleaning under gasification conditions is currently under development, and it will allow for the clean-up of the raw gas without significantly cooling it to below the temperature of the next process step. Released alkali metals can be effectively trapped by getter materials in the ash/slag, e.g. silica

[Müller et al., 2004; Willenborg and Müller, 2006]. Therefore, using the clean-up potential of the slag would be beneficial for the overall efficiency. Qualitative and quantitative data of the released species, as well as a more comprehensive knowledge of the release mechanisms, are needed to develop adequate hot gas cleaning facilities [Scandrett, 1984].

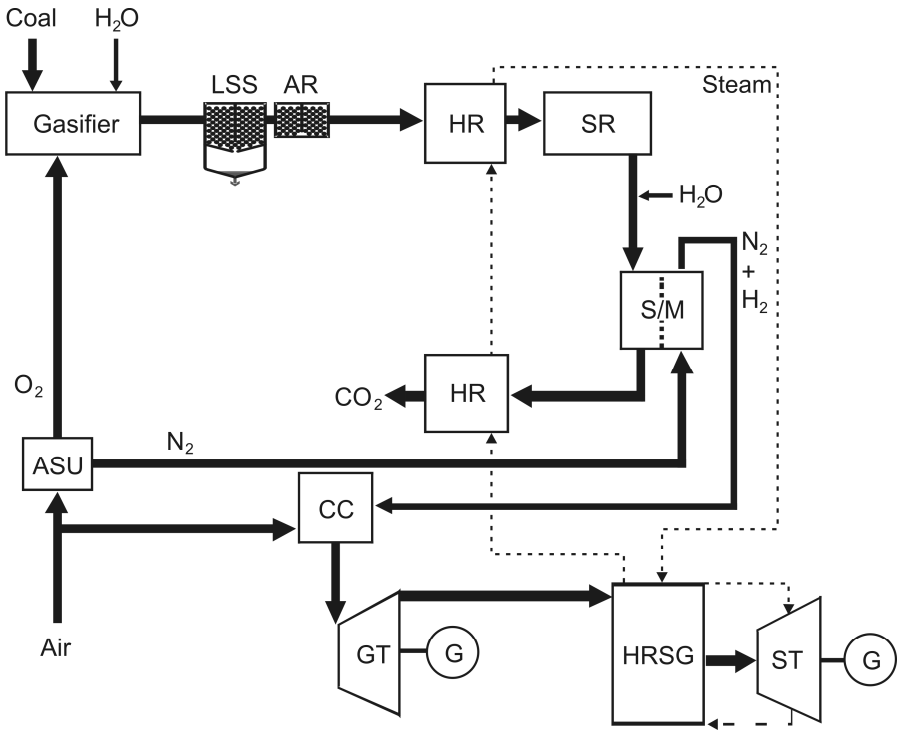

Figure 4. Schematic of an IGCC power plant, adapted from Müller et al. [2009].
Air separation unit (ASU), liquid slag separator (LSS), alkali removal (AR), heat recovery (HR), S removal (SR), catalytic (shift) membrane (S/M), combustion chamber (CC), gas turbine (GT), heat recovery steam generator (HRSG), steam turbine (ST), and generator (G).

2.3 Release of Na, K, S, and Cl species from coal gasification

A review of the literature on the release of Na, K, S, and Cl species is given for thermal utilisation, covering reducing and oxidising conditions, experimental investigations, and thermodynamic predictions. The release of trace elements depends on chemical reactions with other compounds present in the coal and the surrounding gas, the conversion conditions, and the conversion environment (temperature, pressure, gasification agent, temperature gradient in the coal particle, etc.). Coal is a highly complex fuel, as discussed in Section 2.1. The variability of the mineral and organic content of coal increases the diversity of the reactions that can occur during the thermal conversion of coal. Because of the complexity of the reactions, only an outline of reactions involving Na, K, S, and Cl species will be provided. Additionally, a summary will be given on parts of the mineral matter (e.g. SiO_2, aluminosilicate) that are closely related to the release due to several reaction mechanisms, e.g. capture reactions.

Investigations of the release of Na, K, Cl, and S species during thermal treatment of coal and coal ashes were performed by multiple groups using several different experimental approaches, as well as by thermodynamic modelling. Experiments were performed from the lab scale to the pilot-plant scale. Most of the works focused on the quantitative analysis of the release of S, Cl, and N species, but alkali metals and heavy metals were also investigated. A limited number of investigations to discover the release mechanisms have been performed to date. Classical, off-line collective sampling techniques have been frequently used. These methods are commonly available, but they require relatively long sampling/analysis times (usually longer than 30 min). Furthermore, transient release behaviour, for example, cannot be detected in this way. To overcome the limitations of off-line measurement methods, significant efforts have been made to develop and improve online measurement methods. Monkhouse [2002; 2011] has reviewed the state of the art of online diagnostics for metal species, e.g. the excimer laser–induced fluorescence (ELIF) method, which can be used for online analysis of gaseous alkali metal species [Schürmann et al., 2001]. Other online measurement techniques are surface ionisation and molecular beam mass spectrometry. Surface ionisation offers the possibility of detecting gaseous alkali metal species and particles [Davidsson et al., 2002; Kowalski et al., 2007]. Molecular beam mass spectrometry is well established and is able to differentiate a fair number of key gaseous chemical species; it has already delivered a large body of useful data in the area of thermal utilisation of biomass and coal, regarding both the release and capture of inorganic species

[Milne and Soltys, 1983a and 1983b; Krishnan, 1991; French et al., 1994; Wolf, 2003; Oleschko, 2007; Porbatzki, 2008; Stemmler, 2010].

The fate of S during thermal coal utilisation was the object of comprehensive research. Hodges and Richards [1989] identified S as a highly volatile species. Most of the S is released in the early stage of the combustion process. Attar [1978] has given a review of the release of S in coal–gas reactions. Important variables for the release of S species are temperature, pressure, composition of coal and ash, type of reactor, gas composition, and particle size. Most of the S is converted to gaseous forms, e.g. H_2S, COS, SO_2, and CS_2, and only minor amounts can be found in the ash.

The release occurs from inorganic- and organic-bound S as well. The release of inorganic S is closely related to the thermally induced decomposition of sulphides, e.g. pyrite (FeS_2). Halstead and Raask [1969] reported that the decomposition of FeS_2 and the formation of gaseous S and FeS occur in a residence time of approximately 1–5 s during lab-scale experiments under the conditions of pulverised coal-fired boilers. In addition, Raask [1982] reported that pyrite is readily decomposed during devolatilisation in the coal flame. The kinetic of the decomposition of FeS_2 is fast even at moderate temperatures (550–600 °C) [Halstead and Raask, 1969].

S_2 was reported to be the main gaseous S species; it subsequently oxidises to SO_2 in a combustion atmosphere [Halstead and Raask, 1969]. However, a significant fraction of S can remain in unreacted char, and it is released only with the progression of char conversion. It is possible for H_2S to react with the remaining char to form stable thiophenic structures. Indication for the correctness of this assumption was given by the work of Czaplicki and Smolka [1998], which investigated the distribution of total S in products of autothermal pyrolysis in a circulating fluidised bed reactor. They reported that the increase of the coal-to-air ratio results in an increase of S remaining in the char and in a decrease of gaseous S compounds.

The rate of capture is limited by the rate of the mass transfer of gaseous S to the char surface, the diffusivity of S into the char particle, and the rate of the reaction. It is assumed that increasing pressure increases all of these factors; it also increases the residence time, resulting in an enhanced capture.

Attar [1978] reported that the reaction of FeS_2 and H_2 and the formation of H_2S are important and fast reactions at 500 °C, whereas the reaction of FeS and H_2 is rather slow. Xu and Kumagai [2003] investigated the S transformation during rapid hydrodevolatilisation of three coals using a continuous free-fall pyrolyser at 650–850 °C and 50 bar H_2. They found that the decomposition of pyrite is only affected by the temperature. The H_2 pressure had no significant influence.

The dependence on the temperature and the mode of occurrence of the release of S species was investigated by Cernic-Semic [1961]. He used a radioactive marker (^{35}S) to obtain information on the release mechanisms. He found that the release of organic-fixed S began at temperatures below 500 °C, e.g. the decomposition of diethylsulphide begins at 450 °C [Khan, 1989]. The release of inorganic S begins at temperatures above 500 °C. Ibarra et al. reported that the release of H_2S as a function of temperature passes through two peaks between 500–560 °C and 630–700 °C. The release was related to the decomposition of organic and pyritic S. Khan [1989] studied the distribution of S in products during pyrolysis and gasification of a series of coals at 500 °C in a fixed-bed reactor in an inert atmosphere. He reported that an increase in pyrolysis temperature increases the total gaseous S yield at the expense of char S. Nichols et al. [1989] summarised several observations concerning the effects of pressure on the fate of S during entrained gasification. He reported that the amount of S remaining in unconverted char increases and the amount of gaseous S compounds decreases with increasing pressure.

According to Schmidt [1966], the formation of H_2S depends mainly on the occurrence of H_2 and/or H_2O in the gasification atmosphere. The release of S is enhanced by the presence of H_2 [Gryglewicz, 1996]. Additionally, hydrocarbons released during devolatilisation have a significant influence on the release of H_2S. Hydrocarbons are able to undergo reactions with FeS_2 and form highly volatile H_2S [Cernic-Simic, 1961; Attar, 1978]. In agreement with these results, Ibarra et al. reported that the organic matter significantly influences the decomposition of pyrite and the release of H_2S; they highlighted similar trends for COS and H_2S.

The release of COS is influenced by the steam content. Cernic-Simic highlighted the role of the water–gas reaction in this context. Water can react with hydrocarbons and form CO and H (nascendi). CO can undergo secondary reactions and form COS. The formation of H_2S is preferred in H_2-rich atmospheres and at high temperatures [Attar, 1978]. In addition, he pointed out that the reaction of FeS_2 and CO occurs slowly at temperatures below 800 °C. Experimental studies of the transformation of pyrite in a drop tube furnace under pulverised combustion conditions at 1227 °C were carried out by Srinivasachar et al. [1990a]. They found that the pyrite decomposition took about 575 ms for particles of 75–90 µm.

More recently, Yan et al. [2005] reported that S bound to aliphatic and aromatic carbon was released in the form of *SH radicals [Yan et al., 2005]. The *SH radical can undergo several secondary reactions with the remaining char to form H_2S, COS, SO_2, and S structures in the char [Yan et al., 2005]. The release of H_2S, COS, and SO_2 from

the model substances (e.g. benzyl sulphide) started at the same time and at moderate temperatures (215–280 °C). The order of the amount of formed substances was H_2S, SO_2, and COS. S compounds, which do not form the *SH radical, decompose and form S species. The formation of H_2S, but not of COS, was found during model studies in which FeS_2 and FeS were mixed with char and heated to 850 °C under hydrogen. The formation of H_2S was found to begin at 420 °C for FeS_2 and at 480 °C for FeS.

The release of S depends on coal rank. Consequently, the correlation between the coal rank and the release of S species has been the subject of several research groups. Cernic-Semic [1961] stated that, with decreasing rank, more S is released at temperatures below 500 °C. Khan [1989] pointed out that the amount of volatile matter in low-rank coals is usually significantly higher than that in high-rank coals. This leads to significantly higher amounts of S released during devolatilisation because a smaller amount of remaining char results in a lower S capture capability. Attar [1978] reported that the reactivity of S is strongly correlated with the coal rank, as mentioned in Section 2.1. Furthermore, he reported the following order of the reactivity of S (starting with the highest reactivity): thiole and alkyl > aryl.

Gryglewicz [1996] investigated the release and retention behaviour of S of 20 coals in relation to the coal rank during devolatilisation at 723 °C. During the thermal treatment of coal, S-containing structures go through the decomposition processes in a way that depends on the conditions, the coal rank, and the mineral content. Portions of the S remain in the coal matter after devolatilisation. During coalification, part of the thiole is converted to thiophene and sulphide. With increasing temperature, the stability of S structures increases in the following order: aliphatic thiole, disulphide < aromatic thiole and sulphide < thiophene. Aliphatic S is thermally less stable, forms H_2S upon heating or devolatilisation, and is converted, at least in part, to the more stable heterocyclic structures, as mentioned above [Calkins, 1994]. Thiophenes are reported to be very stable up to 1000 °C. In conclusion, primarily aromatic S remains in the coal matter after devolatilisation, and both aliphatic S and inorganic S are released during devolatilisation. Ca-bearing minerals in coal react with released H_2S and form CaS, which remains in the non-volatile coal matter. As mentioned above, acidic slags are capable of capturing large amounts of alkali metal and alkali earth metal oxides. This results in a reduction of volatile alkali metal and alkali earth metal compounds in the gas phase, which reduces the capability of S capture in the gas phase. The influence is significant: Raask [1985] reported that a fraction between 30 and 45% of the alkali metal elements are converted to the alkali metal sulphates under combustion conditions. The remaining amount of alkali metals is dissolved in the surface layer of silicate ash particles.

Sheth and Rasnake [1992] investigated the release of S and K from coal at temperatures up to 1725 °C under combustion conditions. They reported that K can effectively capture S. Also, the capture of S by Ca and Mg is well known [Attar, 1978] and is used in coal combustion power plants to reduce the amount of S in the flue gas.

Cl is a highly volatile species that is usually quantitatively released during thermal coal conversion [Hodges and Richards, 1989]. The fate of Cl during devolatilisation (300–1000 °C) and water steam gasification (1100 °C) of coal was investigated by Gyo et al. [2006]. They found that Cl was almost completely released at moderate devolatilisation temperatures (300–600 °C). In addition, they observed two phases of release. The first phase occurred at 350–750 °C, and the second phase occurred above 850 °C. The two-step release is explained by the mode of occurrence of Cl in the coal. The first-phase release is mainly related to organic-bound Cl, whereas the second-phase release is mainly related to the volatilisation of inorganic Cl species. The second-phase release is enhanced by the presence of char. They also highlighted the decreasing amount of released Cl with increasing pressure. In principle, the release of Cl increases with increasing temperature and decreases with increasing pressure. In the presence of water vapour, the release of HCl increased. This is explained by a shift in the equilibrium to the product side, as shown in Eq. 1 and Eq. 2. However, the contribution of these reactions to the total amount of released HCl is rather small owing to the small amount of $CaCl_2$ mineral in the coal.

$$CaCl_2 + H_2O \leftrightarrow CaO + 2\,HCl \qquad \text{Eq. 1}$$

$$CaCl_2 + SiO_2 + H_2O \leftrightarrow CaSiO_3 + 2\,HCl \qquad \text{Eq. 2}$$

The influence of steam on the release of Cl was investigated by Brinsmead and Kear [1956], who fired coal pellets with steam. The main result was that the release of HCl increased under the influence of steam, whereas the amount of gaseous NaCl decreased. This is explained by the hydrolysis of NaCl and the formation of NaOH and HCl, as mentioned above. Furthermore, they reported that about 95% of the total amount of Cl was already released at 700 °C. They observed significant differences in the release of Na and Cl, and they assumed that Na and Cl are released through independent release mechanisms. They concluded that vaporisation is not the main mechanism of NaCl release. In addition, they found that kaolin is able to capture Na, whereas the release of Cl is unaffected by the presence of kaolin.

Herod et al. [1983] made a mass spectrometric study of the release of HCl and other volatile species from six coals in a He atmosphere at 300 °C. They found that 40–

60% of the Cl content was released during heating at 300 °C over 24 hours. No other Cl species were observed. The release of HCl is not correlated with the amount of Cl in the coal. In addition, they reported that the release of HCl is controlled by the first-order kinetic. The presence of H is important for the formation of HCl.

The release of the alkali metal species Na and K has been the object of comprehensive research. However, the focus was often on biomass, so the results are not always directly transferable to coal; this is especially true for K, which usually occurs in organically fixed form or as KCl in biomass and in non-volatile forms in coal.

Osborn [1992] reported that atomic Na is the main gaseous specie in the conditions of pulverised coal combustion due to high temperature, and especially in the highly reducing environment of the first milliseconds of the combustion process. The atomic Na is oxidised to NaO or NaOH after transportation out of the pyrolysis-like atmosphere around the coal particle. Atomic Na can be formed by a reaction with H (Eq. 3). However, atomic Na is very reactive and will immediately undergo further reactions and form Na_2SO_4, Na-aluminosilicate, and other Na species, as shown by way of example in Eq. 4 and Eq. 5 [Raask, 1985].

$$NaCl + [H] \longrightarrow Na + HCl \qquad \text{Eq. 3}$$

$$2\,NaCl + SiO_2 + H_2O \longrightarrow Na_2O{*}SiO_2 + 2\,HCl \qquad \text{Eq. 4}$$

$$2\,NaOH + SO_2 + 0.5\,O_2 \longrightarrow Na_2SO_4 + H_2O \qquad \text{Eq. 5}$$

Accordingly, Nykänen [2002] reported that NaOH and Na are the main Na species that escape the flame region. At temperatures below 1000–1200 °C, reconversion of NaOH occurs, and the dominant gaseous Na species is NaCl in a pulverised coal combustion atmosphere [Haldstead and Raask, 1969].

Glazer et al. [2005] investigated the release of gaseous alkali metal species during combustion and co-combustion of coal and biomass at 700–900 °C using ELIF. They found that the release of K depends on the K/Cl and K/Si ratios of the fuel. Additionally, Gottwald et al. [2002] measured the alkali metal concentration during coal combustion using ELIF.

Molecular beam mass spectrometry was used by Krishnan et al. [1991] and, more recently, by Oleschko et al. [2007]. Oleschko investigated the release of NaCl and KCl during combustion of hard coal at temperatures of 800–1200 °C and absolute pres-

sures of 1, 3, and 9 bar. One result was that Na and K were mainly released as chloride, although NaOH could not be taken into account because of experimental limitations, as discussed in more detail in Chapter 5. They reported that the amount of gaseous NaCl and KCl decreased with increasing pressure for both the hard coals and the lignites under investigation.

The fate of Na during pulverised coal combustion was investigated by Neville and Sarofim [1985]. They reported that the volatility of Na depends on its mode of occurrence in coal. Na dispersed atomically in the organic matter (i.e., ion-exchangeable organically bound) or present in the form of NaCl is readily volatised, whereas silica-bound Na remains in the ash.

Takarada et al. [1995] investigated the volatilisation of alkali metals during devolatilisation and gasification of coal using leaching experiments and model substances (NaCl, Na_2CO_3, Na_2SiO_3, Kaolin, and SiO_2). They found the following order of release at 840 °C (starting with the highest release amount): NaCl >> Na_2CO_3 > Na_2SiO_3.

The influence of oxygen on the release of Na species was investigated by Steffin [1999]. He found that an increased availability of O_2 leads to an enhanced fixation of Na in non-volatile forms. In addition, he reported that a higher O_2 partial pressure leads to an enhanced coal conversion and a higher temperature, resulting in a shorter residence time of the alkali metal species in the remaining char. Therefore, the alkali metal release outweighs the enhanced binding. The result is a moderate increase of gaseous alkali metal compounds.

Gottwald et al. [2001] reported the disproportionately high increase in alkali metal release in experiments with Cl-doped coals under combustion conditions. Clay minerals were found to suppress the release of alkali metals as a result of the formation of non-volatile alkali metal alumina silicate, e.g. K-alumina silicate. Despite the low temperature and the low residence time in their fluidised bed system (920 °C bed temperature and 7 bar pressure), the capture of alkali metals by aluminosilicates was found to be very effective. The authors suggested that the capture reactions occur before the alkali metals are completely released.

Schürmann et al. [2007] studied the effect of steam, temperature, Cl, and oxygen content on the release of and capture of alkali metal species under pulverised coal combustion conditions (hard coal, 1000–1300 °C, residence time 3–5 s, air/fuel ratio 1.15–1.5). They reported an increased release of K with increasing temperature. Furthermore, they reported that the amount of gaseous K was an order of magnitude higher than the amount of Na; this was assumed to reflect the higher amount of K in the coal.

Similarly, Shet et al. [1992] reported an increasing amount of gaseous metallic K with increasing temperature.

Wei et al. [2008] investigated the transformation of alkali metals during devolatilisation and gasification of lignite. They found that the amount of soluble (H_2O, NH_4CH_3COOH, HCl) Na and insoluble K decreased during devolatilisation, whereas the amount of insoluble Na increased.

Helble et al. [1992] published data of measurements and modelling of vapour-phase NaCl formed during pulverised coal combustion. During experiments with coals of different rank, they found a linear correlation between the formation of NaCl and the Cl content of the coal. The experimental findings have been confirmed by thermodynamic calculations performed using Solgasmix. In addition, the authors reported that NaCl reached equilibrium in hydrogen flames within 10 ms, which is common for gas–gas reactions. Halstead and Raask [1969] performed basic research on the release of Na and Cl species during combustion. They reported on the reaction of NaCl with SiO_2 and on the importance of the formation of HCl and Na-silicate. Additionally, they discussed the hydrolysis of NaCl. They reported that 10% of the NaCl was hydrolysed at 1200 °C, whereas only 4% was hydrolysed at 1000 °C. The hydrolysis of NaCl was also studied by Brinsmead and Kear [1956].

According to Halstead and Raask [1969] and Hodges and Richards [1989], only trace amounts of NaCl are fixed in the slag, indicating that NaCl is a highly volatile species. Hodges and Richards [1989] researched the fate of Cl, S, Na, K, Ca, and Mg during the fluidised bed combustion of coal using off-line analysis equipment. The main finding of their work was that most of the K remains in the ash (especially in the clay mineral fraction). Ca and Mg also remain in the ash.

Wibberley and Wall [1982a and 1982b] researched the thermodynamics of SiO_2, Na, S, and Cl in pulverised coal-fired boilers. They reported that NaCl and NaOH are the main Na species above 1223 °C. A significant increase in atomic Na was found at temperatures above 1423 °C. The formation of Na_2SO_4 occurs mainly as a result of the reaction of NaCl with SO_2 in the presence of O_2 and steam, as shown in Eq. 6. Silica and aluminosilicates are effective getter for Na, as shown by way of example in Eq. 7 and 8. Alkali-silicates have low melting points in the range of 1023 to 1577 °C. This can lead to problems in fluidised bed combustion system resulting from agglomeration of the bed material.

$$2\,NaCl + SO_2 + H_2O + 0.5\,O_2 \longrightarrow Na_2SO_4 + 2\,HCl \qquad \text{Eq. 6}$$

$Na_2SO_4 + 3\ SiO_2 \longrightarrow Na_2O*3\ SiO_2 + SO_2 + 0.5\ O_2$ Eq. 7

$NaCl + H_2O + xAlSi_yO_z \longrightarrow$ Na-aluminosilicates + HCl Eq. 8

Release and capture reactions occur simultaneously during the thermal conversion of coal particles. Thus, a summary will be given on capture reactions with a focus on the capture of Na, K, S, and Cl species. During entrained-flow gasification, most of the original mineral matter melts, and all metal–organic complexes within the fuel are destroyed [Groen et al., 1994]. Therefore, not only highly volatile Na, K, S, and Cl species are released. Several investigations were made regarding the transformation of non-volatile mineral matter during coal combustion [Raask et al., 1965; Tomeczek et al., 2002]. Raask et al. [1965] reported significant volatilisation of silica above 1800 °C. The release mechanism was described as the volatilisation of SiO after reduction of SiO_2 by carbon under highly reducing conditions. Neville and Sarofim [1985] reported that volatised refractory substances (e.g. silica) can form sub-micrometer fume with a high surface area that is capable of effectively capturing alkali metal species. The incorporation of Na and K into silica-rich glasses is well known [Cernic-Simic, 1961; Halstead and Raask, 1969; Groen et al., 1994]. More recently, Wolf [2003] and Stemmler [2010] have confirmed the capture of K and Na by kaolin during laboratory-scale coal combustion and biomass gasification experiments and through thermodynamic calculations.

After and during the release process in the coal particle, the gaseous Na compounds must diffuse through a mineral-rich char matrix, and a significant fraction of the Na can react with silica [Huffman et al., 1989]. The same results were reported by Swift et al. [1979, cited by Nykänen, 2002] during experiments at 900 °C and by Neville and Sarofim [1985] and Takarada et al. [1995]. The suppression becomes increasingly significant at kaolinite ($Al_2O_3*2SiO_2*2H_2O$)/Na molar ratios greater than 1.5 for a devolatilisation temperature of 1220 °C. The results of several research groups proved that in-situ capture of alkali metals in gasifiers is possible through the addition of kaolinite. A low release of Na species has been found for coals with high cross-correlation coefficients between Na and silica/aluminium for combustion and gasification of coal at 850 °C [Murakami, 1999; Murakami and Naruse, 2001]. Tran et al. [2005] studied the kinetics of gaseous alkali metal capture by kaolin using surface ionisation. Kaolin was found to be a very efficient getter for gaseous alkali species at fluidised bed temperatures. Even though mainly gas–solid reactions occur, the kinetic is already fast at temperatures of about 850 °C.

Usually, K can be found in non-volatile form in coal, as mentioned in Section 2.1. Hodges and Richards [1989] reported that K—as well as the alkaline earth metals Mg

and Ca—remains in the ash. K will remain non-volatile in the fused silicate particles in the boiler flame unless there is an exchange reaction with volatilised Na. Na can undergo reactions with SiO_2 and Al_2O_3, or it can be incorporated into K-aluminosilicates through ion-exchange reactions, as shown by way of example in Eq. 9. However, the amount of exchange is limited by the temperature. The ion-exchange occurs at significant rates only above the melting point of K-aluminosilicates as a result of the kinetic limitations of the process in the solid state. However, the reaction kinetic benefits significantly from the formation of eutectics of several multicomponent silicates and aluminosilicates [Schairer, 1957; Schairer and Yoder, 1960; Burnham, 1981; Wu et al., 1993; Ota et al., 1995; Richet et al., 2006]. For example, the melting point of the Na_2O–SiO_2 system was reported by Ryś [2007] to be about 861 ± 9 °C between 78 and 80 mol% Na_2O under coal combustion–like conditions. In conclusion, the kinetic of ion-exchange reactions is significantly enhanced at moderate devolatilisation temperatures, and this can result in an enhanced retention of Na and release of K.

The release of K by ion-exchange reactions has also been reported by Müller et al. [2006] and other authors. There is a small temperature window of retention that depends on the volatility and the melting point of aluminosilicate [Osborn, 1992]. A high temperature can lead to very fast release, and therefore there may not be sufficient time for retention. On the other hand, a temperature that is too low leads to a retarded kinetic.

$$mK_2O * xSiO_2 * yAl_2O_3 + 2\ NaCl \longrightarrow (m\text{-}1)K_2O*Na_2O*xSiO_2*yAl_2O_3 + 2\ KCl \qquad \text{Eq. 9}$$

Gibb and Angus [1983] studied different coals in a bomb combustor. They reported that the fraction of released K was, on average, about 12% (3–28%) of the total amount of K. Furthermore, they concluded that the release of K depends on the amount of K, the amount of Cl, and the composition of the ash, especially the acidity ($SiO_2 + Al_2O_3 + Fe_2O_3$) / (CaO + MgO) ratio. With decreasing acidity, the release of K is enhanced.

Kühn and Plogman [1983] and Formella et al. [1986] studied reactions of K and coal mineral matter in coal gasification. They reported that K compounds (K_2CO_3 and KOH) reacted with the aluminosilicates illite and kaolinite to form K-aluminosilicates, as shown in Eq. 10. However, the actual reaction is more complex as it includes the hydrolysis of K_2CO_3 by steam as well as the dehydration of kaolinite. Formella et al. suggested that the reaction is completed when the coal reaches 600–800 °C. During combustion of K ion–exchanged lignite at 1500 °C under 7% O_2, it was found that the reac-

tion of the ion-exchanged, carboxyl-bound K is comparable, to a significant extent, to the reaction of carboxyl-bound Na in the original coal [Shah et al., 1995]. A possible reaction is shown in Eq. 10.

$$Al_2O_3*SiO_2*2H_2O + K_2CO_3 \longrightarrow K_2O*Al_2O_3*2\,SiO_2 + 2\,H_2O + CO_2 \qquad \text{Eq. 10}$$

Bruno et al. [1986] studied the behaviour of 8 coals at 700 °C and 36 bar. They postulated that, in addition to K-aluminosilicates, other insoluble compounds—especially S and Fe compounds—were formed. In agreement with the results involving alkali metals, the capture of alkaline earth metals was demonstrated by Matsuoka et al. [2008]. They pyrolysed two sub-bituminous coals at 1500 °C in a drop tube furnace; afterwards, the chars were gasified in CO_2. It was found that dispersed Ca is converted into fine ash particles, and these particles undergo reactions with clay minerals and form complex aluminosilicates.

Other relevant studies on the capture of Na and K were performed by Willenborg et al. [2006] and Müller et al. [2004]. They found that network formers (e.g. SiO_2, TiO_2, Fe_2O_3) lead to a lower Na concentration in the gas phase due to an increasing polymerisation of the aluminosilicate network. Furthermore, FeO is a weak network modifier. Increasing amounts of FeO can lead to depolymerisation of the network. As a result, the Na retention of the slag decreases under gasification conditions. This leads to a higher amount of Na in the gas phase. In addition, the acidity of the slag is important for the capture. The ash of a common bituminous coal forms an acidic slag that is capable of absorbing large amounts of basic oxides (e.g. Na_2O and CaO) at high temperature [Raask, 1985].

Adsorption processes of HCl, alkali metal, and alkaline earth metal species were recently investigated by several groups. Sonoyama et al. [2006] found that alkali metal and alkaline earth metal species volatilise from the surface of char mainly as elemental species. Furthermore, they pointed out that the dissociation of carboxylic-bound metal species is enhanced in an atmosphere that is rich in H radicals. Therefore, the release of this species is likely to be enhanced during the gasification of coal and biomass. Partanen et al. [2005] and Shemwell et al. [2001] investigated the capture of HCl by Ca-sorbents. Partanen et al. [2005] made systematic experimental investigations of the effect of temperature, gas atmosphere, and sorbent quality during adsorption of HCl by limestone. They reported two temperature ranges for the concurring reactions of chlorination and recarbonisation. In the presence of CO_2, recarbonisation and chlorina-

tion occur simultaneously at 650 °C, and the chlorination is unaffected by the presence of CO_2 at 850 °C.

The capture of S by Ca is well known and is already a common industrial process. Reactions of gaseous S compounds with basic alkali metal minerals are discussed by Strohbeen [1981]. A possible reaction is shown in Eq. 11. The reaction becomes thermodynamically favoured above 650 °C, and the reaction rate increases at somewhat higher temperatures [Strohbeen, 1981].

$$Na_2CO_3 + H_2S \longrightarrow Na_2S + H_2O + CO_2 \qquad \text{Eq. 11}$$

The given review of the literature indicates that comprehensive research on the release and capture of inorganic species from coal utilisation has already been performed. However, it also reveals that there are many open questions, especially regarding the process conditions of high-temperature coal gasification.

3 Methods and experiments

3.1 Thermodynamic prediction

One method of studying the release of Na, K, S, and Cl species under coal gasification conditions is the use of equilibrium calculations. Chemical thermodynamics have been proven to be helpful in explaining the release and capture of Na, K, and S species as well as the release of Cl species [Blander and Sinha, 1988; Wibberly and Wall, 1982; Scandrett, 1984]. Thermodynamic calculations involve determining the equilibrium composition of the investigated system under predefined conditions. Only the elemental composition of the initial system is relevant to the determination of the equilibrium composition. Knowledge of the mode of occurrence is not needed because equilibrium calculations assume that the starting material is completely converted to the most thermodynamically stable reaction products. In other words, only the composition of the system in equilibrium is important and not the way to equilibrium. However, this approach suffers from some limitations, as summarised by Hansen et al. [1998]:

> Disregarding all kinetic limitations, the primary limitation in the GEA analysis is that the system is considered as being in global equilibrium, i.e., no gradients in temperature, pressure and composition are considered. In a real combustion system, the mixing is far from being perfect. Thus, in a real combustion system gradients in temperature, pressure and composition do exist, causing e.g. different redox conditions in different parts of the system.

The reactor is regarded as zero-dimensional, i.e., there are no spatial variations in temperature or composition. Neither is there any change over time because all forward and reverse reactions are assumed to reach chemical equilibrium. In real equipment, temperature and composition gradients are present along the main flow path.

Additionally, the thermodynamically predicted stable compounds can reach equilibrium only if the temperature is high enough. Otherwise, the system may not be able to reach equilibrium because of the limited residence time of the reaction partners. Also, physical processes—e.g. particle nucleation, agglomeration, and adsorption—are not considered in thermodynamic equilibrium calculations [Wang et al., 2004]. Also, it is possible that kinetic limitations occur such that chemical equilibrium is not reached. Nonetheless, thermodynamic calculations in combination with experimental data are useful in discovering the non-equilibrium effects and kinetic constraints that occur during thermal utilisation of coal and other carbogeneous fuels. Furthermore, the use of calculations can reduce the number of measurements needed to understand the re-

lease mechanisms, especially for conditions that are difficult to provide [Thompson and Argent, 1999]. Kuramochi et al. [2005] attributed overestimation of calculated data compared to experimental results to the lack of kinetic limitations, e.g. mass transfer. Li et al. [2004] presented a calculation model that includes kinetic limitations through empirical modification of the calculations. The results of these advanced calculations were found to be more accurate. A comprehensive kinetic database is needed for this approach, but such data is rarely found; therefore, the best solution for the time being is to compare the calculations to empirical data in order to avoid predictions that are overestimates.

Consequently, chemical equilibrium calculations were performed to support the interpretation of the experimental results. Through comparison with the calculated results, the experimental results were confirmed qualitatively. From a quantitative point of view, it is possible to confirm the release trends. The calculations were performed by FactSage 5.4.1, a common program that uses the principle of the Gibbs free energy minimisation. This program, which is based on ChemSage, is able to calculate the equilibrium in complex multi-component, multiphase systems [Eriksson and Hack, 1990]. The thermodynamic database included in the FACT software package includes about 5000 species and is based on the JANAF thermochemical database [Wang et al., 2004].

Gas phase species were handled as ideal gases based on the dilution of the product gas in the helium carrier gas, which can be handled as ideal [Lindner et al., 2006]. The initial system composition was based on the data given by coal analysis (Tables 4 and 5) and was related to 100 g of coal. C, H, S, O, Na, K, Mg, Ca, Cl, Al, Si, and Fe were included in the computation. The atmosphere of He and O_2 was modelled using an oxygen-to-fuel ratio of $\lambda = 0.5$ with respect to the partial pressure of oxygen during the gasification process and of $\lambda = 1$ with respect to the combustion process. This value was corrected according to the value of oxygen bound in the lignite because a significant portion of the carbon is already partially oxidised. Gaseous, liquid, and solid compounds were included in the computation.

3.2 Hot gas analysis by molecular beam mass spectrometry

3.2.1 Basic principles of mass spectrometry

Mass spectrometry is used for real-time, online determination of gaseous ionised species based on their mass-to-charge ratios (m/z) in an electromagnetic field. A schematic of the basic principles is provided in Figure 5. A mass spectrometer consists of four basic modules: sample inlet, ionisation unit, mass analyser, and detector. A typical MS procedure consists of the following steps: The sample is introduced into the mass spectrometer by a sample inlet system. Solid or liquid matter must be vaporised before the next analysing steps. The gas is ionised by one of a variety of methods, e.g. electron impact or chemical ionisation. The ions are accelerated by an electric field in the direction of the mass analyser, usually a quadrupole or a sector field, where they are separated in an electromagnetic field according to their mass-to-charge ratios. The separated ions are collected by a detector, e.g. a faraday cup or an electron multiplier, which converts the ion flux into proportional electrical current. The current is usually recorded by an automated computer running a specialised software package.

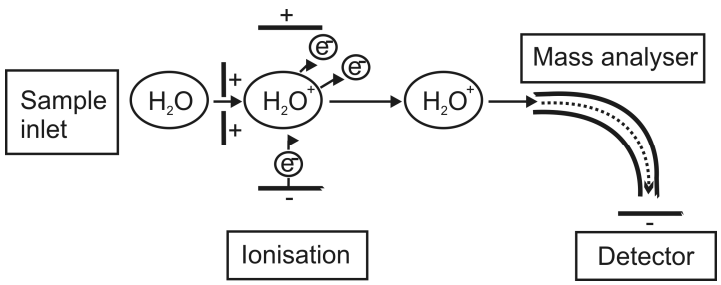

Figure 5. Schematic of the basic principles of mass spectrometry.

3.2.2 Application of molecular beam mass spectrometry

Drowart and Goldfinger [1967] gave a detailed overview of an apparatus intended for the generation and analysis of molecular beams. Hastie et al. [1984 and 2000] were pioneers in the field of high-temperature application of molecular beam mass spectrometry. A comprehensive description of the experimental setup, and especially of the molecular beam mass spectrometer, was given by Wolf [2003]. Molecular beam mass spectrometry is a reliable method for analysing gases under high temperatures and pressures [Wolf, 2003; Oleschko, 2007; Porbatzki, 2008]. The main advantage of molecular beam mass spectrometry is that reactive, condensable species are effectively quenched so that no further condensation and reaction are possible. Detailed speciation can be performed by scanning a broad range of mass-to-charge ratios in a quasi-simultaneous fashion. The released species are cooled to below room temperature in microseconds [Wolf, 2003]. Interaction with underground molecules is inhibited by the high vacuum of the chamber system of the mass spectrometer and by the large distance between the molecules in the so-called molecular beam [Wolf, 2003]. Molecular beam mass spectrometry enables gases in a broad range of different conditions to be analysed. The temperature of the gas can be as high as 1700 °C. Pressurised gas can be analysed up to 12 bar [Oleschko, 2007]. The detected limit is about 20 ppb_{Vol} [Wolf, 2003]. A schematic representation of the molecular beam mass spectrometer (MBMS) is provided in Figure 6.

The MBMS consists of three differentially pumped chambers that are connected by small orifices. A so-called skimmer divides the first stage from the second. Pressures of 10^{-2} mbar for stage 1, 10^{-6} mbar for stage 2, and 10^{-8} mbar for stage 3 are achieved during the measurement. The first stage is evacuated by two Osaka Helical Groove turbo molecular pumps, which must be fairly robust because a relatively large amount of soot and other particles can enter this chamber [Wolf, 2003]. The second chamber is necessary as a pressure stage to reach the high vacuum conditions in the third chamber. The second and the third stages are connected to four Pfeiffer turbo molecular pumps. The ionisation, the deflector, the quadrupole mass filter, and the multiplier are placed in chamber three.

A stainless steel cone (35 mm in length with an interior angle of 108° and an orifice diameter of 0.3 mm) is used for gas sampling under atmospheric pressure, and a reinforced cone with an orifice diameter of 0.1 mm is used for sampling under increased pressure. The cone is fitted to a water-cooled stainless steel flange. This front nozzle is connected to the atmospheric flow channel tube by moving the furnace towards the

MBMS. Because measurements occur under elevated pressure, the furnace and the flange are non-switched and connected in an air-tight fashion.

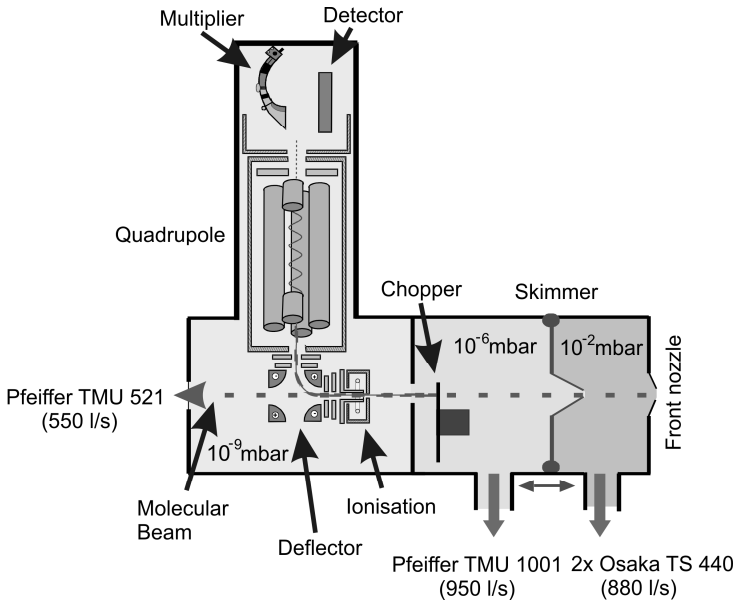

Figure 6. Schematic representation of the molecular beam mass spectrometer [adapted from Porbatzki, 2007].

Gas enters the first chamber of the MBMS through the front nozzle. The ratio of the pressure before the nozzle to the pressure in the first chamber is higher than the critical value, which results in a supersonic expansion [Wolf, 2003]. Therefore, the sampled gas undergoes a free-jet expansion. Within the flow beyond the nozzle, the Mach number is higher than one. The initial expansion is nearly adiabatic and isentropic; consequently, extreme collisional and internal energy state cooling occurs. With transition to molecular flow, collisions between the molecules of the sample gas are minimised. Furthermore, the hot gas is effectively cooled to far below room temperature, such that rotational and vibrational transitions are minimised. As a result, the integrity of the sampled high-temperature gases is preserved and chemical reactions are effectively quenched. The non-equilibrium nature of the free-jet expansion and the subsequent formation of a molecular beam allow reactive and condensable species to remain in the gas phase at temperatures far below their condensation point for time periods that are long in comparison to reaction rates.

About ten orifice diameters downstream from the front nozzle, the expansion attains free molecular flow. The core of the expanded gas is extracted by a conical skimmer with a 1 mm–diameter orifice at the entrance of stage 2. The skimmer is moveable along the axis of the molecular flow. The intensity of the molecular beam can be adjusted by the on-axis movement of the skimmer position. The continual expansion of the gas reduces the density of the stream, resulting in increased mean free path. Also, interaction with underground molecules is reduced. The mean free path (λ) of the gas particles is in the range of several hundred meters in the second chamber. In principle, the second chamber acts as a pressure stage that allows for the very high vacuum in the third chamber. The mass analyser requires an ultra-high vacuum with $\lambda \geq 1$ km, which is reached in the third chamber. The core of the expanding flow is unaffected by the absolute pressure in the chamber. Outside of this zone, the molecular flow is extracted by a skimmer. Usually, skimmers serve as high-intensity, low-temperature sources of molecular beams [Miller, 1984]. With a sufficiently low pressure in the first vacuum chamber and with proper placement of the skimmer, the supersonic flow enters the skimmer without shock formation. This is important, because it suppresses several mass transfer effects (Figure 7) that would otherwise exert a significant influence on the molecular beam.

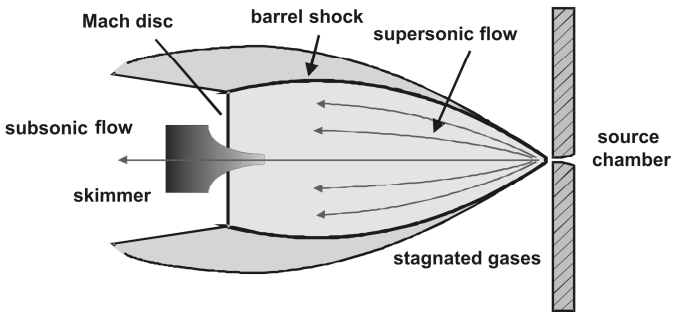

Figure 7. Schematic of the free-jet expansion [Oleschko, 2007].

The molecular beam enters the third chamber through a small aperture with a diameter of 1.5 mm. The molecular beam passes through an annular ioniser where the molecules are ionised by electron impact. Electrons are generated by a tungsten filament; heating the filament results in the thermionic emission of electrons (emission of 1 mA). The ionisation energy for the experiments was 50 eV. However, the energy is continuously adjustable. The electrons are accelerated by a negative current and cross

the molecular beam, where collision leads to the formation of ions. Electron ionisation occurs when an electron abstracts an electron from a gas molecule. When the excess energy in the ion exceeds the bond energies that hold the molecular ion A^+ together, fragmentation occurs. One out of every 10^3 to 10^4 molecules is ionised. The cations are attracted out of the ionisation zone by electrical fields with increasing negative current. The accelerated cations are redirected into the mass analyser by a deflector. The deflector consists of four poles placed in the angles of a square, with each set at the same potential (from 30 to 70 V or from -150 to -250 V) [Questor Manual]. The ion beam is deflected by 90°, focused by electrical lenses, and introduced into the quadrupole mass analyser. Uncharged molecules and anions are not deflected, which helps to prevent contamination of the mass analyser and the detector.

The ions are filtered with an ABB Extrel quadrupole analyser. The quadrupole mass analyser consists of an arrangement of four rods of preferably hyperbolic shape that act as the poles of an electromagnetic field. The quadrupole filters the ions according to their mass-to-charge ratio. AC and DC voltage and a radio frequency component that is variable both in magnitude and frequency are imposed on the rods [Questor Manual]. Opposite filter electrodes are connected. Ions that enter the quadrupole are kept in a straight trajectory by the direct current, and, meanwhile, the radio frequency voltage forces them to jiggle. There is only one path for each mass-to-charge ratio value, depending on the voltage. Only ions of a certain mass-to-charge ratio will reach the detector for a given voltage ratio. Other ions will have unstable trajectories and will collide with the rods. The positive DC voltage is particularly important for stabilising the trajectory of the heavy ions, while lighter ions swing so much that they collide with the rods. On the other two rods, a positive AC voltage is superimposed on a negative DC voltage. The heavier ions are destabilised by the negative voltage and they go out of the rods, while the lighter ions' paths are stabilised by the positive AC voltage. Since mass selection is accomplished simply by varying voltages or frequencies, the quadrupole analyser is able to scan very quickly and to switch rapidly, with negligible dead time, between settings for a number of different ions.

The final element of the mass spectrometer is the detector. The ions are detected by an off-axis Channeltron electron multiplier. A dynode converts incident ions into secondary electrons, which are then amplified in a number of stages. Electron multiplier gains of 10^4 to 10^7 are routinely obtained. The 'electron shower' hits an anode, and the current is recorded by the software and computer package. Control of the scanning parameters and collection of the multiplier signal, as a function of time and mass-to-charge ratio, are performed using ABB Extrel's Merlin Automation Data System.

3.2.3 Sensitivity test of the molecular beam mass spectrometer

To confirm the sensitivity of the MBMS, the amount of Kr in air was determined. The tune-up of the MBMS is described in Table 3. The main isotopes—^{82}Kr, ^{83}Kr, ^{84}Kr, and ^{86}Kr—were detected in air. The signal intensity of the isotopes was normalised to the signal of the main isotope, ^{84}Kr. The determined distribution of the isotopes is in good agreement with the data in the literature, as shown in Figure 8. The variance is related to pollution of the air in the laboratory and in the mass spectrometer [Wolf, 2003]. The content of Kr in dry air is 1.14 ppm_{Vol} [Earth fact sheet]. The fractions of the main isotopes of Kr in air are shown in Figure 8.

In conclusion, the detection of species with a content as low as 0.1 to 0.2 ppm_{Vol} is possible. With regard to the content of the species of interest (Na, K, Cl, and S species) in the product gas, the resolution is sufficient. However, Wolf [2003] was able to determine the main isotopes of Xe in air using an MBMS that was identical in construction; this indicates a detection limit of about 20 ppb_{Vol}.

Table 3. Tune-up of the molecular beam mass spectrometer.

Multiplier	1900 V
Sample rate	50 samples per mass
Scan time	1 s
Electron emission	0.5 mA
Electron energy	50 eV

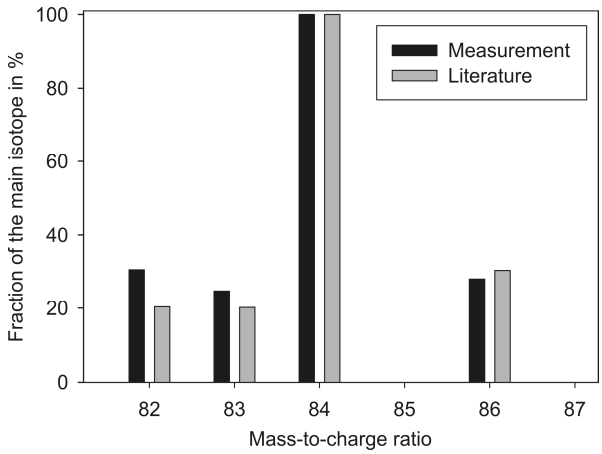

Figure 8. Results of the sensitivity test of the MBMS.

3.3 Sample preparation and analysis

Samples from 19 coals were collected and prepared for analysis. The low-rank coals were mined in Germany. K3-1, -2, and -3 were mined in Lower Lusatia. K2-2, HKN-S-, HKN-S+, HKS, and HKT are Rhenish lignites and K2-1 is a blend of different lignites. The high-rank coals were mined in Germany (STD-x and K2-3), Columbia (K2-4), Spain (K2-5), and Norway (STN-x). The coals were ground in a mill and air dried at room temperature. The coals were graded, and the particles that were smaller than 100 µm were stored under dry conditions at room temperature, as recommended by Speight [2005].

The ultimate analysis of the coals under investigation was performed by the central division of analytical chemistry (ZCH) of the Forschungszentrum Jülich. The major elements of coal matter, including C, H, N, and S, were analysed by CHNS Analysator (system LECO). As such, coal samples of 2 mg were burned in oxygen. The CO_2, H_2O, and SO_2 were analysed by IR absorption. N_2 was analysed using heat conductivity, and Cl was analysed using ion chromatography according to the Wickbold combustion method. Inorganic elements were analysed by inductively coupled plasma optical emission spectrometry (ICP-OES). Sample preparation included the following steps: A sample of 100 mg was mixed with 0.5 g lithium borate and heated to about 1000 °C for about 30 min. The melt was dissolved with 50 ml of 3% HCl and filled up to 100 ml.

The results of the analysis are given in Tables 4 and 5. The relative variance of ICP-OES was reported from the ZCH: for amounts >1%, ±3%; for amounts 0.1–1%, ±10%; and for amounts <0.1%, ±20%. The relative variance of Cl ion–chromatography was reported to be ±10%. The relative variance of CHNS was calculated from the analysis report to be ±0.2–5%. The coals represent a broad range of fuels. The elements Na, K, S, Cl, Si, Al, and Ca as well as their elemental ratios, are especially significant to the release during the conversion of coal and biomass [Oleschko and Müller, 2007a,b; Müller et al., 2006; Dayton et al., 1999; Krishnan and Wood, 1991; French et al., 1994; Milne and Soltys, 1983a and 1983b; Porbatzki, 2008].

Table 4. Chemical composition of the high-rank coals (mass%).

	K2-3	K2-4	K2-5	STD-1	STD-2	STD-3	STD-4	STD-5	STN-1	STN-2
C	79.4	65.5	31.6	83.6	80.3	78.4	65.2	59.8	78.8	74.8
H	2.76	4.72	2.60	4.22	4.72	4.98	3.67	4.14	5.54	4.52
O	10.5	21.9	34.3	6.26	8.47	10.62	16.38	20.90	8.86	15.3
N	0.978	1.241	0.73	1.72	1.65	1.68	1.36	1.41	1.61	1.25
S	0.9	0.49	0.98	0.75	0.77	0.89	0.77	0.94	0.64	1.25
Cl	0.127	0.011	0.032	0.116	0.156	0.185	0.136	0.237	0.015	0.009
Al	3.06	1.84	7.81	0.96	0.91	0.90	3.30	3.10	0.64	1.35
Fe	0.69	0.73	2.35	0.52	0.55	0.43	1.30	1.30	0.60	0.99
Ca	0.3	0.21	0.72	0.15	0.43	0.26	0.78	0.77	0.72	1.09
Mg	0.16	0.17	0.45	0.094	0.2	0.11	0.49	0.44	0.21	0.25
K	0.73	0.22	1.93	0.16	0.16	0.17	0.75	0.87	0.11	0.17
Na	0.3	0.32	0.19	0.053	0.088	0.072	0.16	0.19	0.25	0.50
Si	4.57	4.89	16.1	1.4	1.6	1.3	5.7	5.9	1.60	2.46

Table 5. Chemical composition of the low-rank coals (mass%).

	K2-1	K2-2	K3-1	K3-2	K3-3	HKN-S-	HKN-S+	HKS	HKT
C	54.8	56.9	51.0	55.5	54.6	65.8	65.8	62.0	57.3
H	5.604	5.563	5.134	4.861	5.03	4.81	4.98	4.89	4.18
O	33.8	33.2	37.6	37.6	37.2	28.1	26.6	28.0	27.5
N	0.574	0.585	0.5	0.577	0.636	0.78	0.84	0.69	0.75
S	0.24	0.3	1.35	0.28	0.31	0.205	0.508	0.365	0.478
Cl	0.035	0.037	0.022	0.023	0.0207	0.01	0.025	0.023	0.011
Al	0.069	0.042	0.27	0.051	0.06	0.034	0.034	0.12	1.5
Fe	0.58	0.49	1.3	0.8	0.66	0.25	0.25	0.48	0.28
Ca	1.39	1.26	1.01	1.03	0.89	1.0	1.2	1.4	1.3
Mg	0.37	0.51	0.26	0.36	0.28	0.37	0.44	0.48	0.47
K	0.014	0.021	0.061	0.014	0.016	0.02	0.023	0.024	0.085
Na	0.16	0.39	0.008	0.017	0.017	0.22	0.22	0.22	0.23
Si	0.25	0.22	1.33	0.22	0.18	0.01	0.023	0.72	3.6

3.4 Experimental setup

The experiments were carried out in atmospheric and pressurised flow channel reactor furnaces. For the determination of the composition of the product gas, the electrical heated flow channel reactors were coupled to an MBMS system. A summary of the experimental conditions for all experimental runs is given in Table 6.

Table 6. Overview of the experimental conditions.

Experimental run	Atmosphere	Temperature	Pressure	Coals
Influence of the oxygen content	He/20 v% O_2 and He/7.5 v% O_2	1400 °C	1 atm	5 Hard coals 4 Lignites
Influence of the coal rank	He/7.5 v% O_2/ 2.5 v% steam	1400 °C	1 atm	9 Hard coals 8 Lignites
Influence of the temperature	He/7.5 v% O_2	1100 °C 1400 °C 1700 °C	1 atm	5 Hard coals 4 Lignites
Influence of the steam content	He/7.5 v% O_2/ 2.5 v% steam	1400 °C	1 atm	6 Hard coals 4 Lignites
Influence of the pressure	He/7.5 v% O_2	1325 °C	2 bar 4 bar 6 bar	10 Hard coals 9 Lignites

3.4.1 Atmospheric flow channel furnace

The experimental setup is depicted in Figures 9 and 10. The setup mainly consisted of a heated flow channel housed in a furnace with four independent heating zones. For the channel, a high density alumina tube was used to prevent reaction of the tube walls with the released species. The inner diameter of the tube was 25 mm, and the total length of the tube was 820 mm. Helium was selected as the carrier gas because its low atomic mass leads to the highest signal intensities in the MBMS [Wolf, 2003]. The gas flow was calibrated and confirmed using a DryCal Calibration Set. The gas stream was controlled by BROOKS gas flow controllers. During the experiments involving the influence of steam and coal rank, a nebuliser was used to provide the gas with a steady moisture content of 2.5 v%.

All parts of the reactor downstream of the reaction zone were kept at a temperature above the condensation point of the Na, K, Cl, and S species of interest, making it impossible for these species to condense in this region. The temperature profile of the reactor is provided in Figure 10.

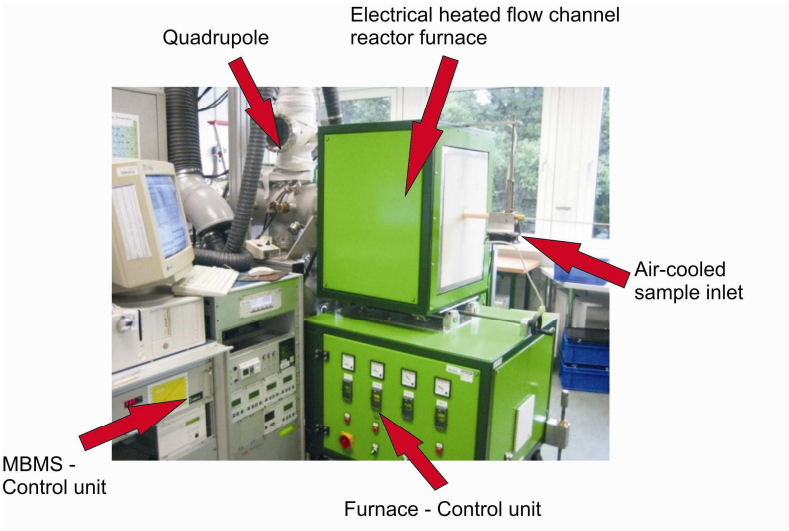

Figure 9. Flow channel reactor: experimental setup.

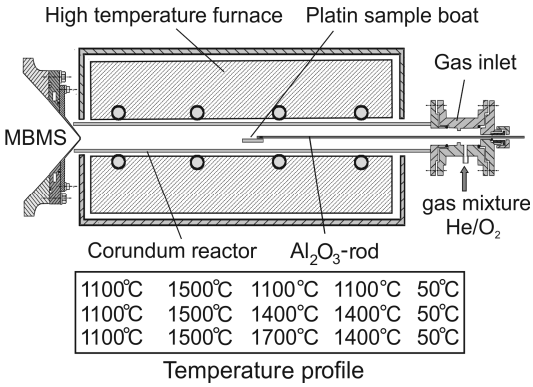

Figure 10. Flow channel reactor: schematic of the experimental setup.

A typical experimental run consisted of the following steps: At the start of the experiment, a platinum sample boat loaded with 50 mg of coal was inserted into the air-cooled end of the heated flow channel. The gas flow was switched on, and a back-

ground spectrum was recorded for 20 s. The end of the alumina reactor was coupled to the sampling orifice of the MBMS device to sample the high-temperature conversion products. The orifice extended into the furnace to maintain an elevated temperature and thus prevent condensation of gas-phase species on the tip of the orifice (Figure 11). Then, using a horizontally displaceable corundum rod, the sample boat was inserted into the reaction zone of the furnace, where the coal sample was gasified (Figure 12). The gaseous reaction products flowed to the end of the reactor. All parts downstream of the reaction zone were maintained over the condensation point of the Na, K, S, and Cl species of interest. The reaction products entered the MBMS through a nozzle with a diameter of 0.3 mm.

Figure 11. Flow channel furnace coupled with the MBMS.

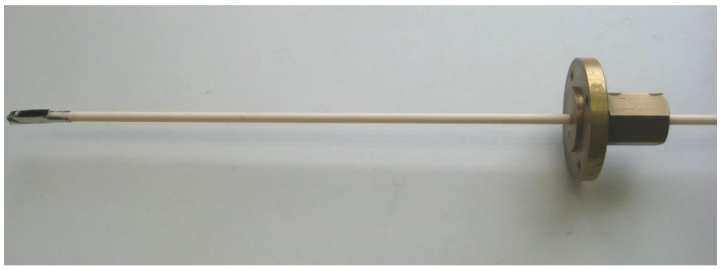

Figure 12. Sample inlet with moveable corundum rod.

A type S thermocouple was used to determine the heat-up rate of the coal samples. The sample boat was fixed at the tip of a corundum rod, and the tip of the thermocouple was in contact with the coal sample. A representative heat-up profile is shown in Figure 13. In general, the coal samples were heated up at about 350 °C/s. The coal samples reached devolatilisation temperature in about 1 s.

The heat-up rate is lower than that reported in the literature, as mentioned in Section 2.2.2. However, the rates are not directly comparable as a result of the different methods used to determine the temperature.

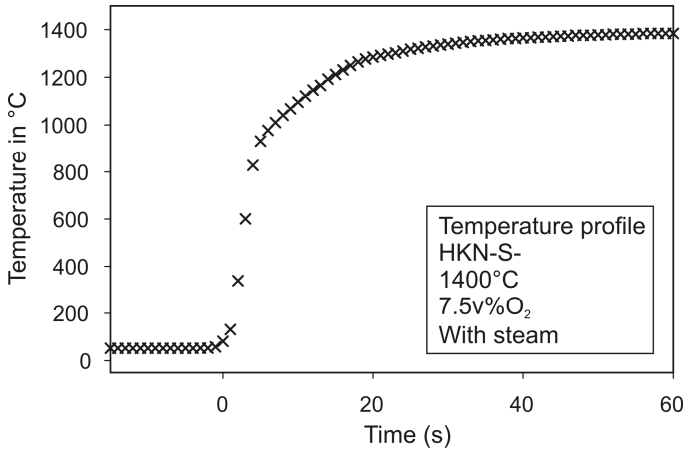

Figure 13. Heat-up profile of an experimental run with HKN-S- at 1400 °C and 7.5 v% O_2.

In preliminary measurements, mass spectra from 10 to 150 amu were scanned. In order to enable monitoring of the gasification process with sufficient temporal resolution, 10 scans per second were acquired. Comparison of the spectra produced no sign of the appearance of organic species, as reported by Dayton et al. [1995]. Due to the high temperature (1400 °C), most of the volatile organic matter was effectively cracked or reacted, despite the short residence time of 0.1–0.2 s. There was even no characteristic mass peak at m/z = 78 $(C_6H_6)^+$, indicating a very stable aromatic hydrocarbon. During the measurements, $^{58}NaCl^+$, but no $^{142}Na_2SO_4{}^+$ and no $^{40}NaOH^+$, could be observed in the gas phase as Na-containing species. $^{40}NaOH^+$ is not easily detectable because it has the same mass-to-charge ratio as $^{40}Ar^+$, which causes the two peaks to overlap. Ar is always present in the gas phase to a small extent because the oxygen that is used for

the experiments is slightly contaminated with Ar resulting from the production process. However, NaCl and NaOH are the most dominant gas-phase alkali metal species for temperatures up to 1400 °C [Oleschko, 2007]; NaOH exceeds NaCl only above this temperature. Therefore, the monitored species were $^{23}Na^+$, $^{34}H_2S^+$, $^{36}HCl^+$, $^{39}K^+/^{39}NaO^+$, $^{58}NaCl^+$, $^{60}COS^+/^{60}NaCl^+$, $^{64}SO_2{}^+$, and $^{74}KCl^+$. The isotope ratio of the species $^{36}HCl^+$ and $^{38}HCl^+$ was in good agreement with the data in the literature [Burdo and Morrison]. The isotope ratio of the species H_2S, K^+/NaO^+, KOH, NaCl, COS, and SO_2 was not checked because only a limited number of different species can be detected simultaneously.

The qualitative information of the spectra was transformed into semi-quantitative data by normalising the intensity of the $^{34}O_2{}^+$ signal. Thus, the peak areas were calculated and divided by the peak area of the first 20 s of the $^{34}O_2{}^+$ signal. The result is a normalised peak area, which allows for further interpretation of the data by comparison of the different coals and for mathematical analysis using correlation analysis. The averaged, normalised peak areas are based on six to ten experimental runs for each coal. The peak areas were calculated for the devolatilisation phase only because most of the species under investigation have a low signal-to-noise ratio during the char reactions phase.

The mass spectrometer shows linear behaviour for the $^{34}O_2{}^+$ signal intensity and the oxygen concentration. For other species, the situation is more complex and linearity cannot be assumed [Wolf, 2003]. In conclusion, the signal intensity for Na, K, S, and Cl species could not be directly compared for gasification and combustion experiments, but it is still possible to make conclusions regarding trends. In addition to the experimental results, the results of the thermochemical modelling will be presented.

3.4.2 Pressurised flow channel furnace

The experimental setup is shown in Figures 14 and 15. The gasification reactor mainly consisted of a heated flow channel housed in a pressurised vessel. The inner diameter of the alumina flow channel was 25 mm, and the total length of the tube was 350 mm. The sample boat was carried in the cold part of the pressure furnace by a horizontally displaceable corundum rod coupled to a stainless steel rod. The gas flow was controlled by BROOKS gas flow controllers, and the pressure was controlled by a BROOKS pressure controller. The reaction zone is heated by an SiC heating element. The highest reachable temperature in this zone is 1325 °C at an absolute pressure of 6 bar. An additional heating element kept the connection between the pressure furnace and the MBMS at temperatures above 825 °C, which inhibits condensation, as mentioned above. In general, the experimental run was similar to the atmospheric experiments. A platinum sample boat loaded with 50 mg of coal was inserted into the cold end of the heated flow channel (about 70 °C). A gas flow of 4 l/min He and 0.324 l/min O_2—corresponding to 92.5% He and 7.5% O_2—was fed into the reactor to simulate a gasification environment. When the absolute pressure reached the desired value of 2, 4, or 6 bar, the background signal was recorded, then the sample boat was placed in the hot reaction zone. The hot reaction products flowed to the end of the reactor where they entered the MBMS through a reinforced nozzle with a diameter of 0.1 mm.

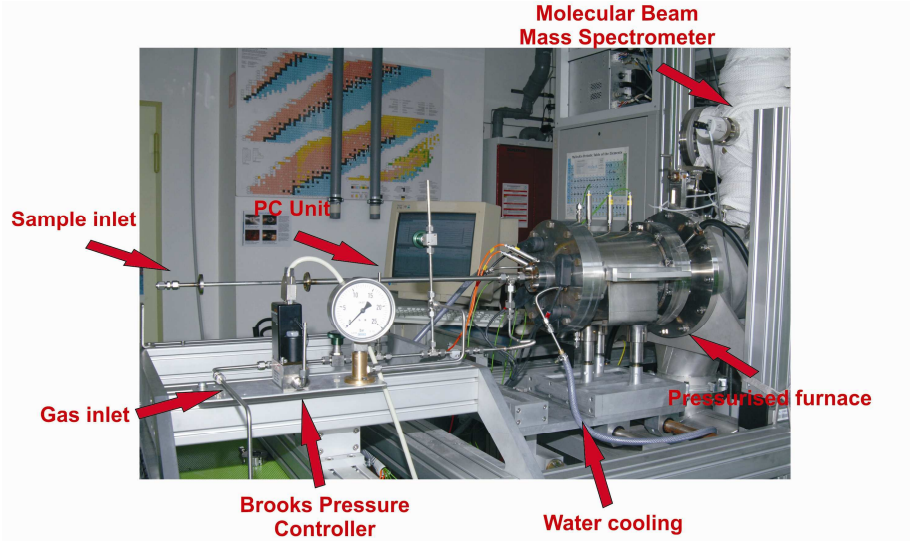

Figure 14. Experimental setup for measurements under elevated pressure.

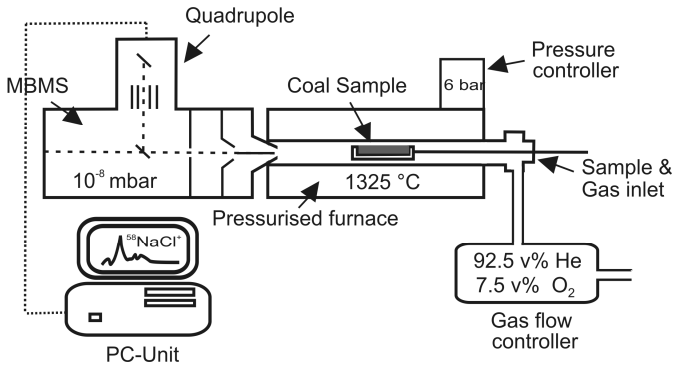

Figure 15. Schematic of the experimental setup for measurements under elevated pressure.

4 Results

4.1 Influence of gasification and combustion like conditions

Qualitative: The experiments simulate the thermal conversion of coal under gasification- and combustion-like conditions. Primarily fast gas–solid reactions and reactions occurring during char gasification are relevant to the obtained results because the gas–solid interaction times for the released species and the remaining non-volatile coal matter are very short (0.1–0.2 s); these times are basically set by the batch nature of the experimental run. Therefore, the results represent conditions in a pulverised coal combustor [Müller, 2006] or an entrained-flow gasifier. The main species detected during gasification and combustion experiments were $^{34}H_2S^+$ (m/z = 34), $^{36}HCl^+$ (m/z = 36), $^{58}NaCl^+$ (m/z = 58), $^{64}SO_2^+$ (m/z = 64), $^{74}KCl^+$ (m/z = 74), $^{142}Na_2SO_4^+$ (m/z = 142), which were qualitatively investigated for both lignites and hard coals. Sample results of the measurements from the MBMS are provided in Figures 16 to 25. In addition, two phases of thermal conversion—devolatilisation and char reactions—could be observed for the lignites and hard coals.

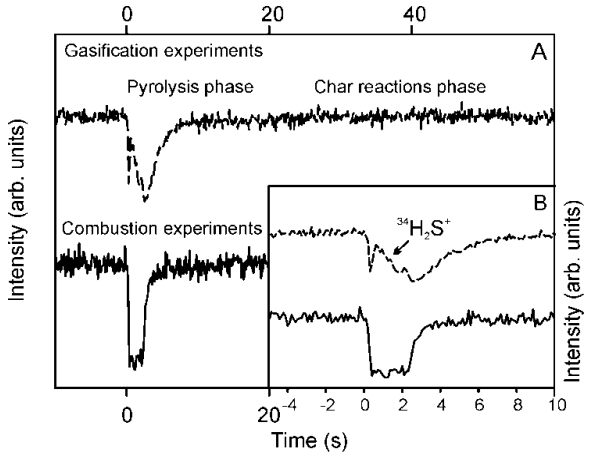

Figure 16. Intensity–time profile of $^{34}O_2^+/^{34}H_2S^+$ for the lignite HKN-S+ and a magnification of the intensity–time profile at 1400 °C in He/20% O_2 and He/7.5% O_2.

Shortly after sample insertion, the sample reached the temperature necessary for devolatilisation. The released volatile organic and inorganic matter immediately reacted with oxygen. This caused a lack of oxygen, as shown by the sharp drop-off of the $^{34}O_2^+$ signal intensity in Figures 16 and 17. After devolatilisation, the remaining non-volatile coal matter reacted with oxygen, as can be seen in the $^{34}O_2^+$ signal that is lower than the base level.

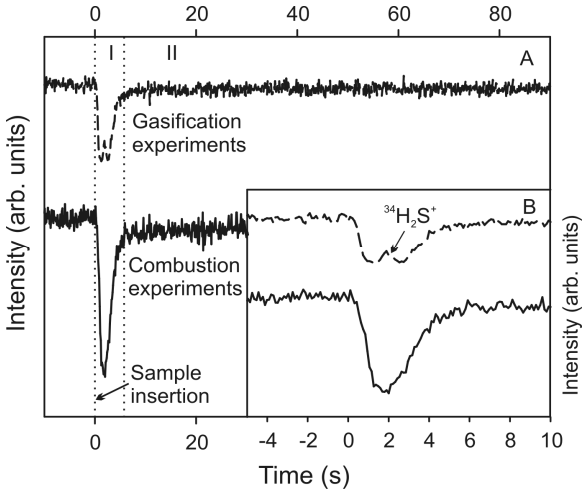

Figure 17. Intensity–time profile of $^{34}O_2^+/^{34}H_2S^+$ during thermal conversion of STD-5 and a magnification of the intensity–time profile at 1400 °C in He/20% O_2 and He/7.5% O_2.

Under the reduced oxygen partial pressure during the gasification experiments, the signal intensity of the specie with m/z = 34 exhibited a sharp increase during the devolatilisation phase, as depicted in Figures 16 and 17. This increase in signal intensity was considered to be caused by the formation of the S species H_2S instead of SO_2. The occurrence of H_2S leads to an overlapped spectra as a consequence of the overlapping mass-to-charge ratio of $^{34}H_2S^+$ (m/z = 34) and $^{34}O_2^+$ (m/z = 34). In contrast to that observation, the $^{34}O_2^+$ signal was relatively stable after the sharp drop-off that occurred when the sample was inserted during the combustion experiments. Because of its low resolution, the quadrupole system used is not able to distinguish between $^{34}H_2S^+$ and $^{34}O_2^+$. For higher resolution and determination of $^{34}H_2S^+$ and $^{34}O_2^+$, a sector field mass spectrometer is needed.

Another detected S species was $^{64}SO_2^+$. Typical release profiles are shown in Figures 18 and 19. $^{64}SO_2^+$ was released in two notable steps during the devolatilisation phase,

with very high intensity over a short time period, and during the char reactions phase, with low intensity over a long time period.

In comparison with the hard coals the lignites showed a more complex release behaviour, especially during devolatilisation phase. For the hard coals the signal intensity of $^{64}SO_2^+$ increased after sample insertion, reached a maximum and decreased again. The signal of the lignites showed two maximums and a minimum shortly after sample insertion. Of special interest is the overlapping of the maximum of the release of $^{34}H_2S^+$ during gasification of the lignites with the minimum of the release of $^{64}SO_2^+$ during gasification experiments as can be seen by comparison of Figs. 16 and 18.

The second release step during char reactions phase lasted longer, during gasification experiments for the lignites and hard coals. Even though the MBMS detected a significant amount of $^{64}SO_2^+$, which should enhance the formation of Na_2SO_4, there was no evidence for the release of $^{142}Na_2SO_4^+$.

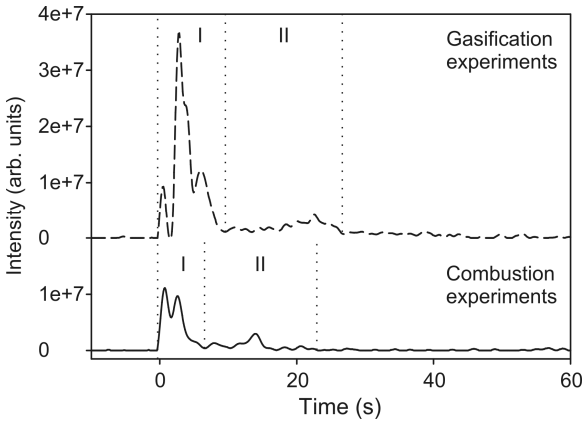

Figure 18. Intensity–time profile of $^{64}SO_2^+$ during thermal conversion of HKN-S+ at 1400 °C in He/20% O_2 and He/7.5% O_2. I—Devolatilisation phase; II—Char reactions phase.

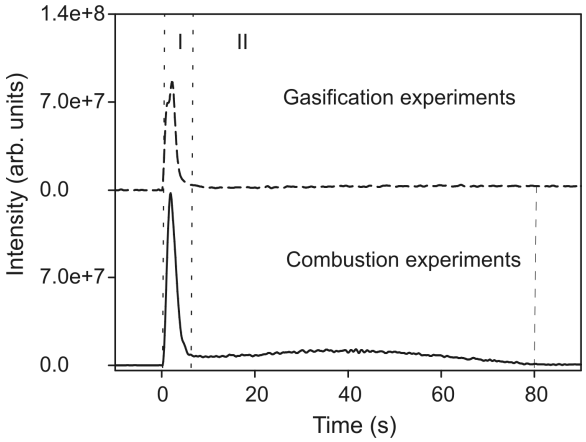

Figure 19. Intensity–time profile of $^{64}SO_2^+$ during thermal conversion of STD-5 at 1400 °C in He/20% O_2 and He/7.5% O_2. I—Devolatilisation phase; II—Char reactions phase.

The release of $^{36}HCl^+$ is shown in Figures 20 and 21. $^{36}HCl^+$ was released with high signal intensity during devolatilisation for both gasification and combustion experiments. The signal intensity was higher during gasification experiments for the lignites and was steady for the hard coals. Additionally, a low-intensity release of $^{36}HCl^+$ was observed during the char reactions phase. However, the signal-to-noise ratio was too low for further interpretation.

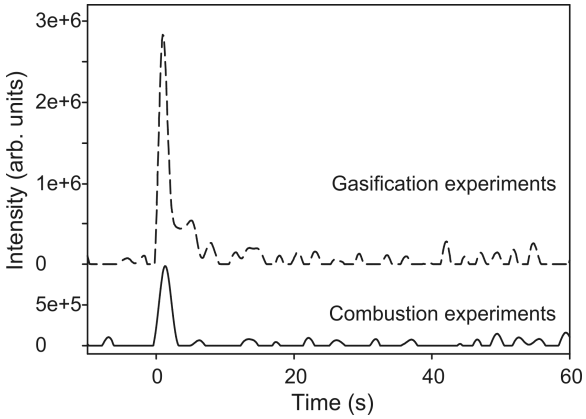

Figure 20. Intensity–time profile of $^{36}HCl^+$ during thermal conversion of HKN-S+ at 1400 °C in He/20% O_2 and He/7.5% O_2.

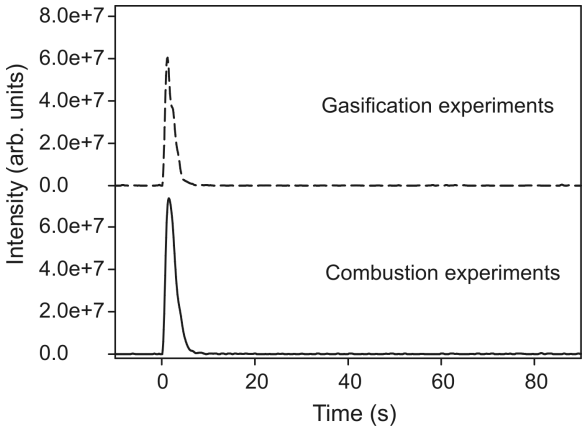

Figure 21. Intensity–time profile of $^{36}HCl^{+}$ during thermal conversion of STD-5 at 1400 °C in He/20% O_2 and He/7.5% O_2.

Intensity–time profiles for the release of $^{58}NaCl^{+}$ are shown in Figures 22 and 23. $^{58}NaCl^{+}$ was released with high intensity during the devolatilisation phase. Also, low-intensity signals of $^{58}NaCl^{+}$ were observed during char reactions. The signal intensity was slightly higher than the background noise. During the gasification experiments, the signal intensity of $^{58}NaCl^{+}$ was higher than that from the combustion experiments for the lignites and slightly higher than that from the combustion experiments for the hard coals.

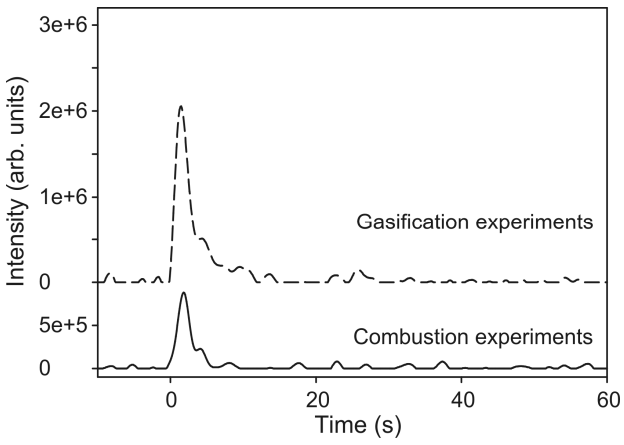

Figure 22. Intensity–time profile of $^{58}NaCl^{+}$ during thermal conversion of HKN-S+ at 1400 °C in He/20% O_2 and He/7.5% O_2.

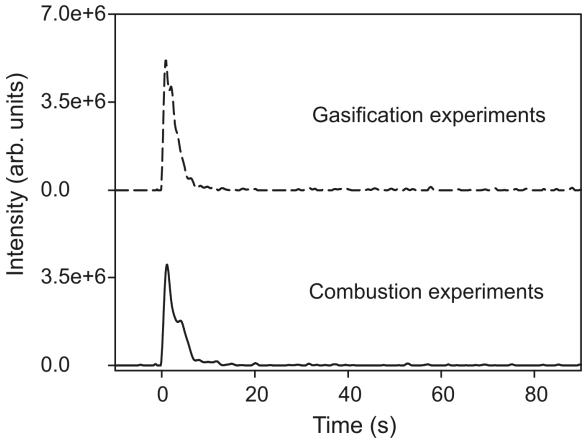

Figure 23. Intensity–time profile of $^{58}NaCl^{+}$ during thermal conversion of STD-5 at 1400 °C in He/20% O_2 and He/7.5% O_2.

$^{74}KCl^{+}$ was detected with a reliable signal-to-noise ratio only for the hard coals (Figure 24). The signal for the lignites was not determinable. The signal-to-noise ratio was very low as shown in Figure 25. Therefore, only the release of the hard coals is considered in the following. The release occurred in two steps, as shown in Figure 24. The first release step occurred during devolatilisation with high intensity in only about 5 s for STD-5. The second release step occurred with very low intensity over a long time period during the char reactions phase. However, on account of the low signal-to-noise ratio, further interpretation must be undertaken with care.

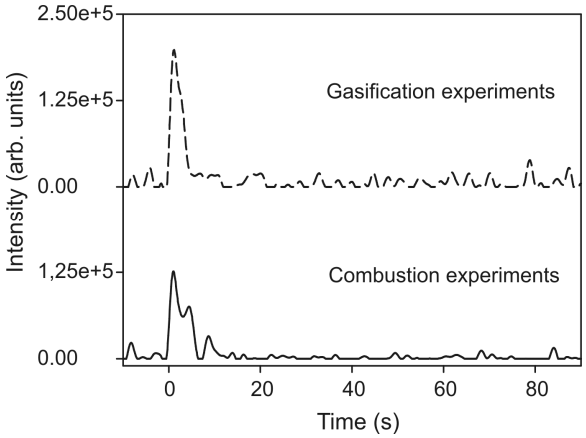

Figure 24. Intensity–time profile of $^{74}KCl^{+}$ during thermal conversion of STD-5 at 1400 °C in He/20% O_2 and He/7.5% O_2.

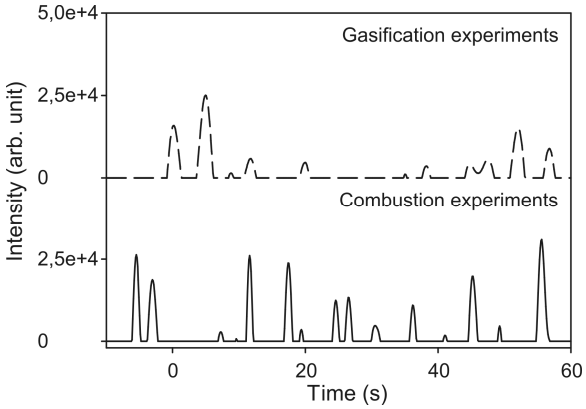

Figure 25. Intensity–time profile of $^{74}KCl^{+}$ during thermal conversion of HKN-S+ at 1400 °C in He/20% O_2 and He/7.5% O_2.

Quantitative results for the German hard coals: The averaged, normalised peak areas of $^{34}H_2S^+$, $^{36}HCl^+$, $^{58}NaCl^+$, $^{64}SO_2^+$, and $^{74}KCl^+$ are depicted in Figure 26. The release of $^{34}H_2S^+$ was only observed during the gasification experiments. The release of $^{34}H_2S^+$ was highest for STD-3 (peak area of about 0.055) and lowest for STD-4, with a release that was lower by an order of magnitude. In contrast, the order of the released amount of $^{64}SO_2^+$ was STD-5 > STD-3 > STD-4 > STD-1 > STD-2. In general, the peak areas of $^{64}SO_2^+$ were found to be smaller for the gasification experiments. The release of $^{36}HCl^+$ was higher during the combustion experiments by an average factor of 1.5. The order of the released amount of $^{36}HCl^+$ was similar for both conditions. The release of $^{58}NaCl^+$ was considerably higher for STD-1, STD-2, and STD-3 during gasification than it was during the combustion experiments, and the release during gasification and during combustion were similar for STD-4 and STD-5. The release of $^{74}KCl^+$ during gasification experiments was slightly higher than during combustion experiments for the hard coals STD-1, STD-2, and STD-3. The value of STD-5 exhibited no significant difference. The amount of $^{74}KCl^+$ was higher during the combustion experiments. S-containing species were the main gaseous species under combustion and gasification conditions. HCl was the most abundant Cl species under combustion and gasification conditions. The amount of NaCl was about one order of magnitude lower than the amount of S species for both combustion and gasification experiments, and the amount of KCl was two orders of magnitude lower. The order was the same for combustion and gasification experiments.

Quantitative results for the German lignites: The results are depicted in Figure 27. For the combustion experiments, the order of detected species, starting with the species with the highest amount, was $^{64}SO_2^+$ > $^{58}NaCl^+$, $^{36}HCl^+$. For the gasification experiments, the order was $^{34}H_2S^+$ > $^{58}NaCl^+$, $^{36}HCl^+$. As mentioned above, the release of $^{34}H_2S^+$ was only observed during gasification experiments. HKN-S+ showed the highest amount of $^{34}H_2S^+$, with an averaged, normalised peak area of about 0.43, and HKS showed the lowest amount, with a peak area of about 0.24. $^{64}SO_2^+$ was the main S species during combustion experiments. HKN-S+ showed the highest release, with a peak area of about 0.34, and HKN-S- showed the lowest release, with a peak area of about 0.1. The released amount of $^{36}HCl^+$ during gasification experiments was about two times higher than that during combustion experiments. The released amount of $^{58}NaCl^+$ during gasification experiments was a factor of about two to three higher than that during combustion experiments. The order of the released amount, expressed by the peak areas of $^{36}HCl^+$ and $^{58}NaCl^+$, was similar for both conditions.

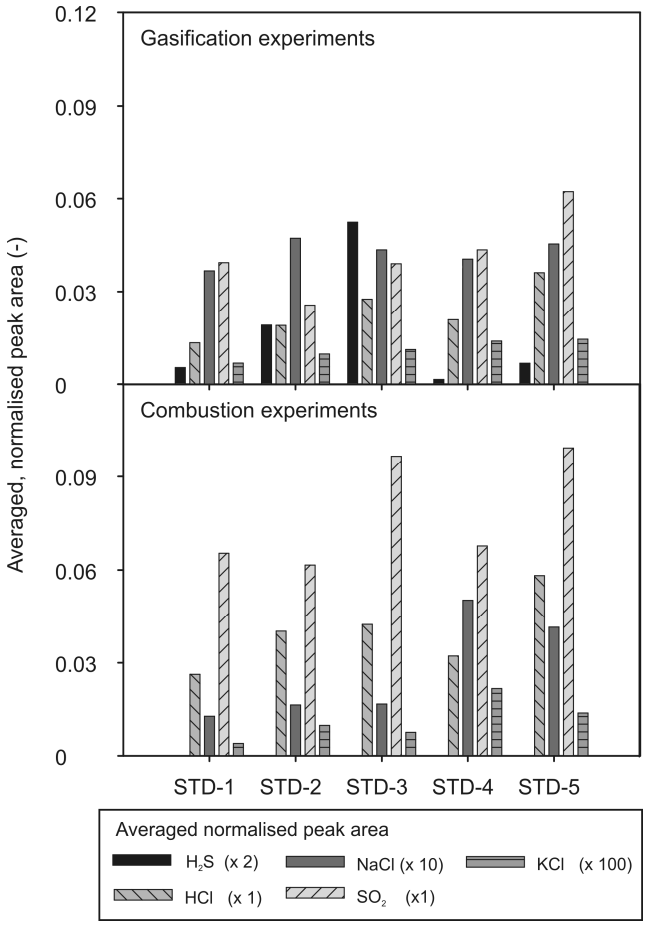

Figure 26. Averaged, normalised peak area of the hard coals for the gasification and combustion experiments at 1400 °C.

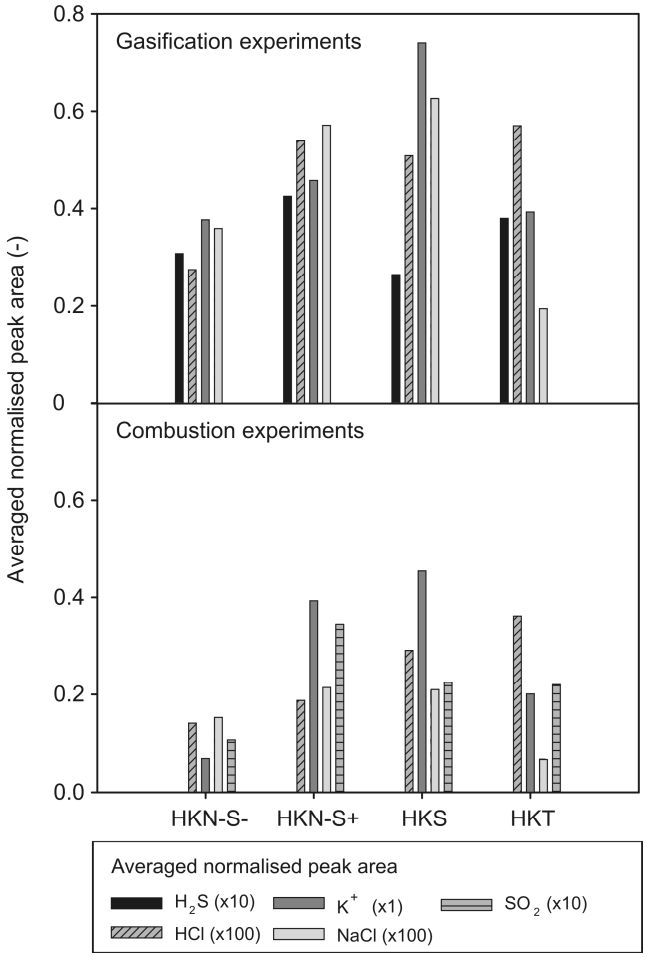

Figure 27. Averaged, normalised peak area of the lignites for the gasification and combustion experiments at 1400 °C.

4.2 Influence of the temperature

The species $^{34}H_2S^+$, $^{36}HCl^+$, $^{39}K^+/^{39}NaO^+$, $^{56}KOH^+$, $^{58}NaCl^+$, $^{60}COS^+/^{60}NaCl^+$, $^{64}SO_2^+$, and $^{74}KCl^+$ were detected and qualitatively/semi-quantitatively investigated.

Representative results of the MBMS measurements are provided in Figures 28 and 29. The depicted graphs show the intensity–time profiles of the species under investigation during gasification experiments with the hard coal STD-5 and the lignite HKT. Two phases of gasification can be observed in the spectra of $^{34}O_2^+$: devolatilisation (phase I) and char reactions (phase II), as mentioned in Section 4.1.

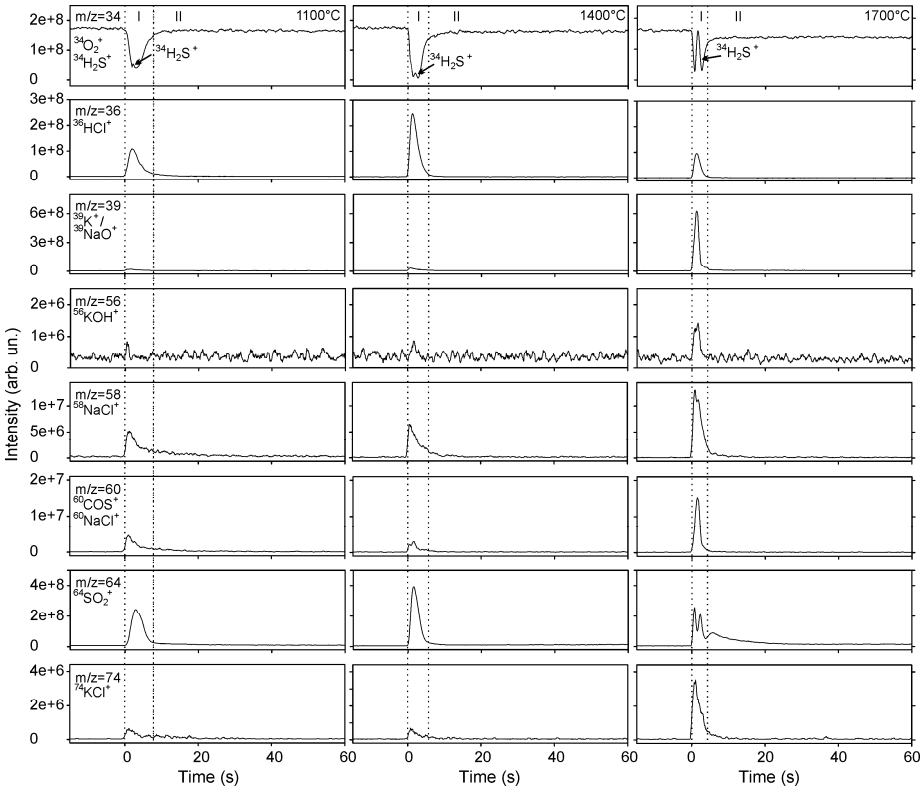

Figure 28. Intensity–time profiles obtained during gasification experiments with STD-5 at 1100–1700 °C in He/7.5% O_2.

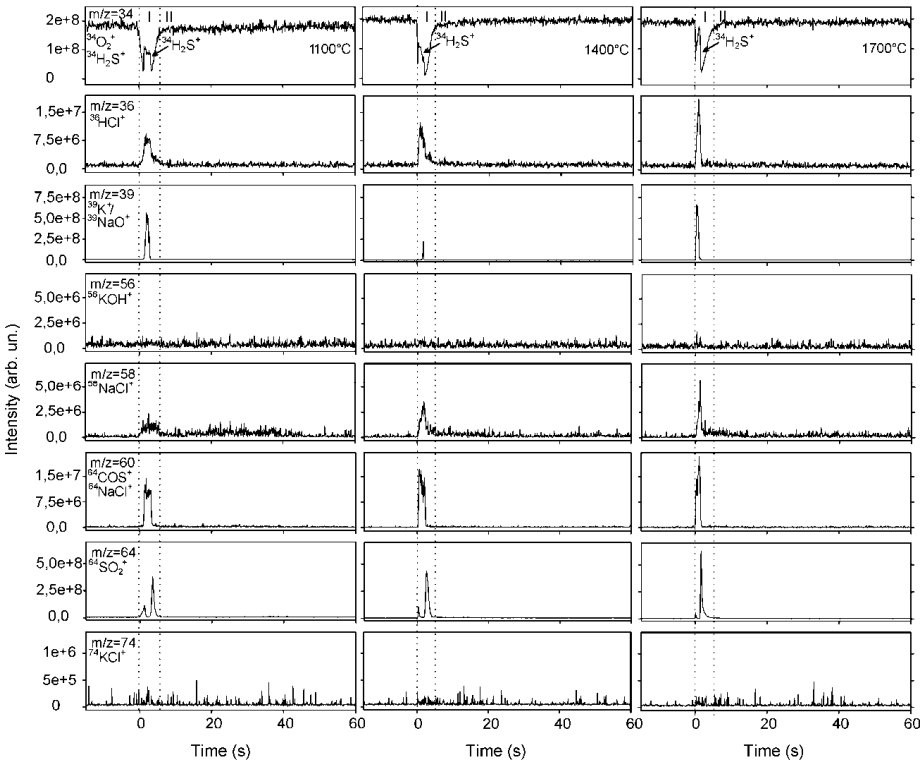

Figure 29. Intensity–time profiles obtained during gasification experiments with HKT at 1100–1700 °C in He/7.5 % O_2.

In recent publications, m/z = 39 was related to $^{39}K^+$ [Bläsing and Müller, 2010a,b]. However, the authors are sceptical about this exclusive relation because there has been evidence that m/z = 39 is also occupied by other species. The release of the species with m/z = 39 was detected with high intensity, occurring mainly during devolatilisation and therefore at moderately high temperatures (Figure 30). Based on the results of previous release experiments under combustion conditions at 800 °C and 1200 °C [Oleschko and Müller, 2007a,b], $^{39}K^+$ originates primarily from the fragmentation of released KCl. Additionally, the fragmentation of KOH can lead to $^{39}K^+$. Experiments with leached hard coals showed that K is mainly fixed in silicates [Oleschko, 2007] and, therefore, can be released in significant amounts only during secondary reactions that occur at temperatures above the devolatilisation temperature, e.g. ion exchange, as mentioned above. In conclusion, the high-intensity release of the species with m/z = 39 at moderate devolatilisation temperatures cannot be related exclusively

to K species. Therefore, the assumption was made that $^{39}NaO^+$ (a fragment of released NaOH), organic species like $^{39}C_3H_3^+$, or even un-cracked or unreacted double-ionised benzol ($^{78}C_6H_6^{2+}$) were formed. As a consequence of this assumption and in order to obtain more information, further experiments with model substances in place of coal were performed. The experimental conditions were the same as those for the experiments with the hard coals. The model substances were sodium salicylate, which has a coal-like structure despite the fact that it is not a macromolecule, and trisodium citrate, which contains three carboxylic-bonded Na ions. Sodium salicylate is similar to the hydroxyl acid sodium salts found in coal. Similarly, Strohbeen [1981] used sodium gluconate and vanillic acid during model experiments on the release of alkali metals. The results of the model experiments with sodium salicylate and trisodium citrate are provided in Figure 30. The lack of oxygen is an indicator of reducing conditions during the experiments. The release of $^{23}Na^+$ during decomposition was observed for the experiments with both sodium salicylate and trisodium citrate. The signal intensity of the species with m/z = 39 and m/z = 41 increased during the experiments. However, there was no signal for m/z = 78. Therefore, the occurrence of double-ionised benzol ($^{78}C_6H_6^{2+}$), which would lead to a signal at m/z = 39, is rather unlikely. It is concluded that $^{39}NaO^+$ and $^{41}NaO^+$ as fragments of formed NaOH were detected by the MBMS. Transferring the results of the model experiments to the experiments with coal, it is concluded that the signal of m/z = 39 is not exclusively related to $^{39}K^+$. In addition to $^{39}K^+$, $^{39}NaO^+$ is part of the signal of m/z = 39.

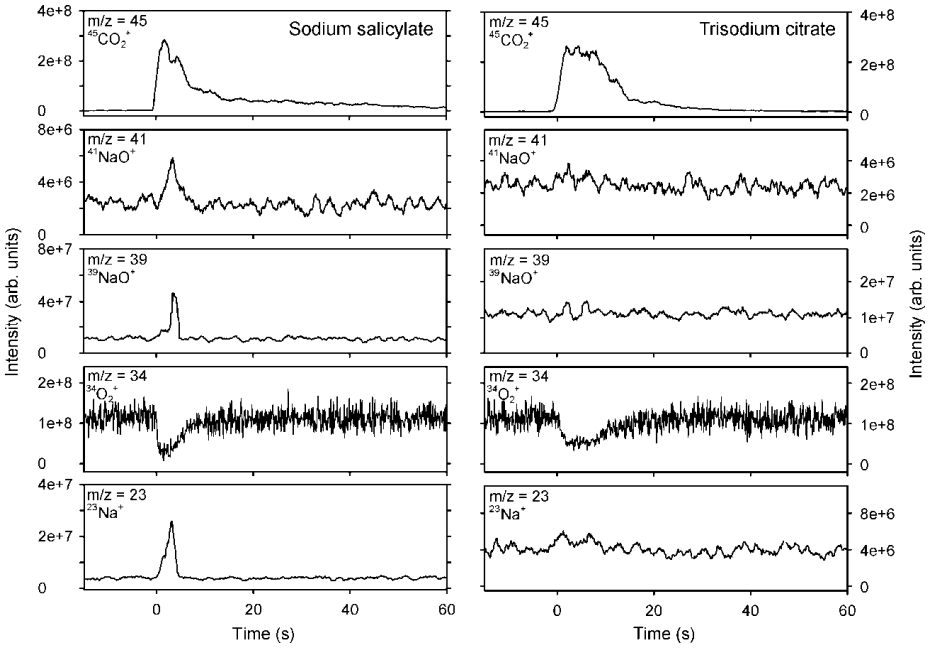

Figure 30. Intensity–time profiles obtained during gasification experiments with sodium salicylate and trisodium citrate at 1100 °C in He/7.5% O_2.

The averaged, normalised peak areas of $^{34}H_2S^+$, $^{36}HCl^+$, $^{58}NaCl^+$, and $^{64}SO_2^+$ at 1100–1700 °C are shown in Figures 31 to 39. The release of $^{56}KOH^+$ and $^{74}KCl^+$ is not discussed from a quantitative point of view on account of the low signal-to-noise ratio. Also, the release of $^{60}COS^+/^{60}NaCl^+$ was not quantified because of its overlapping spectra, as mentioned above.

Lignites: The averaged, normalised peak areas of $^{34}H_2S^+$ are depicted in Figure 31. With regard to the release trend, the four lignites can be divided into two groups. The released amount increased slightly from 1100 to 1400 °C and strongly decreased from 1400 to 1700 °C for HKN-S- and HKN-S+. The released amount strongly decreased for HKS (decrease of 26% from 1100 to 1400 °C and 77% from 1100 to 1700 °C) and slightly decreased for HKT.

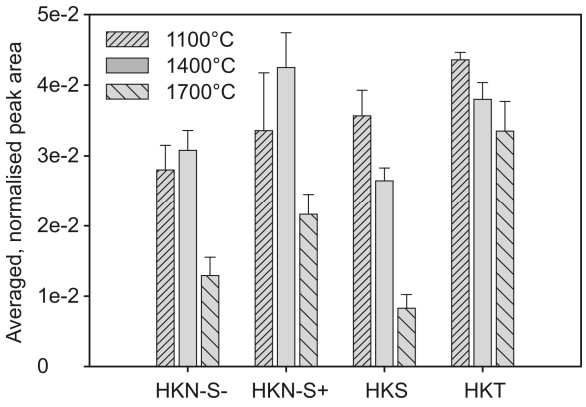

Figure 31. Averaged, normalised peak area of $^{34}H_2S^+$ at 1100–1700 °C in He/7.5% O_2.

The averaged, normalised peak areas of $^{64}SO_2^+$ are depicted in Figure 34. The release trend is the same for HKN-S- and HKN-S+. The amount decreased from 1100 to 1400 °C and increased from 1400 to 1700 °C. Within the variance of the measurements, the released amount of HKS increases and the amount of HKT slightly decreases.

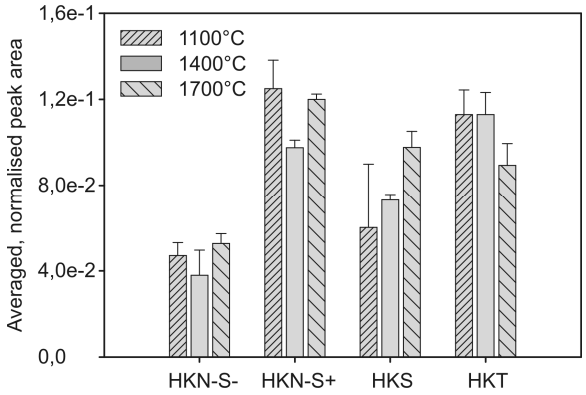

Figure 32. Averaged, normalised peak area of $^{64}SO_2^+$ at 1100–1700 °C in He/7.5% O_2.

The averaged, normalised peak areas of $^{36}HCl^+$ are depicted in Figure 33. The release trend is negative for the entire temperature range within the variance of the measurements, e.g. HKS showed a 20% decrease from 1100 to 1400 °C and a 60% decrease from 1100 to 1700 °C. The averaged, normalised peak areas of $^{58}NaCl^+$ are depicted in Figure 34. The release of $^{58}NaCl^+$ increases within the temperature range of 1100–1700 °C for HKN-S- (slightly positive), HKN-S+ (strongly positive), and HKS (strongly positive). The data for HKT are nearly constant.

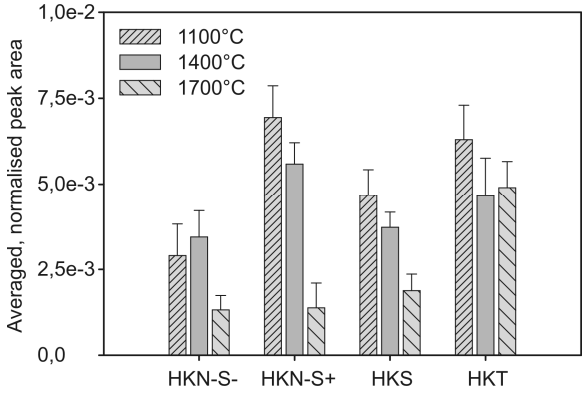

Figure 33. Averaged, normalised peak area of $^{36}HCl^+$ at 1100–1700 °C in He/7.5% O_2.

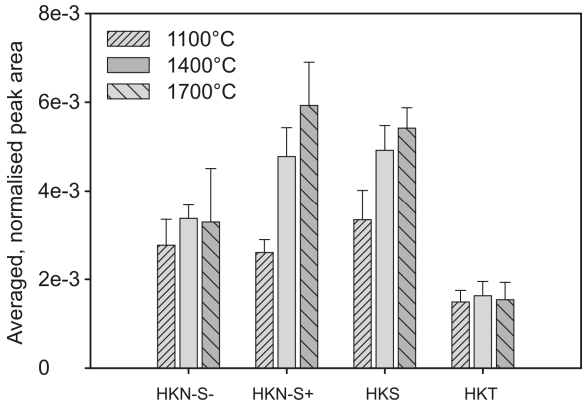

Figure 34. Averaged, normalised peak area of $^{58}NaCl^{+}$ at 1100–1700 °C in He/7.5% O_2.

Hard coals: The averaged, normalised peak areas of $^{34}H_2S^{+}$ are depicted in Figure 35. The released amount strongly increased with increasing temperature, e.g. for STD-5, the released amount was 5.1 times higher at 1400 °C than it was at 1100 °C and 58.9 times higher at 1700 °C than it was at 1100 °C.

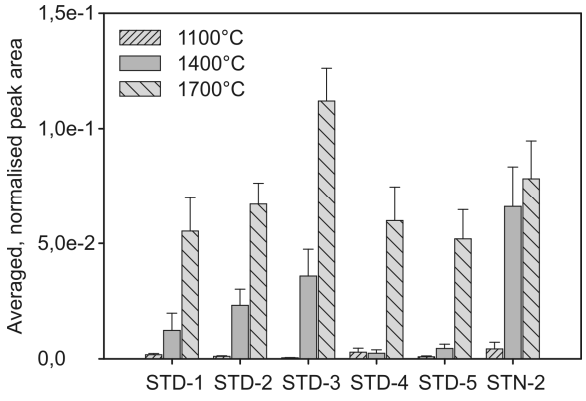

Figure 35. Averaged, normalised peak area of $^{34}H_2S^{+}$ at 1100–1700 °C in He/7.5% O_2.

The averaged, normalised peak areas of $^{64}SO_2^+$ are depicted in Figure 36. In general, the released amount decreased with increasing temperature, e.g. STN-2 showed a decrease of 40% from 1100 to 1400 °C and a decrease of 70% from 1400 to 1700 °C.

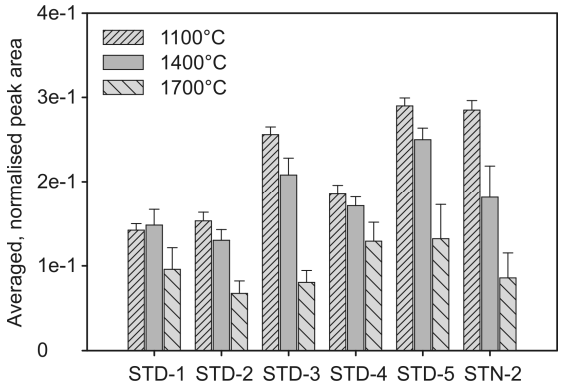

Figure 36. Averaged, normalised peak area of $^{64}SO_2^+$ at 1100–1700 °C in He/7.5% O_2.

The averaged, normalised peak areas of $^{36}HCl^+$ are depicted in Figure 37. The released amount of $^{36}HCl^+$ increases from 1100 to 1400 °C and decreases from 1400 to 1700 °C. However, the differences are moderate in comparison with those of most of the other species under investigation, e.g. STD-3 showed a 10% increase from 1100 to 1400 °C and a 30% decrease from 1400 to 1700 °C.

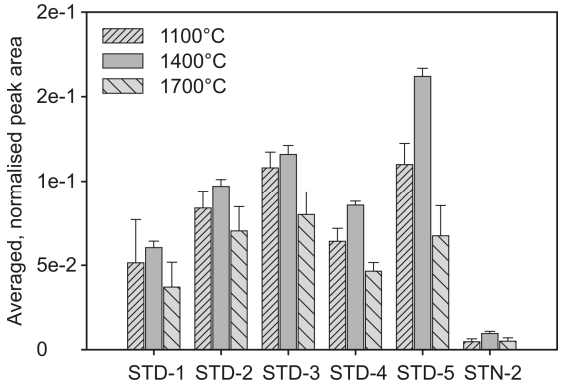

Figure 37. Averaged, normalised peak area of $^{36}HCl^+$ at 1100–1700 °C in He/7.5% O_2.

The averaged, normalised peak area of $^{58}NaCl^{+}$ is depicted in Figure 38. The release of $^{58}NaCl^{+}$ increases within the temperature range of 1100–1700 °C for STD-1, STD-2, STD-3, and STN-2. For STD-4 and STD-5, the release decreases from 1100 to 1400 °C and strongly increases from 1400 to 1700 °C.

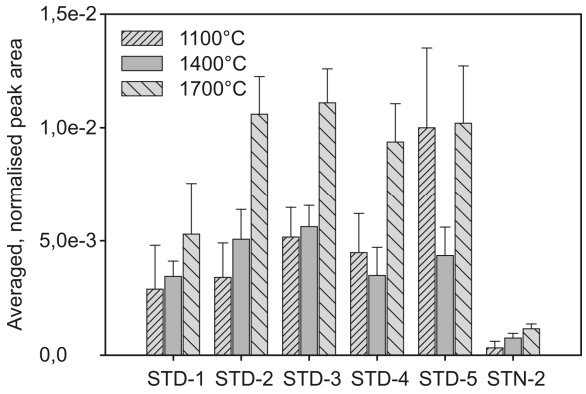

Figure 38. Averaged, normalised peak area of $^{58}NaCl^{+}$ at 1100–1700 °C in He/7.5% O_2.

The averaged, normalised peak areas of $^{74}KCl^{+}$ are depicted in Figure 39. In general, the released amount increased with increasing temperature—e.g. compared to the released amount at 1100 °C, the release was 1.6 times higher at 1400 °C and 21.7 times higher at 1700 °C for STD-5. However, there are exceptions, e.g. STD-2 showed a decrease of about 50% from 1100 to 1400 °C and an increase of about 400% from 1400 to 1700 °C. Compared to the other four hard coals, STD-4 and STD-5 showed a very high increase at 1700 °C.

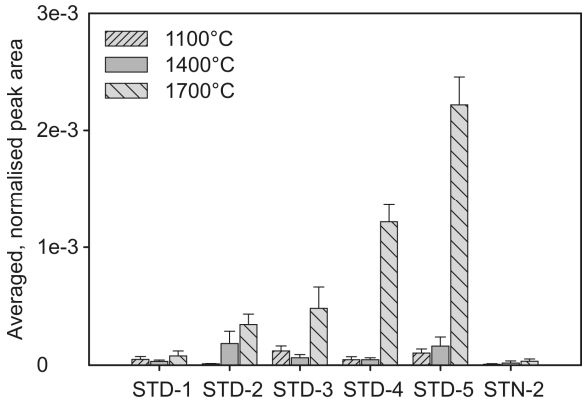

Figure 39. Averaged, normalised peak area of $^{74}KCl^{+}$ at 1100–1700 °C in He/7.5% O_2.

4.3 Influence of the steam content

Results of the MBMS measurements are presented in Figures 40 and 41. The key species detected by the MBMS were $^{23}Na^+$, $^{34}H_2S^+$, $^{36}HCl^+$, $^{39}K^+/^{39}NaO^+$, $^{56}KOH^+$, $^{58}NaCl^+$, $^{64}SO_2{}^+$, and $^{74}KCl^+$. Takuwa and Naruse [2007] reported the release of metallic Na during the combustion of coal. However, $^{23}Na^+$ detected by molecular beam mass spectrometry is most likely a product of the fragmentation of Na species—e.g. NaCl and NaOH—during ionisation.

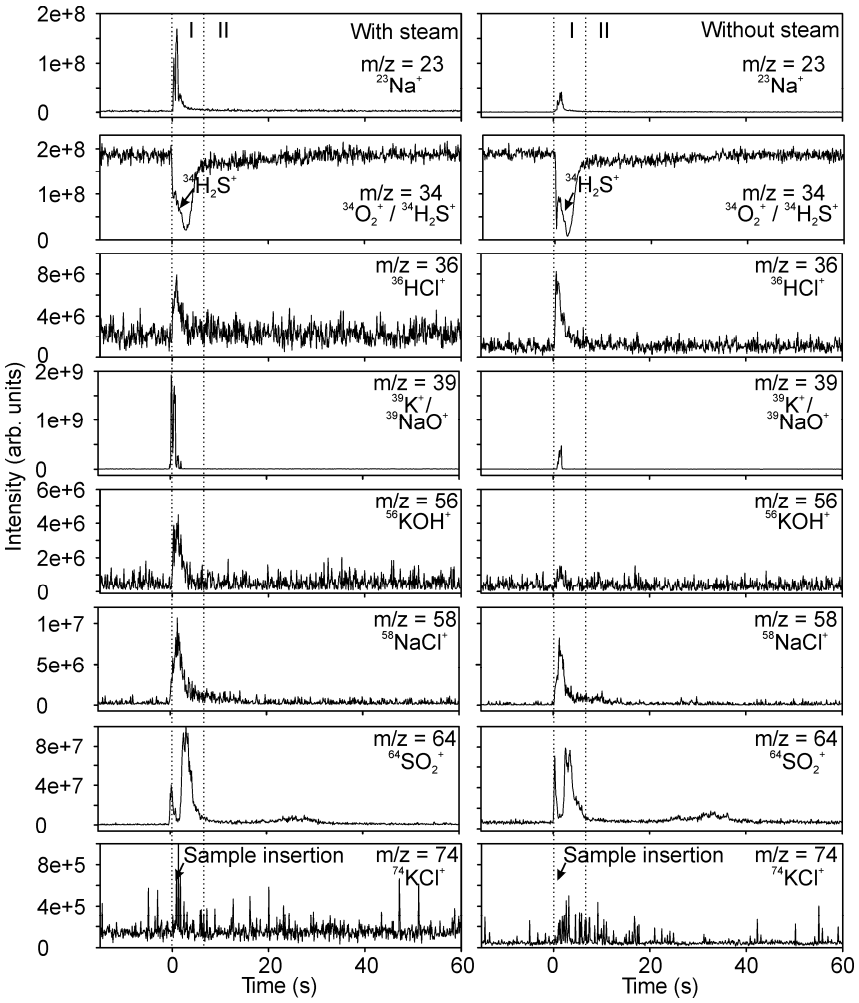

Figure 40. Intensity–time profiles of the lignite HKN-S- at 1400 °C in He/7.5% O_2 with and without water vapour.

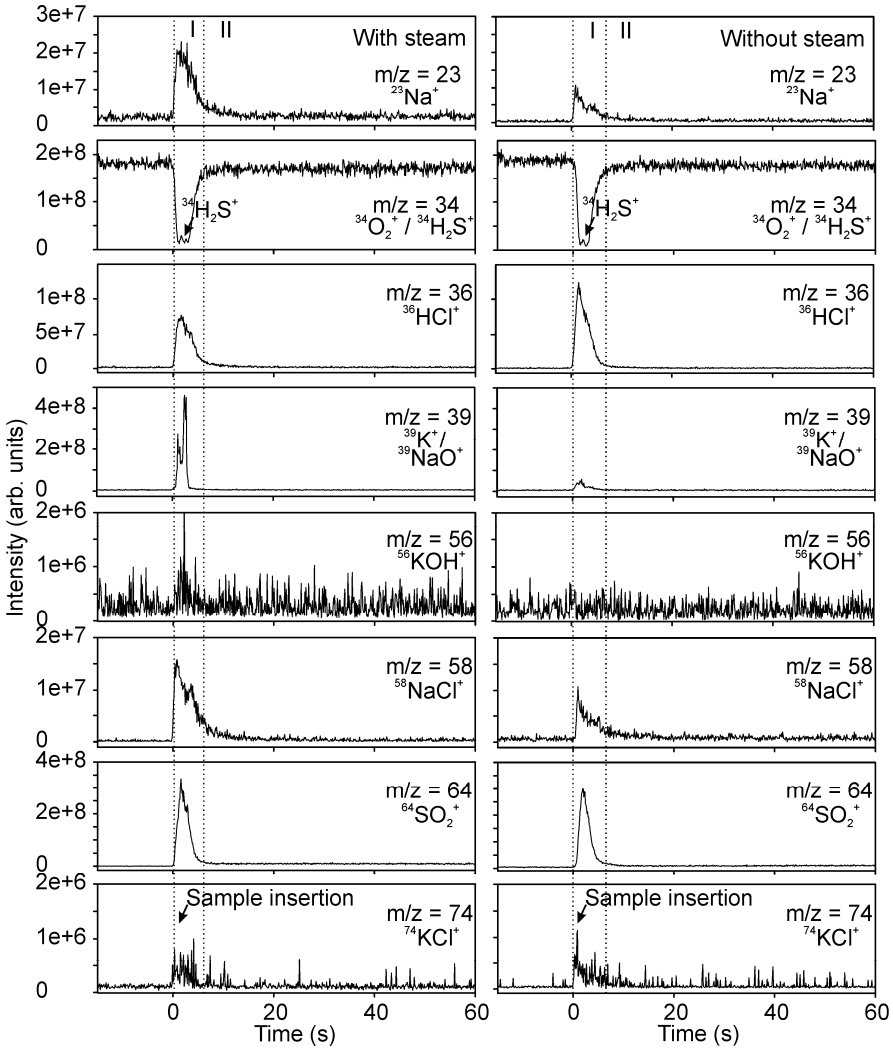

Figure 41. Intensity–time profiles of the hard coal STD-4 at 1400 °C in He/7.5% O_2 with and without water vapour.

The majority of the release occurred during the devolatilisation phase with high intensity. Therefore, quantification of the spectra was performed only for the devolatilisation phase. Quantification was performed through normalisation of the peak area during the devolatilisation phase to the $^{34}O_2^+$ signal of the first 20 s of the experimental run, during which time the steady oxygen concentration led to a steady signal. The averaged, normalised peak areas of the coals under investigation are depicted in Figures 42 and 43.

Recent studies showed that a mass-to-charge ratio of 39 is occupied by $^{39}K^+$, most likely a fragment of KCl and other K species, and by $^{39}NaO^+$, most likely a fragment of NaOH [Bläsing et al., 2010c]. The normalised peak areas of $^{39}K^+/^{39}NaO^+$ strongly increased for all lignites under investigation under the influence of steam. HKN-S- and HKN-S+ increased by a factor of 5.2 to 36.9. HKS and HKT increased by a factor of 46.7 to 68.8. In contrast to the lignites, most of the hard coals increased by a moderate factor of 1.7 to 3.9. However, the hard coal STN-2 increased by a factor of 20.

The amount of $^{58}NaCl^+$ moderately increased during the experiments with steam for all coals under investigation (a factor of 1.1 to 4.1). The amount of $^{23}Na^+$ moderately increased for most of the hard coals and for the lignites HKN-S-, HKN-S+, and HKT (a factor of 1.2 to 3.9). However, STN-2 and HKS showed a very high increase—a factor of 12.9 and 8.2, respectively. $^{56}KOH^+$ was detected in significant quantities only during experiments with steam. In the experiments with steam, the normalised peak areas of $^{56}KOH^+$ increased by a factor of about 1.4 to 4.3 for the lignites and by a factor of about 13.8 to 646.5 for the hard coals. The 646.5 factor (STN-2) is noticeably high. However, the signal-to-noise ratio was very low during the experiments without steam, especially during the experiments with hard coal. Therefore, the results should be handled with some care. Under the influence of steam, the amount of $^{74}KCl^+$ increased by a factor of about 1.05 to 3.6 for the lignites and by a factor of about 1.5 to 7.1 for the hard coals. However, the variance is high as a result of the low signal-to-noise ratio.

All coals under investigation showed a decrease of $^{36}HCl^+$ under the influence of steam. The decrease was slight in most cases, e.g. -16% for HKT and -15% for STD-5, but the value was constant for HKN-S-.

Key sulphur bearing species detected during the experiments with and without steam were $^{34}H_2S^+$ and $^{64}SO_2^+$. The amount of $^{34}H_2S^+$ slightly increased under the influence of steam (by a factor of about 1.2 to 2.2) for the lignites and for the hard coals STD-4 and STD-5. The hard coals STD-1, STD-2, STD-3, and STN-2 showed a moderate decrease, e.g. 22% for STN-2. The amount of $^{64}SO_2^+$ slightly increased in the experiments with steam for all coals under investigation, e.g. by a factor of about 1.5 for the lignite HKS and the Norwegian hard coal STN-2.

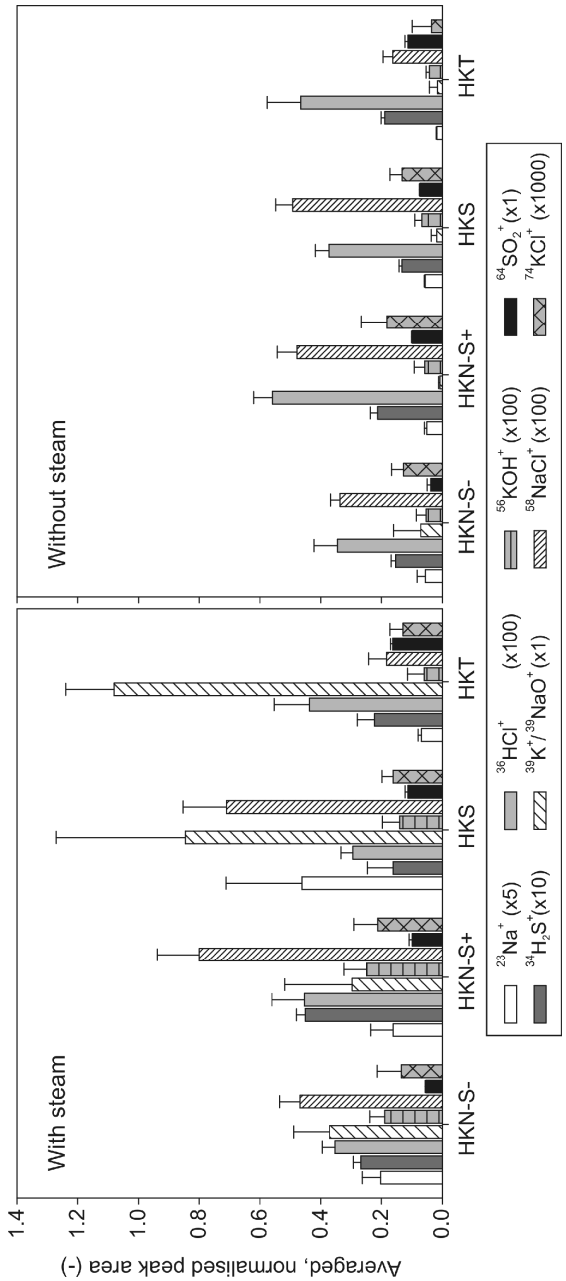

Figure 42. Averaged, normalised peak areas of $^{23}Na^+$, $^{34}H_2S^+$, $^{36}HCl^+$, $^{39}K^+/^{39}NaO^+$, $^{56}KOH^+$, $^{58}NaCl^+$, $^{64}SO_2^+$, and $^{74}KCl^+$ detected during experiments with lignites at 1400 °C with and without water vapour.

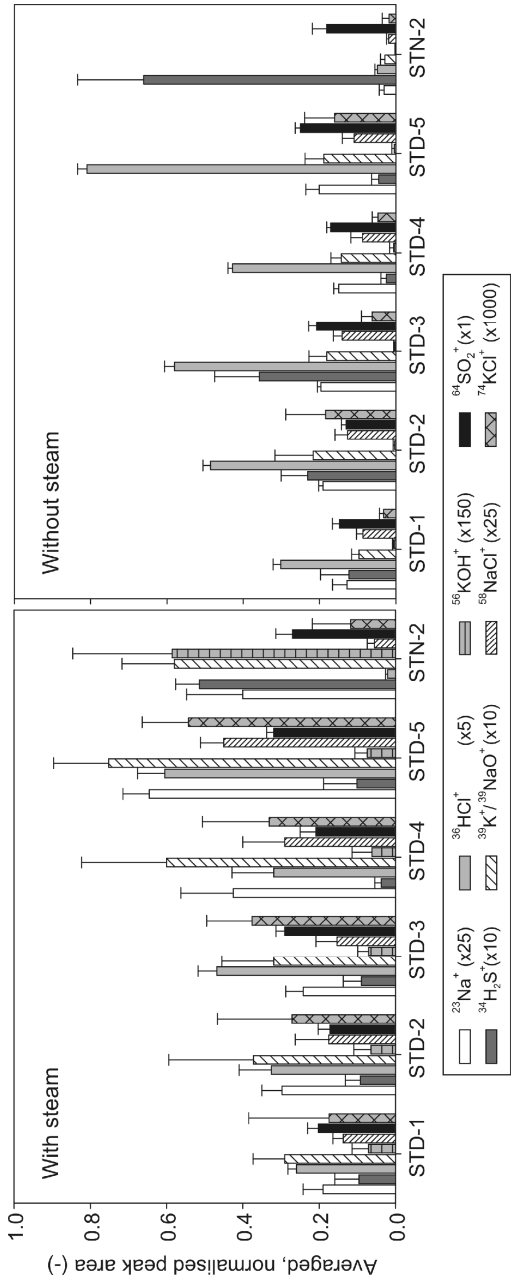

Figure 43. Averaged, normalised peak areas of $^{23}Na^+$, $^{34}H_2S^+$, $^{36}HCl^+$, $^{39}K^+/^{39}NaO^+$, $^{56}KOH^+$, $^{58}NaCl^+$, $^{64}SO_2^+$, and $^{74}KCl^+$ detected during experiments with hard coals at 1400 °C with and without water vapour.

4.4 Influence of the coal rank

The main species detected by the MBMS were $^{23}Na^+$ (m/z = 23), $^{34}H_2S^+$ (m/z = 34), $^{36}HCl^+$ (m/z = 36), $^{39}K^+/^{39}NaO^+$ (m/z = 39), $^{56}KOH^+$ (m/z = 56), $^{58}NaCl^+$ (m/z = 58), $^{60}COS^+/^{60}NaCl^+$ (m/z = 60), and $^{74}KCl^+$ (m/z = 74). The averaged, normalised peak areas are shown in Figures 44 to 50 (bars – left axis). Additionally, the content of the elements of interest has been depicted (symbols – right axis). For the high-rank coals, the detected species ordered by the size of the peak areas are $^{39}K^+/^{39}NaO^+ > ^{34}H_2S^+$, $^{36}HCl^+ > ^{58}NaCl^+$, $^{60}COS^+ > ^{56}KOH^+ > ^{74}KCl^+$. For the low-rank coals, the order is $^{39}K^+/^{39}NaO^+ > ^{58}NaCl^+$, $^{60}COS^+$, $^{36}HCl^+ > ^{34}H_2S^+ > ^{56}KOH^+ > ^{74}KCl^+$. The Spanish hard coal K2-5 showed the highest release of $^{34}H_2S^+$, with a peak area of 8.32×10^{-2}. In comparison, the German anthracite K2-3 showed the lowest peak area (2.44×10^{-3}).

The quantity of the released $^{34}H_2S^+$ was equal to that of the hard coals, as shown in Figure 44. The S-rich lignite K3-1 showed the highest release, with a peak area of 7.04×10^{-2}, and HKS showed the lowest release, with a peak area of 7.74×10^{-3}. The low rank coals showed a good correlation with the sulphur content (Figure 44). On the contrary, the released amount of $^{34}H_2S^+$ was not correlated with the sulphur content of the high rank coals.

The peak areas of $^{60}COS^+/^{60}NaCl^+$ (Figure 45) were one order of magnitude lower than the peak areas of $^{34}H_2S^+$ for both hard coals and lignites, e.g. the peak area of m/z = 60 was about 6×10^{-3} and the peak area of $^{34}H_2S^+$ was about 5.1×10^{-2} for the Norwegian hard coal STN-2.

The mass-to-charge ratio of 60 is occupied by $^{60}COS^+$ and $^{60}NaCl^+$. It is not possible to distinguish between the two species with the low-resolution quadrupole system of the MBMS. However, calculations with $^{58}NaCl^+$, the main NaCl isotope, were performed to estimate its participation in the peak area of m/z = 60. The amount of $^{60}NaCl^+$ was calculated on the basis of the peak area of $^{58}NaCl^+$ and the ratio of $^{35}Cl/^{37}Cl$, and it is depicted together with the measured value of m/z = 60 in Figure 45. For most of the hard coals under investigation, the fraction of $^{60}NaCl^+$ of the peak area of m/z = 60 was significantly higher than the fraction of $^{60}COS^+$. Notable exceptions were the Colombian hard coal K2-4, the Spanish hard coal K2-5, and the Norwegian hard coal STN-2, all of which showed a relatively large fraction of $^{60}COS^+$. The fraction of $^{60}COS^+$ was much higher than the fraction of $^{60}NaCl^+$ for all the lignites.

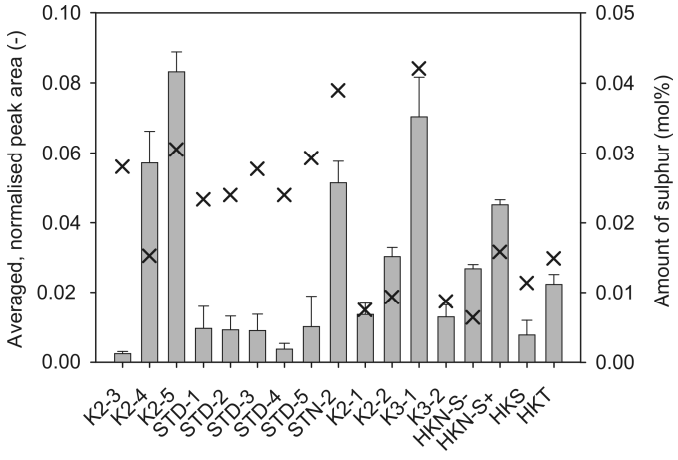

Figure 44. Averaged, normalised peak areas of $^{34}H_2S^+$ (bars) at 1400 °C in He/7.5% O_2 with water vapour.

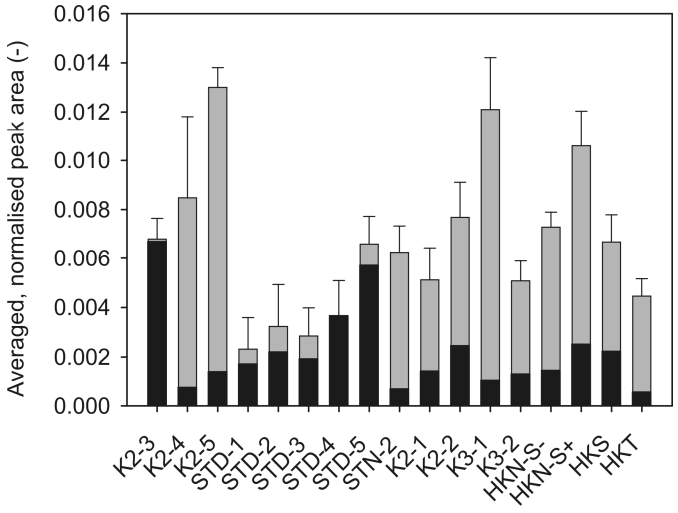

Figure 45. Averaged, normalised peak areas of $^{60}COS^+$ (grey) / $^{60}NaCl^+$—calculated (black).

The mass-to-charge ratio of 39 is occupied by $^{39}K^+$ and $^{39}NaO^+$, as recently shown by Bläsing and Müller [2010c]. The averaged, normalised peak areas of the alkali metal species $^{58}NaCl^+$ and $^{39}K^+/^{39}NaO^+$ are depicted in Figures 46 and 47. The anthracite K2-3 showed the highest amount of $^{58}NaCl^+$ (peak area of 2.11×10^{-2}) and the lowest amount of $^{39}K^+/^{39}NaO^+$ (peak area of 1.12×10^{-2}). The lignite HKT showed the lowest amount of

$^{58}NaCl^+$ and the highest amount of $^{39}K^+/^{39}NaO^+$. The peak areas of $^{39}K^+/^{39}NaO^+$ for the lignites were about two orders of magnitude higher than the peak areas of $^{58}NaCl^+$. The sodium content of the coals and the amount of $^{58}NaCl^+$ showed a weak correlation. There was no correlation between the sodium and potassium content and the amount of $^{39}K^+/^{39}NaO^+$.

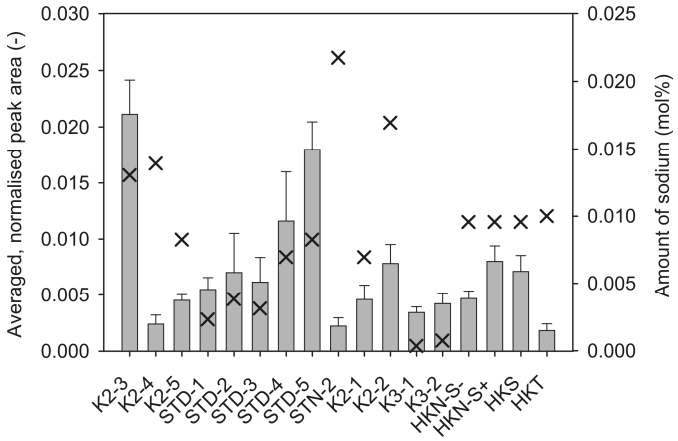

Figure 46. Averaged, normalised peak areas of $^{58}NaCl^+$ (bars) at 1400 °C in He/7.5% O_2 with water vapour.

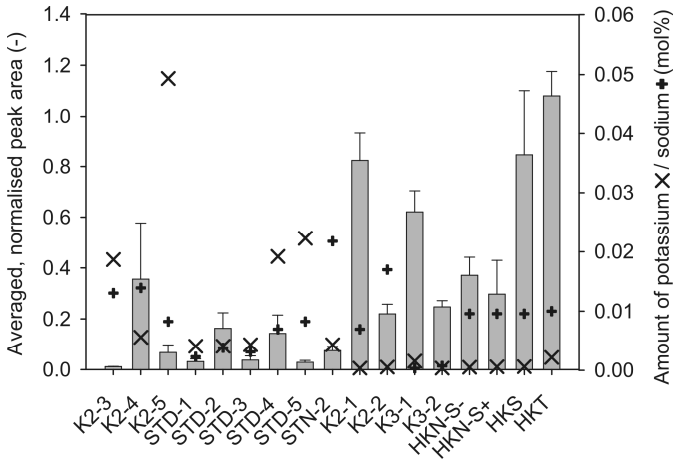

Figure 47. Averaged, normalised peak areas of $^{39}K^+/^{39}NaO^+$ (bars) at 1400 °C in He/7.5% O_2 with water vapour.

The peak areas of the K species $^{74}KCl^+$ and $^{56}KOH^+$ are depicted in Figures 48 and 49. The peak areas of $^{56}KOH^+$ were about one order of magnitude smaller than the peak area of $^{74}KCl^+$, as shown by the following examples. The lignite K3-1 showed a strong release. The averaged, normalised peak area of $^{74}KCl^+$ was 1.52×10^{-4}. The peak area of $^{56}KOH^+$ was 4.2×10^{-3}. In contrast, the hard coal K2-4 showed a small release of 1.04×10^{-4} for $^{74}KCl^+$ and 1.98×10^{-3} for $^{56}KOH^+$. The peak areas of $^{39}K^+/^{39}NaO^+$ for the lignites were about four and five orders of magnitude higher than the peak areas of $^{56}KOH^+$ and $^{74}KCl^+$, respectively. For the hard coals, the difference was lower—three and four orders of magnitude. Neither the high rank coals nor the low rank coals showed a significant correlation of the potassium content and the release of $^{56}KOH^+$ and $^{74}KCl^+$.

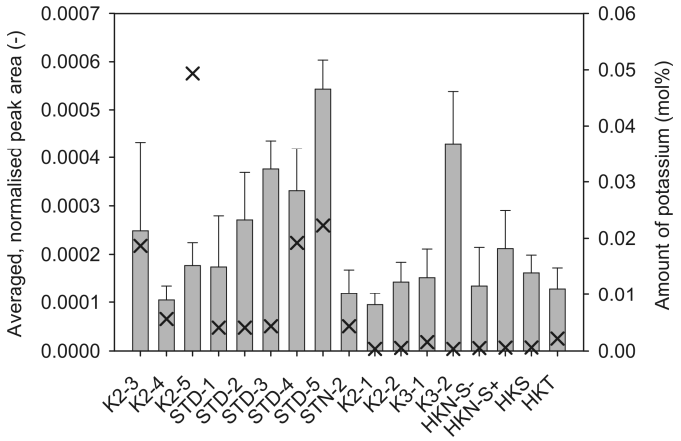

Figure 48. Averaged, normalised peak areas of $^{74}KCl^+$ (bars) at 1400 °C in He/7.5% O_2 with water vapour.

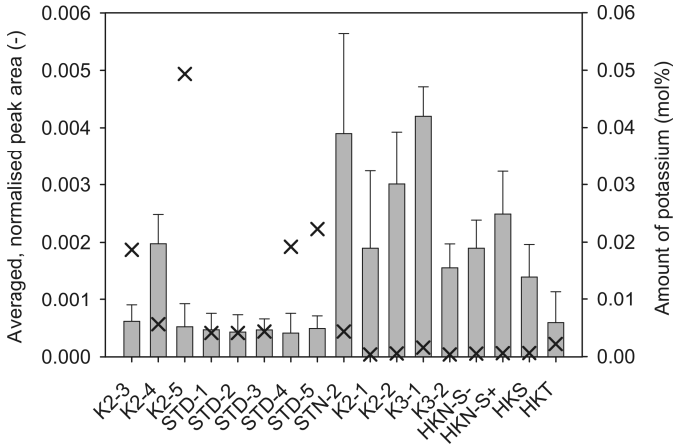

Figure 49. Averaged, normalised peak areas of $^{56}KOH^{+}$ (bars) at 1400 °C in He/7.5% O_2 with water vapour.

In general, the hard coals showed a higher release of $^{36}HCl^{+}$ than did the lignites, as shown in Figure 50. The peak areas of the lignites were between 3.4 and 3.8% of the hard coal STD-5, which showed the highest release with a peak area of 1.21×10^{-1}. Exceptions were the hard coals K2-4 and STN-2, which showed relatively low peak areas, similar to those of the lignites. The high rank coals showed a significant correlation with the chlorine content, whereas the low rank coals showed no correlation.

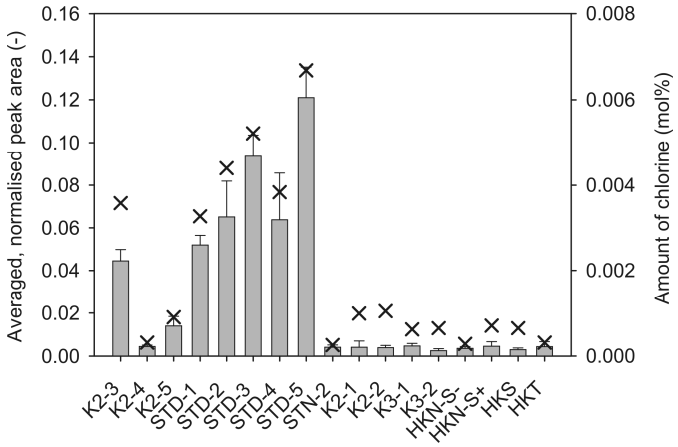

Figure 50. Averaged, normalised peak areas of $^{36}HCl^{+}$ (bars) at 1400 °C in He/7.5% O_2 with water vapour.

4.5 Influence of the pressure

The experiments simulate the batch-scale gasification of coal under pressure. Based on the qualitative results of the MBMS measurements, spectra of the Norwegian hard coal STN-2 are depicted in Figure 51. Key species were $^{30}CO^{+}$, $^{34}H_2S^{+}$, $^{36}HCl^{+}$, $^{41}K^{+}/^{41}NaO^{+}$, $^{58}NaCl^{+}$, $^{64}SO_2^{+}$, and $^{74}KCl^{+}$, all of which were released mainly during devolatilisation.

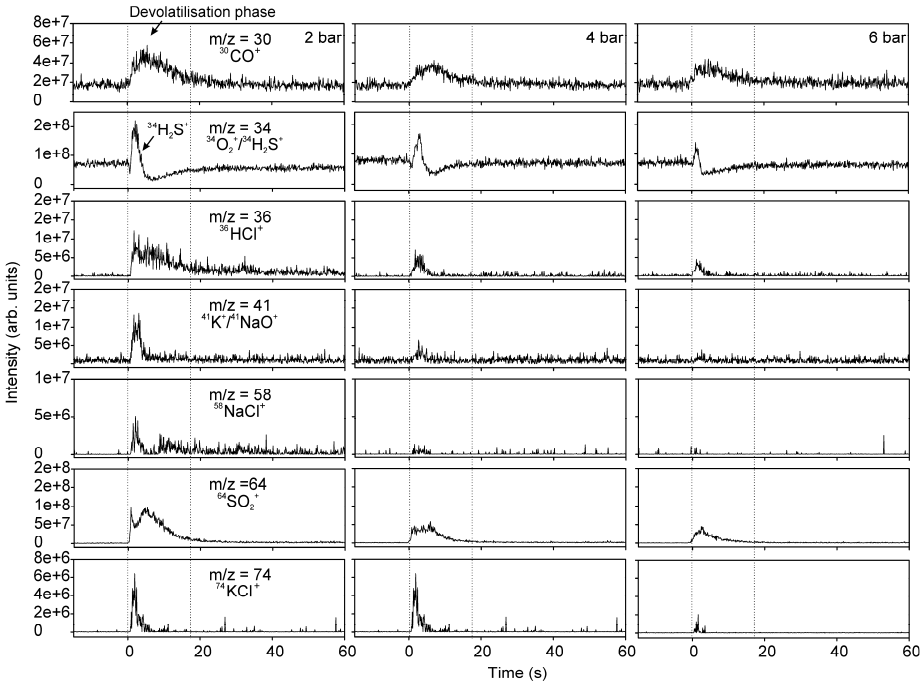

Figure 51. Intensity–time profiles of several inorganic compounds released during gasification experiments with the Norwegian hard coal STN-2 at 1325 °C and at 2, 4, and 6 bar.

In order to quantify the detected species, the signal intensities were integrated over time and normalised to the $^{34}O_2^{+}$ signal. The quantitative results are depicted in Figures 52 to 57.

Both the hard coals and the lignites under investigation showed a decrease of the averaged, normalised peak areas of $^{34}H_2S^{+}$ with increasing pressure (Figure 52)—e.g. the hard coal STD-5 showed a very strong $^{34}H_2S^{+}$ decrease of 66.0% at 4 bar and 87.2% at 6 bar. In contrast, the lignite K2-1 indicated a smaller influence of pressure on the

release of $^{34}H_2S^+$—29.5% at 4 bar and 34.0% at 6 bar. Additionally, the release of $^{64}SO_2^+$ decreased with increasing pressure, e.g. K2-5 by 65.8% at 4 bar and 88.4% at 6 bar (Figure 53).

The averaged peak areas of $^{36}HCl^+$ decreased for both the hard coals and the lignites (Figure 54). The variance of the decrease is high, e.g. STD-3 showed a decrease of 3.5% at 4 bar and 42.4% at 6 bar and K2-5 showed a decrease of 52.8% at 4 bar and 85.5% at 6 bar.

The averaged peak areas of $^{58}NaCl^+$ and $^{74}KCl^+$ decreased with increasing pressure (Figures 55 and 56). STN-2 showed a very strong $^{58}NaCl^+$ decrease of 88.7% at 4 bar and 95.6% at 6 bar. Additionally, the decrease of $^{74}KCl^+$ was strong for STN-2—75.8% at 4 bar and 85.1% at 6 bar.

The averaged peak areas of $^{41}K^+/^{41}NaO^+$ decreased with increasing pressure over a broad range (Figure 57). K2-3 showed a moderate decrease of 7.5% at 4 bar and 26.2% at 6 bar, whereas STD-1 showed a strong decrease of 75.8% at 4 bar and 85.5% at 6 bar.

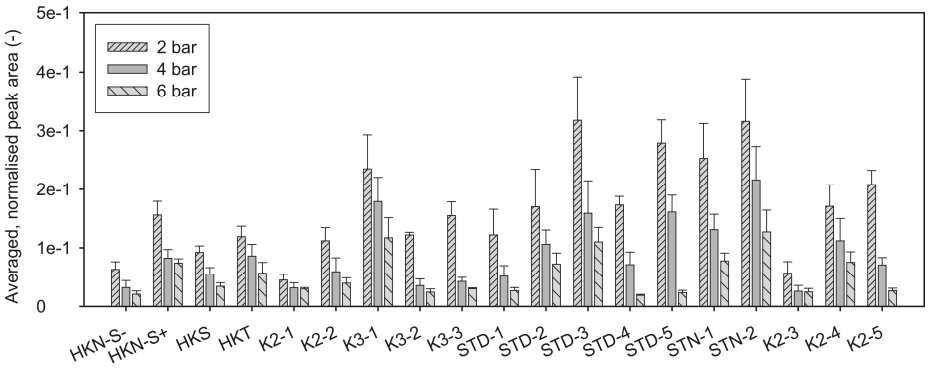

Figure 52. Averaged, normalised peak areas of $^{34}H_2S^+$ at 1325 °C and 2–6 bar.

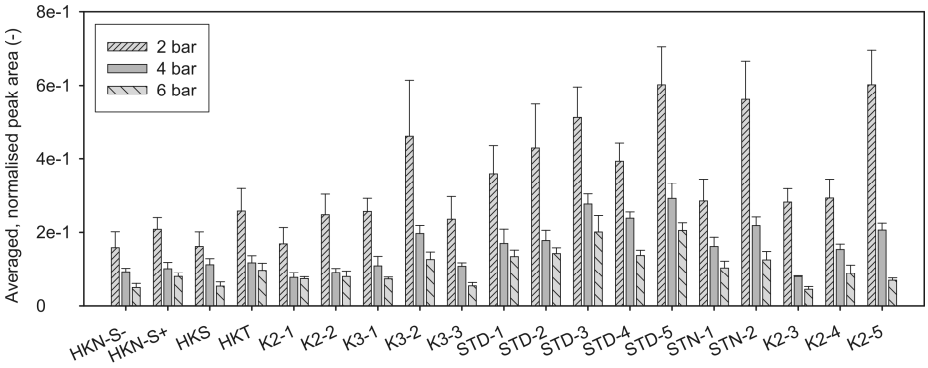

Figure 53. Averaged, normalised peak areas of $^{64}SO_2^+$ at 1325 °C and 2–6 bar.

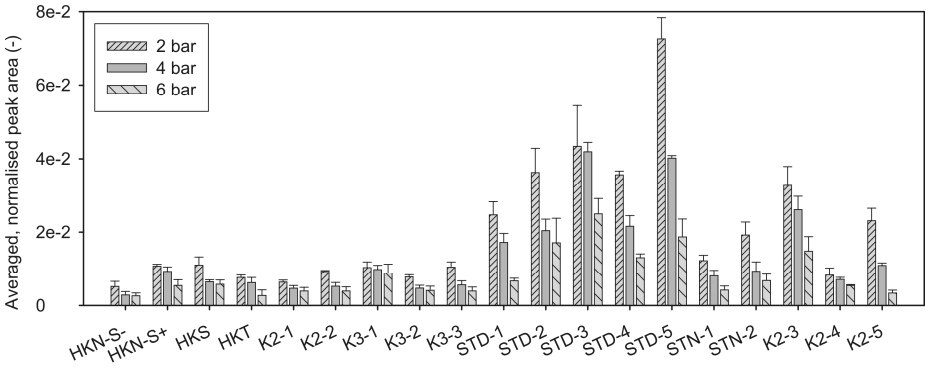

Figure 54. Averaged, normalised peak areas of $^{36}HCl^+$ at 1325 °C and 2–6 bar.

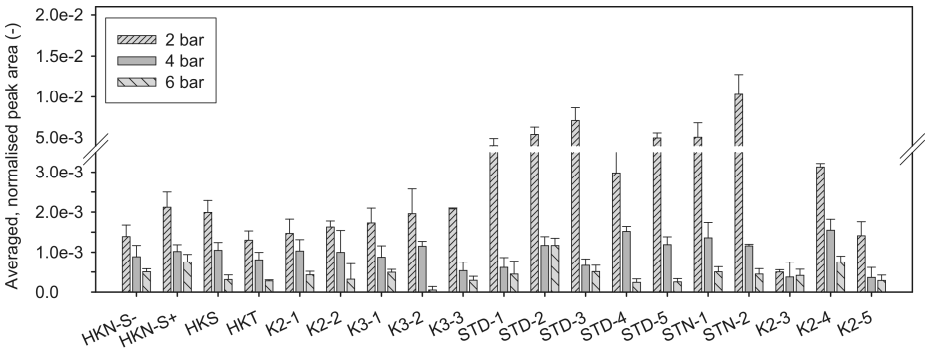

Figure 55. Averaged, normalised peak areas of $^{58}NaCl^+$ at 1325 °C and 2–6 bar.

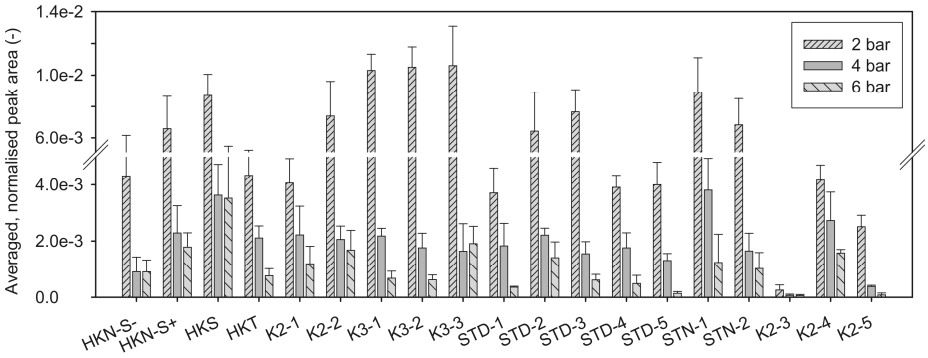

Figure 56. Averaged, normalised peak areas of $^{74}KCl^{+}$ at 1325 °C and 2–6 bar.

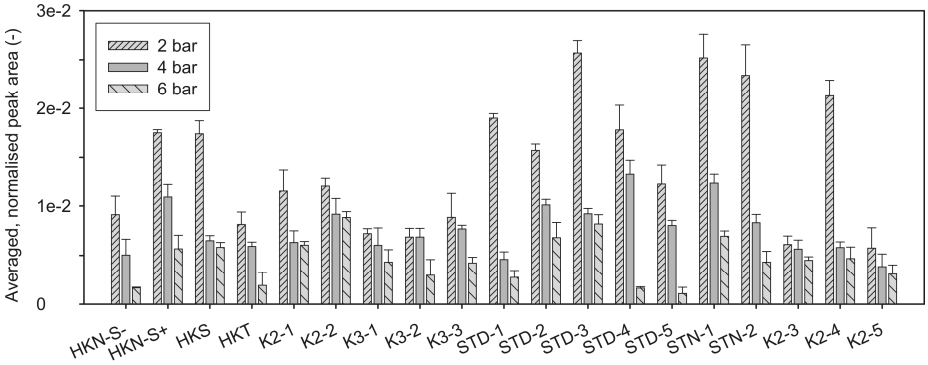

Figure 57. Averaged, normalised peak areas of $^{41}K^{+}/^{41}NaO^{+}$ at 1325 °C and 2–6 bar.

5 Discussion

5.1 Influence of gasification and combustion like conditions

The main S species detected by the MBMS were $^{34}H_2S^+$ and $^{64}SO_2^+$. The release of S species during the devolatilisation phase is representative for weakly bound S, which is released relatively easily at moderate temperatures of coal devolatilisation (500–800 °C). Pyrite decomposes thermally during devolatilisation, as shown in Eq. 12 [Raask, 1985].

$$FeS_2 \longrightarrow FeS + S \ (T > 500\ °C) \qquad \text{Eq. 12}$$

The released S can undergo several reactions depending on the reaction partner. The formation of H_2S instead of SO_2 depends on the oxygen partial pressure. During combustion experiments, released S can react with oxygen, leading to the formation of SO_2. $^{34}H_2S^+$ was not detected.

The detection of $^{64}SO_2^+$ during gasification experiments indicated that the oxygen partial pressure was high enough to allow for the formation of SO_2. The second release step of $^{64}SO_2^+$ can be explained by the release of char-bound S during the char conversion phase and secondary reactions, as shown in Eq. 7 in Section 2.3. For the hard coals, the second release step occurred with a significant intensity during the combustion experiments, whereas the intensity of the second release step of $^{64}SO_2^+$ was low during the gasification experiments. This can be explained by kinetic constraints, which are likely to occur during gasification because unreacted carbon can form a layer that causes retarded mass transfer. It is suggested that the limiting factors in the release mechanism are the transportation of gaseous reactants and products in the char/boundary layer and the diffusion of gaseous reaction partners and products through the pore system of the remaining char. Accordingly, the release occurred over a long time period with lower intensity during gasification.

Despite the detection of a significant amount of $^{64}SO_2^+$, which can stabilise the formation of Na_2SO_4, the release of $^{142}Na_2SO_4^+$ was not detected. A likely explanation is given by the temperature dependence of the formation of $^{142}Na_2SO_4^+$ in combination

with the oxygen content of the reaction atmosphere. Additionally, the effect of the oxygen content is modified by the temperature. Wibberley and Wall [1982] showed that Na_2SO_4 is only stable below 1127 °C under combustion conditions in the furnace gas and below 827 °C under extreme reducing conditions in the burning char.

The majority of the $^{58}NaCl^+$ was released with high intensity during the devolatilisation phase at the start of the thermochemical conversion. Recently, the release of $^{58}NaCl^+$ during devolatilisation was explained by the vaporisation of NaCl that occurs as a result of its relatively low melting point (801 °C) [Oleschko, 2007]. However, considering the low vapour pressure of NaCl at the devolatilisation temperature (<800 °C), vaporisation cannot satisfactorily explain the high intensity of the release. According to Brinsmead and Kear [1956], vaporisation is not the main mechanism of the NaCl release: the explanation must also consider the desorption of organically bound Na and Cl.

During the gasification experiments, the amount of released $^{58}NaCl^+$ (expressed by the averaged, normalised peak areas) was higher than that during the combustion experiments for the lignites and slightly higher for the hard coals. Several explanations for this are the following: Under the influence of a hydrogen-rich atmosphere, the dissociation of carboxylic-bound Na is enhanced, as mentioned in Section 2.3. Therefore, the release of Na is likely to be enhanced during the gasification experiments. In addition, the capture of Na by Al-silicates is inhibited during the gasification experiments because H_2O and oxygen play an important role in the capture mechanism, as shown by Eq. 6 and 8 in Section 2.3 [Steffin, 1999]. These effects seem to overcome the enhanced capture capability: During the release process in the coal particle, the gaseous Na compounds must diffuse through a mineral-rich char matrix, and a significant fraction of the Na can react with silica [Huffman et al., 1989]. Retarded mass transfer, such as that caused by a carbon layer, as mentioned above, should lead to a longer residence time of the released species and to an enhanced capture if a significant amount of getter is available.

The high-intensity release of $^{36}HCl^+$ during the devolatilisation phase of both gasification and combustion experiments is assumed to originate mainly from weakly bound Cl from the coal surface. Adsorbed Cl can react with hydrogen (such as that released from coal during devolatilisation) and form highly volatile $^{36}HCl^+$. Because of the hydrogen-rich gasification atmosphere, the reaction of Cl with H is enhanced; this could lead to the increased formation of HCl. Furthermore, the low-intensity long-term release of $^{36}HCl^+$ after the devolatilisation phase can be partly explained by the release of trapped Cl due to the slower conversion of the coal matter under the reduced oxygen content of the gasification experiments. The slightly higher signal intensity of $^{36}HCl^+$

during the char reactions phase of the gasification experiments (Figure 20 in Section 4.1) is an indication of the slower release of Cl. This agrees with the observations regarding the release of $^{58}NaCl^+$.

$^{74}KCl^+$ was detected with a reliable signal-to-noise ratio only for the hard coals. The release occurred in two steps. The first release step occurred during devolatilisation, with high intensity in only a few seconds, e.g. about 5 s for STD-5. The release can partly be explained by the desorption of surface-bound K and Cl, and to a much smaller extent, by the vaporisation of KCl (melting point: 790 °C). Also notable is the second release step, which occurred during the char reactions phase with lower intensity over a long time period. The second release step can be partly explained by the replacement of K by Na in Al-silicates at 1400 °C, as mentioned in Section 2.3, and by the release of trapped KCl or secondary reactions. A lower oxygen partial pressure leads to a slower char conversion, which traps some of the K species. These species were released during char conversion. Additionally, the residence time of trapped species is higher, which can lead to an enhanced capture due to higher temperature as well as to a longer time of contact between the mostly volatile K species and the remaining mineral matter. The slightly higher released amount of $^{74}KCl^+$ during gasification experiments can be explained by an enhanced release of carboxylic-bound K as well as by reduced capture, as mentioned above in regards to the alkali metal Na.

Thermodynamic calculations: The results of thermodynamic calculations for the species HCl, NaCl, H_2S/SO_2, and KCl are provided and compared to the experimental results in Figures 58 and 59.

German lignites: For combustion conditions (λ = 1), the order of the formed species calculated by FactSage 5.4.1, starting with the highest amount, is SO_2 > NaCl, K species > HCl. The order for the released species measured by the MBMS is $^{39}K^+$ > $^{64}SO_2^+$ > $^{58}NaCl^+$, $^{36}HCl^+$. The extended release of the species with m/z = 39, discovered during experimental investigations, cannot be satisfactorily explained by the fragmentation of different K sources, e.g. $^{58}KOH^+$ and $^{74}KCl^+$. The release of $^{58}NaCl^+$ is smaller than that predicted by thermodynamic modelling.

For reducing conditions (λ = 0.5), the order of the formed species calculated by FactSage 5.4.1, starting with the highest amount, is H_2S > NaCl > HCl. The order for the released species measured during the gasification experiments is $^{34}H_2S^+$ > $^{58}NaCl^+$, $^{36}HCl^+$. The predicted release of H_2S in place of SO_2 was confirmed by the experimental results, but the order of the released amounts was not correctly predicted. A likely explanation is the thermodynamic stability of the alkali metal species: NaOH > NaCl > Na_2S, as shown by thermodynamic calculations. There may be kinetic constraints so

that Na_2S is more stable than was predicted by thermodynamic calculations, and therefore less $^{34}H_2S^+$ and $^{58}NaCl^+$ are released, as was predicted. Consequently, the order of the species according to released amount has been changed.

The experimental results, the calculated results for H_2S for the gasification experiments, and the calculations with $\lambda = 0.5$ are in good agreement. H_2S is the most abundant gaseous S species. The predicted order of the release amount of H_2S is identical to the order from the experimental results. The trend of the released amount is similar to the calculated fugacity. The highest fugacity and one of the highest peak areas were found for HKN-S+. HKN-S- exhibited larger differences between the experimental findings and the calculated fugacity. The release was much higher during the experiments than was predicted by the thermodynamic calculations. A reasonable explanation is yet to be found.

German hard coals: The order of the released amount of $^{36}HCl^+$ cannot correctly be predicted for the gasification-like environment. The order of the released amounts for STD-1, STD-2, and STD-4 is different than the order of the predicted amounts. In contrast, the calculated order of the amount of HCl for the combustion-like environment agrees well with the experimental results from the combustion experiments. This can be partially explained by the differences between the experiments and the calculations. The release of $^{36}HCl^+$ during the experiments is a result mainly of desorption and further gas-phase reactions and is therefore a fast process. Equilibrium cannot be reached because the gas flow carries away parts of the released $^{36}HCl^+$ before the temperature is high enough to support secondary reactions with the coal minerals. In the gasification experiments, this effect was amplified as a result of the layer of unreacted carbon, as mentioned above.

The prediction for NaCl agrees with experimental results for STD-1, STD-2, and STD-3, but the predicted release of STD-4 and STD-5 are much lower than what was detected during experimental investigation. This can be explained by the occurrence of kinetic constraints in the exchange mechanism of K in K-aluminosilicates caused by Na. For combustion-like conditions, the prediction becomes much closer to the experimental results. Thus, the conclusion is that a layer of unreacted carbon may block the reaction between NaCl and K-aluminosilicate during gasification experiments.

The predicted release of H_2S is in partial agreement with the experimental results. For STD-1, STD-2, and STD-3, the calculated amount is in agreement with the experimental results, but for STD-4 and STD-5, the calculated amount is much higher than the amount released during the gasification experiments. A possible explanation is that the retention of S by Na and Ca is more effective than is indicated by the thermody-

namic equilibrium calculations; this discrepancy is attributable to the layer of unreacted carbon, which inhibits the incorporation of Na and Ca in the K-aluminosilicate.

The predicted release of SO_2 is in good agreement with the experimental results, but the released amount of STD-3 is much higher than predicted.

The formation of KCl predicted by thermodynamic calculations is higher than the amount of NaCl. In contrast, the amount of released $^{58}NaCl^+$ measured by the MBMS is much higher than the amount of released $^{74}KCl^+$. This can be partially explained by the fragmentation of KCl due to the ionisation process [Krishnan and Wood, 1991; Milne and Soltys, 1983b; French et al., 1994; Oleschko, 2007; Porbatzki, 2008]. An additional explanation involves the different modes of occurrence and, accordingly, the different release mechanisms of Na and K species. Part of the ionic bound Na is released at the moderate temperatures of devolatilisation. Part of the released Na flows away in the gas stream before ion-exchange reactions can occur, leading to the release of K. Therefore, it is likely that there will be differences between release experiments and thermodynamic calculations.

Krishnan et al. [1994] performed thermodynamic calculations and experiments under various conditions. They reported that the partial pressure of Na_2SO_4 increased with increasing oxygen content, whereas the partial pressures of Na, NaCl, and NaOH decreased. The predominant gaseous Na species at low oxygen partial pressure were Na, NaOH, NaCl, and Na_2Cl_2. Discrepancies between calculated and observed values were related to absorption of vapour species on the surface of fume particles [Krishnan et al., 1994]. They found that gaseous Na species were present at about 14 ppm under gasification conditions at a temperature of 827 °C.

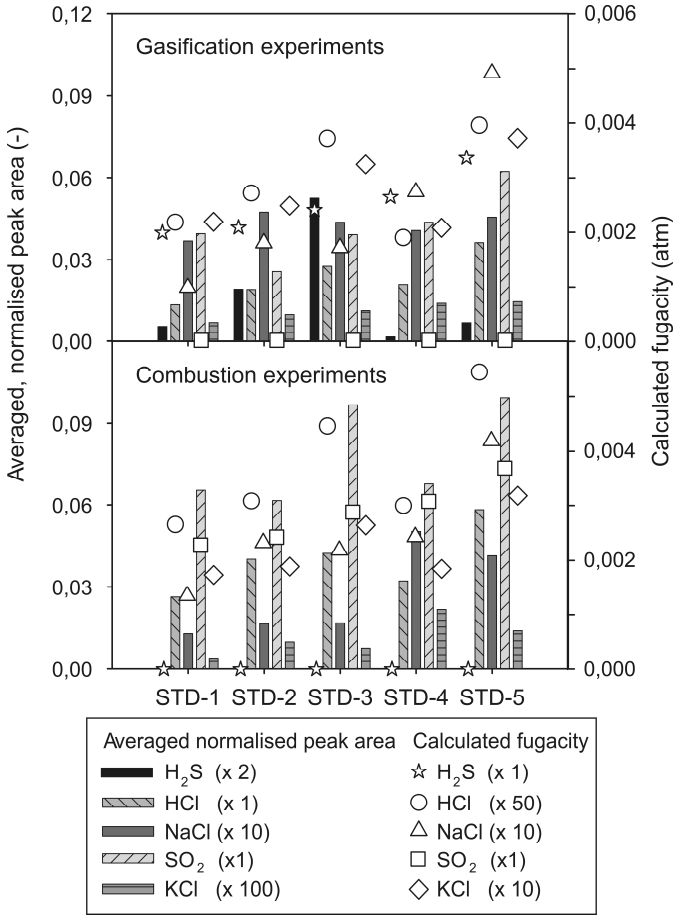

Figure 58. Averaged, normalised peak areas and the results of thermodynamic calculations by FactSage 5.4.1 for the release of H_2S, HCl, NaCl, SO_2, and KCl (hard coals).

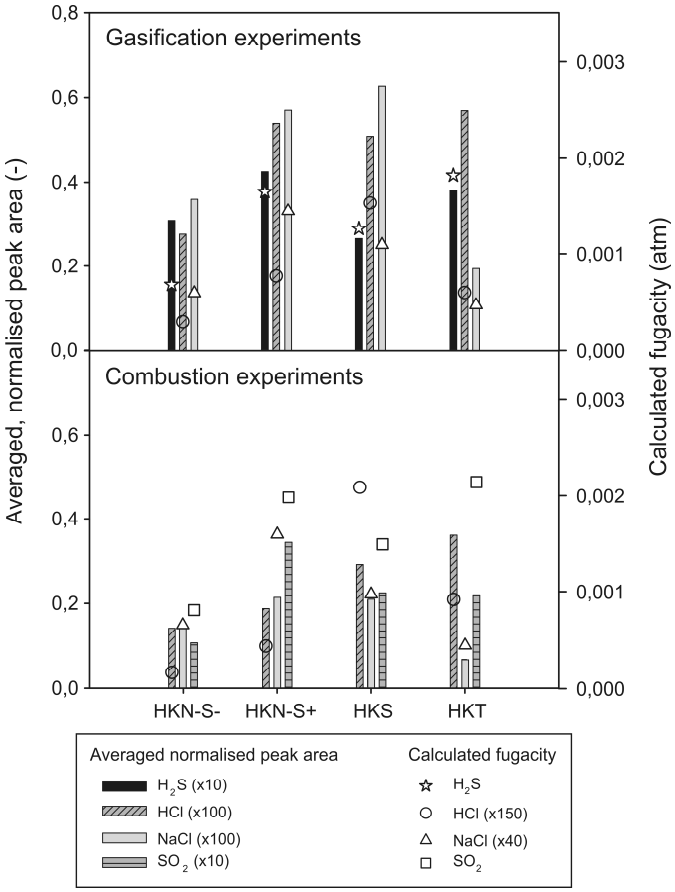

Figure 59. Averaged, normalised peak areas and the results of thermodynamic calculations by FactSage 5.4.1 for the release of H_2S, HCl, NaCl, and SO_2 (lignites).

5.2 Temperature

Lignites: The $^{34}H_2S^+$ and $^{64}SO_2^+$ release behaviour of the lignites was very complex. The release trends were contradictory and cannot be satisfactorily explained by the known release mechanisms of S.

The released amount of $^{58}NaCl^+$ increased within the temperature range from 1100 to 1700 °C for HKN-S- (slightly positive), HKN-S+ (strongly positive), and HKS (strongly positive). The amount is nearly constant for HKT. A likely explanation for the contrary release trends of $^{36}HCl^+$ and $^{58}NaCl^+$ is the following: The lignites HKN-S-, HKN-S+, and HKS have a high Na/Si ratio. It can be concluded that the main fraction of Na is highly volatile, e.g. fixed to the organic matter or dispersed in the form of NaCl. However, the lignites are characterised by a shortage of Cl, and therefore the fraction of NaCl is small as well. Additionally, vaporisation of NaCl is assumed to play a minor role during the release of NaCl, as mentioned in Section 5.1. An important release mechanism is the desorption of the organically fixed Na and Cl. Sonoyama et al. [2006] found that alkali metal and alkaline earth metal species volatilise from the surface of char mainly as elemental species. They emphasised that the dissociation of carboxylic-bound metal species is enhanced in an atmosphere that is rich in H radicals. The amount of H radicals increases with increasing temperature. This leads to the enhanced release of carboxylic-bound metallic species. Furthermore, organically bound Cl is almost completely released at moderate temperatures (300–600 °C). In conclusion, organically fixed Na as well as Cl should be completely released during the devolatilisation phase of the high-temperature gasification experiments (1100–1700 °C) and should form Na and Cl species. The reaction products are HCl and NaCl as well as KCl, depending on the reaction partner and the conditions. Gaseous NaCl is one of the most stable reaction products under the experimental conditions. However, owing to the lack of Cl, the main fraction of Na will form other species, most likely intermediate NaOH [Wei et al., 2008]. The increased amount of NaOH shifts the equilibrium of NaOH and HCl with NaCl and H_2O to the product side. With increasing temperature, the volatility of Na increases as a result of the enhanced dissociation of carboxylic-bound Na species. This results in an enhanced release of $^{58}NaCl^+$, whereas the release of $^{36}HCl^+$ decreases. The proposed mechanisms constitute a likely explanation of the negative release trend of $^{36}HCl^+$ and the positive trend of $^{58}NaCl^+$ for HKN-S-, HKN-S+, and HKS. In the case of HKT, it is assumed that the enhanced release of Na is compensated for by the enhanced capture by aluminosilicates contained in the ash of this clay-rich lignite.

The majority of the release of $^{39}K^+/^{39}NaO^+$, $^{56}NaOH^+$, $^{58}NaCl^+$, and $^{74}KCl^+$ occurred during devolatilisation at relatively low temperatures of 600–1000 °C. Therefore, the

occurrence of ion-exchange reactions is assumed to be less important due to kinetic limitations of the process. In conclusion, the contribution of K species to the signal of m/z = 39 is likely to be marginal in the present experiments. The model experiments in Section 4.2 showed that m/z = 39 is most likely occupied by $^{39}NaO^+$. Complementary explanations of the increase of the m/z = 39 signal are given below. Additionally, the species of KOH and KCl could have led to an increase of the m/z = 39 signal as a result of the fragmentation of KOH and KCl and the detection of $^{39}K^+$ by the MBMS. However, the signal intensity of $^{56}KOH^+$ and $^{74}KCl^+$ was about two to three orders of magnitude lower than the signal intensity of m/z = 39. Therefore, it is unlikely that the signal of m/z = 39 is caused mainly by $^{39}K^+$.

Hard coals: In general, the released amount of $^{34}H_2S^+$ increased strongly with increasing temperature, whereas the released amount of $^{64}SO_2^+$ decreased. It is assumed that the increased concentration of hydrogen led to the increased formation of $^{34}H_2S^+$ with increasing temperature.

$^{64}SO_2^+$ was released in two steps during the devolatilisation phase and char reactions phase. Comparing the spectra of $^{64}SO_2^+$ at 1100–1700 °C, the second low-intensity release step of $^{64}SO_2^+$ was observed with increased signal intensity and with a compressed spectrum, especially at 1700 °C. The second release step of $^{64}SO_2^+$ can be explained by the long-term release of low-volatility S fixed in the coal matrix in the form of S bound in heterogeneous aromatic carbon rings (e.g. thiophene). S bound in aromatic systems is stable up to high temperatures and is only released during gasification of the residual coal matter after devolatilisation. Therefore, a faster heat-up in combination with a higher furnace temperature leads to a faster consumption of the residual coal matter and to enhanced release of char-bound S. The enhanced release leads to a significant peak at 1700 °C, as shown in Figure 28. The slower heat-up at 1100–1400 °C leads to a slower consumption of the coal matter, and therefore the S is released with lower intensity over a longer period.

The released amount of $^{36}HCl^+$ increased from 1100 to 1400 °C and decreased from 1400 to 1700 °C. However, the differences are moderate in comparison with those of most of the other species under investigation, as mentioned above. The contrary release trends cannot be satisfactorily explained by the known release mechanisms of Cl.

$^{58}NaCl^+$ was released in two steps. The high-intensity release during the devolatilisation phase can be explained by desorption of adsorptively bonded Na and Cl and by the vaporisation of NaCl. The low-intensity release during the char reactions phase can be explained by the release of trapped NaCl that occurs during progressive char conversion, as mentioned in Section 5.1. The intensity of the signals increased

with increasing temperature during the devolatilisation phase. Additionally, the second-step release during the char reactions phase became shorter with increasing temperature. This can be explained by faster conversion of the remaining coal matter at higher temperatures, e.g. carbon layers that inhibit further reactions between mineral matter are consumed more quickly. The released amount of $^{58}NaCl^{+}$ increases within the temperature range from 1100 to 1700 °C for STD-1, STD-2, STD-3, and STN-2. For STD-4 and STD-5, the release decreases from 1100 to 1400 °C and strongly increases from 1400 to 1700 °C. The Na content of the coals is of secondary importance, e.g. STN-2 has an Na content that is ten times higher than that of STD-1, but the released amount of $^{58}NaCl^{+}$ is much lower. The release of $^{58}NaCl^{+}$ is positively correlated with the Cl content of the coals. The present results highlight the importance of Cl in the release mechanism of alkali metal during the gasification of coal. This is discussed in more detail in Section 5.4.

The majority of $^{74}KCl^{+}$ (m/z = 74) was released during the devolatilisation phase. However, there was a low-intensity, long-term release during the char reactions phase. The second-phase release during the char reactions phase can be explained by secondary reactions, as mentioned above. In general, the released amount of $^{74}KCl^{+}$ increased with increasing temperature; exceptions include STD-2, which showed a decrease of about 50% from 1100 to 1400 °C and an increase of about 400% from 1400 to 1700 °C. In comparison to the other four hard coals, STD-4 and STD-5 showed a very large increase at 1700 °C. The temperature dependence of the K release agrees with the data reported by Novakovic et al. [2009]. They reported a release of K that was higher at 1000 °C than at 900 °C in an atmosphere of N_2/H_2O for model experiments with K_2CO_3–CaO–SiO_2 mixtures. Osborn [1992] highlighted the important influence of temperature on the release and capture of alkali metals. He assumed that there is a small window of temperature retention that depends on the volatility and the melting point of aluminosilicates. High temperatures can lead to very fast release, and thus there may not be sufficient time for retention. However, Gottwald et al. [2001] reported a high-efficiency capture of alkali metals by aluminosilicates at 920 °C during combustion experiments. The authors suggested that the capture reactions occur before the alkali metals are completely released.

The release of KCl from the Spitsbergen hard coal STN-2 was very low, despite contents of K, Si, and Al that were similar to those of the hard coals STD-1, STD-2, and STD-3. It is assumed that the low Cl content of STN-2 limits the release of KCl. Another K species under investigation is KOH. The release of $^{56}KOH^{+}$ (m/z = 56) was detected with high intensity at 1700 °C. In contrast, only low-intensity signals were detected at 1100–1400 °C. This can be explained by the shift in the equilibrium of KCl and KOH.

5.3 Steam content

The experimental results indicate that, in general, the release of vapour alkali metal compounds ($^{39}K^+/^{39}NaO^+$, $^{56}KOH^+$, $^{58}NaCl^+$, $^{74}KCl^+$) increases under the influence of steam. Previous investigations have highlighted the importance of Cl during the release of alkali metals [French et al., 1994]. Gottwald et al. reported the disproportionately high increase in alkali metal release in experiments with Cl-doped coals under the conditions of fluidised bed combustion [2001]. Regarding the chemical analysis, the amount of Cl is of a quantity that is similar to the amount of Na in the five German hard coals. In contrast, there is a lack of Cl in the four Renish lignites and the Norwegian hard coal STN-2. The latter showed a very high release of $^{39}K^+/^{39}NaO^+$. Furthermore, the amount of Cl is about one order of magnitude smaller than the amount of Na. In conclusion, the release of Na in the form of NaCl is limited by the amount of Cl for coals that lack Cl, as proven by the present experimental results. The noticeably high release of $^{39}K^+/^{39}NaO^+$ indicates that during the experiments with steam, highly volatile NaOH is formed, as proposed in the reactions of Eq. 13 [Wei et al., 2008]. In other words, steam acts as a carrier and enhances the release of Na. Wei et al. proposed a reaction mechanism for the transformation of Na bound to the organic coal matter in the form of Na-silicates [2008]. In the proposed mechanism, the formation of NaOH under the influence of steam and the formation of Na_2CO_3 play an important role (see Eq. 14 and 15).

$$2\,Na + 2\,H_2O \leftrightarrow 2\,NaOH + H_2 \qquad \text{Eq. 13}$$

$$2\,NaOH + CO \leftrightarrow Na_2CO_3 + H_2 \qquad \text{Eq. 14}$$

$$Na_2CO_3 + nSiO_2 \rightarrow Na_2SiO_3 + CO_2 \qquad \text{Eq. 15}$$

Analogous to the present experiments, NaOH could have led to an increased signal of m/z = 39 due to fragmentation of the mother molecule ($^{40}NaOH \rightarrow {}^{39}NaO^+$). Additionally, Kosminski et al. [2006a-c] reported the formation of NaOH and Na_2CO_3 and the enhanced formation of liquid Na_2CO_3 and Na-disilicate under the influence of steam. The enhanced release of $^{39}NaO^+$ under the influence of steam is an indication for the correctness of the above-mentioned assumptions and the proposed reaction mechanism. However, the majority of NaOH flowed away in the gas stream before further reactions occurred, resulting in a high m/z = 39 signal intensity.

Complementary explanations of the increase of the m/z = 39 signal are the following: Osborn [1992] reported that atomic Na is one of the main gaseous species as a result of the high temperature and, especially, of the highly reducing environment that is present in the first milliseconds of the combustion process. Furthermore, atomic Na is oxidised into NaO^+ or NaOH, which can form NaCl, Na_2SO_4, Na-aluminosilicates, and other species [Raask, 1985]. Concerning this, in the present experiments, the MBMS may have detected non-converted NaO^+.

Additionally, the fragmentation of KOH and KCl could have led to an increase of the m/z = 39 signal on account of the fragmentation of KOH and KCl and the detection of $^{39}K^+$ by the MBMS. However, the signal intensity of $^{56}KOH^+$ and $^{74}KCl^+$ was about two to three orders of magnitude lower than the signal intensity of m/z = 39. Therefore, it is unlikely that the m/z = 39 signal is caused primarily by $^{39}K^+$. Furthermore, K present in coal minerals is almost exclusively fixed in aluminosilicates and, therefore, is commonly a non-volatile compound. However, the author also discussed ion-exchange reactions, as mentioned in Section 2.3. The majority of the release of $^{39}K^+/^{39}NaO^+$, $^{56}NaOH^+$, $^{58}NaCl^+$, and $^{74}KCl^+$ occurred during devolatilisation at relatively low temperatures of 600 to 1000 °C. Therefore, the occurrence of ion-exchange reactions is assumed to be less important, as already discussed above. In contrast, Gottwald et al. [2001] reported a high-efficiency capture of alkali metals by aluminosilicates at 920 °C during combustion experiments. The authors suggested that the capture reactions occur before the alkali metals are completely released. Furthermore, the capture reaction is enhanced by the presence of steam as shown by Eq. 8 in Section 2.3. Steam lowers the melting point of Na_2CO_3 and promotes the formation of liquid Na-disilicate [Wei, 2008]. It is assumed that K is influenced in the same way. As a result, less alkali metal chlorides are released from low-rank coals in the presence of steam if significant amounts of SiO_2 are available. This influence can be seen for the four lignites, which have nearly equal amounts of Na but have different amounts of Al and Si. HKT in particular showed a relatively low release of alkali metal compounds.

The release of $^{56}KOH^+$ was strongly enhanced under the influence of steam for all coals under investigation. The coals with under-stoichiometric amounts of Cl in comparison with K showed an especially high increase under the influence of steam. A likely explanation for this increase is the enhanced formation of highly volatile KOH under the influence of steam. In the experiments without steam, the amount of Cl is the limiting factor of the release of K owing to its ‘carrier function’ during the release of alkali metal, as mentioned above.

The increase in the amount of $^{58}NaCl^+$ and $^{74}KCl^+$ is likely a result of the enhanced release of NaOH and KOH and of the reaction equilibrium, as shown in Eq. 16 (Me = Na

or K). An increased amount of NaOH or KOH leads to an increased amount of NaCl due to the shift of the reaction balance. However, one must keep in mind that the amount of Cl is limited, as mentioned above.

$$MCl + H_2O \leftrightarrow MOH + HCl \qquad \text{Eq. 16}$$

In general, the amount of $^{36}HCl^+$ decreased for all coals under investigation under the influence of steam. A likely explanation is the reaction of NaOH and/or KOH with HCl and the resulting formation of alkali metal chloride. This is in agreement with the slightly increased formation of NaCl and KCl.

The ten coals under investigation showed no clear trend regarding the release of $^{34}H_2S^+$. On the contrary, the release of $^{64}SO_2^+$ increased under the influence of steam. Cernic-Simic highlighted the role of the water–gas reaction in the release of S species [1962]. However, the kinetic of the reaction is rather slow, and a shift would lead to a general increase of $^{34}H_2S^+$ for all coals under investigation (Eq. 17). Steam can react with hydrocarbons and form CO and H (nascendi). The CO can undergo further reactions, e.g. to form COS [Brinsmead and Kear, 1956]. The result of this would also be a shift to the side of H_2S. Therefore, it can be concluded that the release mechanism of H_2S is more complex and may depend also on the capture of S by alkaline earth metals, which are known to form excellent getter materials for S under combustion conditions.

$$COS + H_2O \leftrightarrow CO_2 + H_2S \qquad \text{Eq. 17}$$

The slightly increased release of $^{64}SO_2^+$ can be explained by the enhanced reaction of alkali metal and alkaline earth metal with silica or aluminosilicate under the influence of steam, which results in a depressed capture capability. But this does not explain the different behaviour regarding $^{34}H_2S^+$.

To aid in the interpretation of the experimental results regarding the release of alkali metal compounds, thermodynamic calculations were performed. The results are depicted in Figures 60 and 61.

K-aluminosilicate was the main K compound, from a thermodynamic point of view, when sufficient alumina and silica were available, as shown for all hard coals and the lignite HKT. In this case, KCl > KOH > K were found to be minor compounds. The lignites

HKN-S-, HKN-S+, and HKS, which lack alumina and silica, showed some differences. For these lignites, the formation of alkali metal aluminosilicate was not predicted. The main alkali metal species were KOH, K, and KCl.

The calculations predicted that Na-aluminosilicate was the main Na compound for all hard coals and the lignite HKT. Other important Na compounds were NaCl, NaOH, and Na. The formation of Na-aluminosilicate was not predicted for the lignites HKN-S-, HKN-S+, and HKS. The main compounds were NaOH, NaCl, and Na. Aluminosilicates were found to be efficient getters of alkali metals under gasification conditions at 1400 °C from a thermodynamic point of view. In general, the predicted amount of alkali metal aluminosilicate slightly increased under the influence of steam. Steam leads to a shift in the equilibrium and enhances the capture of Na by kaolin, as shown in Eq. 3. However, the predicted enhanced capture of alkali metals by aluminosilicate has not been clearly confirmed by the experimental results. This is likely caused by the non-equilibrium character of the discontinuous experiments. The reaction kinetic of the capture is strongly favoured by the thermodynamics, but it could not be reached by the experimental setup. Most of the released alkali metals were simply carried away by the gas stream before effective capture could occur.

In general, the enhanced formation of alkali metal hydroxide was correctly predicted by thermodynamic calculations for both hard coals and lignites. However, the calculated increase is much lower than the experimental findings. The main Cl compound predicted by FactSage for the lignites HKN-S-, HKN-S+, and HKS is NaCl, which is followed by KCl and HCl. The differences between the experimental findings and the thermodynamic calculations are mainly kinetic in nature. Equilibrium is not reached during the batch-scale experiments, as mentioned above.

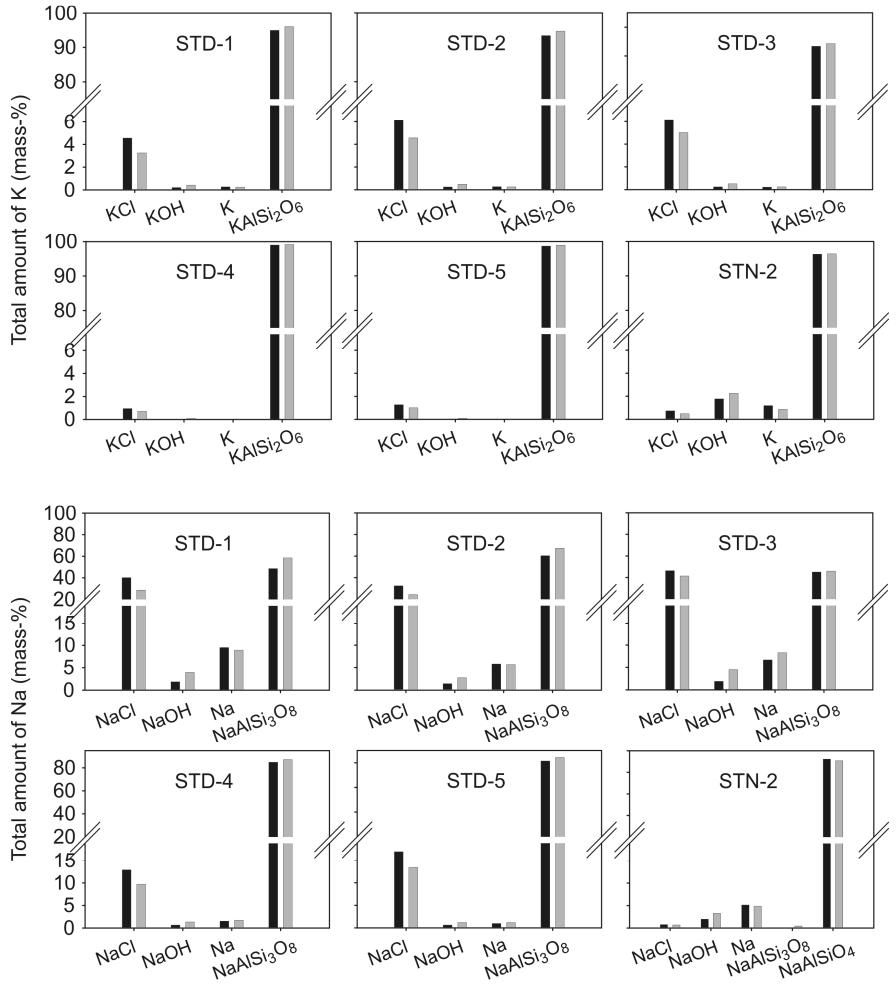

Figure 60. Results of the thermodynamic calculations by FactSage at 1400 °C and λ = 0.5 for hard coals (black: without steam, grey: with steam).

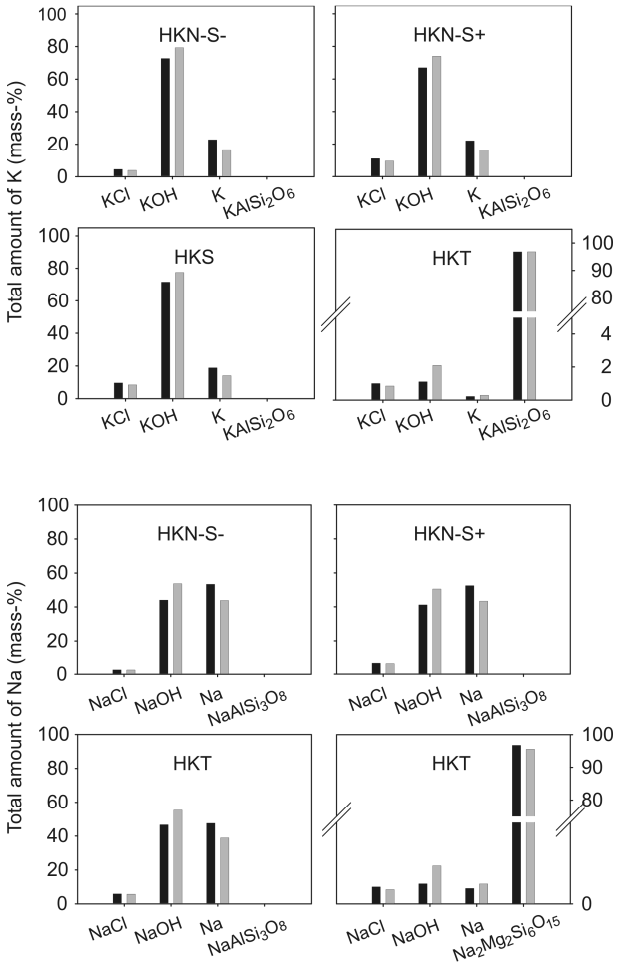

Figure 61. Results of the thermodynamic calculations by FactSage at 1400 °C and λ = 0.5 for lignites (black: without steam, grey: with steam).

5.4 Coal rank

The interpretation of the experimental results was supported by data from coal analysis (Tables 4 and 5), correlation analysis (Tables 7 and 8), and thermodynamic calculations (Figures 63 and 64).

The low rank coals show a high positive correlation of the peak areas of $^{34}H_2S^+$ with the S content, as shown by the correlation analysis and depicted in Figure 44 in Section 4.4. The release trend of the hard coals is more complex. The high-rank coals can be divided into two groups: K2-3 and the German hard coals STD-1 to STD-5 had a lower peak area than did K2-4, K2-5, and STN-2, despite comparable amounts of S. For example, the hard coals K2-3 and K2-5 have equal amounts of S, but the peak area of $^{34}H_2S^+$ of K2-3 is 97.1% smaller than the peak area of K2-5. Furthermore, the release of $^{34}H_2S^+$ for the lignites was found to exhibit a good negative correlation with the Ca/S ratio. This can be explained by the well-known capability of Ca to capture S. However, the release of the high-rank coals did not show a significant correlation with the Ca/S ratio. The correlation of the German hard coals STD-1 to STD-5 exhibited a moderate negative correlation (-0.63) with the peak areas of $^{34}H_2S^+$. This agrees with recently published data [Bläsing and Müller, 2010b]. In summary, the release of H_2S can be estimated with sufficient accuracy using the S and Ca content of the lignites under investigation.

Table 7. Correlation matrix of important species and the composition of the low-rank coals.

	$^{34}H_2S^+$	$^{36}HCl^+$	$^{39}K^+$ / $^{39}NaO^+$	$^{56}KOH^+$	$^{58}NaCl^+$	$^{74}KCl^+$
S	**0.858**	0.554	0.146	0.684	-0.286	-0.113
Cl	-0.047	0.023	-0.270	0.397	0.557	-0.035
Al	-0.028	0.344	0.691	-0.472	-0.667	-0.230
Ca	-0.518	0.062	0.574	-0.420	0.267	-0.449
Fe	0.499	0.040	-0.036	0.646	-0.300	0.230
K	0.388	0.546	0.613	-0.057	-0.657	-0.297
Mg	-0.503	-0.131	0.069	-0.484	0.497	-0.167
Na	-0.253	0.134	-0.060	-0.181	0.531	-0.501
Si	0.064	0.356	**0.740**	-0.352	-0.685	-0.247
Ca/S	**-0.770**	-0.453	-0.036	-0.451	0.184	-0.143
S/Cl	**0.716**	0.562	0.374	0.336	-0.591	-0.194
Na/Cl	-0.233	0.117	0.229	-0.513	-0.128	-0.450
Na/Si	0.091	0.022	-0.398	-0.009	0.161	-0.151

Table 8. Correlation matrix of important species and the composition of the high-rank coals.

	$^{34}H_2S^+$	$^{36}HCl^+$	$^{39}K^+$ / $^{39}NaO^+$	$^{56}KOH^+$	$^{58}NaCl^+$	$^{60}COS^+$	$^{64}SO_2^+$	$^{74}KCl^+$
S	-0.290	0.582	0.357	-0.452	-0.069	-0.348	-0.002	0.496
Cl	-0.568	**0.830**	0.090	-0.426	0.223	-0.524	-0.160	**0.755**
Al	0.561	-0.220	-0.139	-0.238	0.134	**0.824**	**0.719**	-0.010
Ca	0.306	-0.097	-0.181	0.468	-0.013	0.288	0.417	0.118
Fe	0.624	-0.212	-0.101	-0.057	-0.010	**0.776**	**0.807**	0.017
K	0.462	-0.086	-0.243	-0.324	0.233	**0.769**	**0.715**	0.119
Mg	0.230	0.129	-0.045	-0.132	0.232	0.434	0.528	0.368
Na	0.466	-0.614	0.196	0.871	-0.081	0.441	-0.006	-0.437
Si	0.666	-0.285	-0.014	-0.175	0.010	**0.874**	**0.770**	-0.076
Ca/S	0.410	-0.455	-0.200	0.786	-0.199	0.269	0.225	-0.310
S/Cl	**0.789**	0.487	-0.114	0.005	-0.286	**0.812**	**0.800**	-0.351
Na/Cl	**0.699**	**-0.670**	-0.181	0.654	-0.275	0.617	0.457	-0.513
Na/Si	0.195	-0.438	0.020	0.923	-0.312	-0.074	-0.189	-0.414

A likely explanation for the observed dependence of the release of $^{34}H_2S^+$ on rank was found in the mode of occurrence of S. S can be found in the form of inherent mineral matter or as organically bound S. There is a strong correlation between the form of S and the coal rank. Maes et al. [1997] reported that the most common S functionalities in low-rank coals are aryl–aryl and diaryl sulphides. The amount of thiophenes increases with increasing coal rank, and thiophenes are the main S group for bituminous coals. Nearly all S is fixed in the form of thiophenes in anthracites. Furthermore, the authors mentioned that the distribution of S structures can differ widely, even among coals of the same rank. The thermal stability of organic-bound S increases from sulphide to thiophene. The release of H_2S from pyrite and aryl sulphides occurs in the same temperature range [Maes et al., 1997]. Therefore, it can be concluded that S in the lignites, the Norwegian hard coal STN-2, and the hard coals K2-4 and K2-5 is mostly bound in a volatile form, and it is assumed that the main S forms are inorganic and organic sulphides. In contrast, the anthracite K2-3 and the German hard coals STD-1 to STD-5 showed a smaller released amount than was expected on the basis of the S content. It can be concluded that a significant part of the S is bound in the form of thiophenes and, therefore, is thermally more stable and is released during the char reactions phase. Support for the correctness of this conclusion can be found in the release of $^{64}SO_2^+$, as shown in Figure 62. The spectra of several coals of different ranks are depicted. All coals showed a high-intensity release of $^{64}SO_2^+$ during the devolatilisation phase (I), whereas only the anthracite K2-3 and the German hard coals showed a significant second-phase release during the char reactions phase (II). A likely explanation is that the thermally more stable thiophene-bound S was released during the char reactions phase. The thermally less stable S, which can occur in the form of inorganic and organic sulphides, was released during the devolatilisation phase at relatively low temperatures. The release during the char reactions phase was not quantified because the conditions ranged between gasification and combustion conditions.

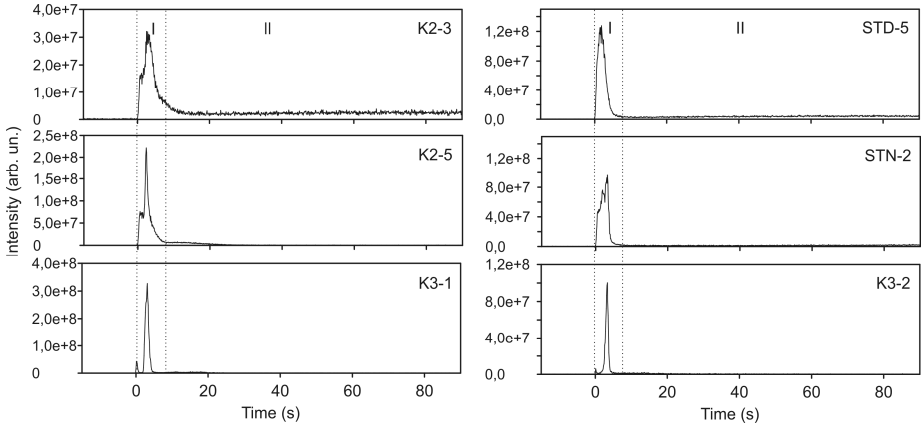

Figure 62. Spectra of $^{64}SO_2^+$ for several coals of different rank at 1400 °C and 7.5 v% O_2 with steam.

An additional explanation for the observed rank dependence of the release of $^{34}H_2S^+$ was found in the mode of occurrence of Ca. Correlations between coal rank and coal composition were investigated using 43 coals by Vassilev et al. [1996]. They highlighted the differences between low- and high-rank coals. Usually, low-rank coal ash is rich in basic oxides (e.g. MgO, CaO), whereas high-rank coal ash is rich in acid oxides (e.g. SiO_2, Al_2O_3). Commonly, the amount of organically fixed inorganic elements—e.g. organically fixed Ca—decreases with increasing coal rank. This can be explained by the decrease of functional groups (e.g. –COOH) that occurs with increasing rank. Weakly fixed, easily exchangeable ions can be removed or can form more stable compounds during coalification (e.g. ion-exchangeable fixed Ca can form calcite or water soluble alkali, and alkaline earth compounds can even be leached by ground water). The content of volatile organic sulphides and the content of available Ca decrease with increasing coal rank. Organically fixed Ca and S are released during devolatilisation, and, therefore, reactions of S and Ca can occur immediately; this is expressed by the negative correlation of the Ca/S ratio with the peak areas of $^{34}H_2S^+$ for the lignites (Table 7). The correlation for the hard coals was not of statistical significance (Table 8).

The S/Cl ratio also seems to be important to the release of $^{34}H_2S^+$ for both high- and low-rank coals. The release of $^{34}H_2S^+$ exhibited a moderate-to-good positive correlation with the S/Cl ratio, as shown in Tables 7 and 8. This indicates the occurrence of competing reactions between S and Cl.

The interpretation of the release of $^{60}COS^+/^{60}NaCl^+$ is somewhat arguable because of the overlapping mass-to-charge ratio. An estimation of the ratio of $^{60}COS^+$ and

$^{60}NaCl^+$ in the peak area was performed using calculations, as mentioned in Section 4.4. The amount of $^{60}COS^+$ was much higher for the lignites compared with the hard coals (except K2-4, K2-5, and STN-2). A likely explanation of the differences involves the release mechanism of COS. The decomposition of pyrite leads to the formation of H_2S under reducing conditions. COS is not formed, as shown by experimental studies [Van Krevelen, 1993]. Furthermore, the reaction of H_2S with CO_2 leads to the formation of COS and H_2O. However, the reaction kinetic is rather slow, and its contribution to the release of $^{60}COS^+$ is assumed to be rather small, as mentioned above. Pyrite and thermally stable thiophenes are commonly the main modes of occurrence of S in hard coals. Therefore, the significant release of $^{60}COS^+$ for the lignites and the hard coals K2-4, K2-5, and STN-2 must have its origin in organic sulphide. In contrast, according to the calculations, the anthracite K2-3 showed no release of $^{60}COS^+$; this can be explained by the modes of occurrence of S, which are assumed to be mostly pyrite and thiophenes.

The peak areas of $^{36}HCl^+$ exhibited good positive correlation (0.83) with the Cl content of the high-rank coals. However, the lignites showed no significant correlation. For the high-rank coals, a moderate negative correlation was found between the release of $^{36}HCl^+$ and the Na/Cl ratio. A likely explanation is that a high Na/Cl ratio leads to an enhanced formation of NaCl, which results in a smaller amount of Cl for the formation of HCl. In contrast, the low-rank coals showed a very poor correlation. Furthermore, the peak areas of $^{36}HCl^+$ were found to exhibit a negative correlation with the S/Cl ratio for the hard coals, whereas the lignites showed a positive correlation. A likely explanation of these different trends is given by the mode of occurrence of Cl in coal. Yudovich and Ketris [2006] highlighted two broad modes of occurrence of Cl in coal: inorganic-bound Cl in the form of discrete minerals—such as salt-like Cl (e.g. NaCl, a common Cl-bearing mineral) or, to a much smaller extent, Cl-containing silicates—and organic-bound Cl, with 'semi-organic' Cl sorbed to the coal matrix as the main form of organic-bound Cl. In addition, it was pointed out that the majority of Cl in coal seems to be associated with functional groups of the coal matter [Yudovich and Ketris, 2006; Tillman et al., 2006; Sheth and Rasnake, 1992]. Therefore, it can be concluded that the amount of organic-bound Cl decreases with increasing coal rank.

The release of $^{58}NaCl^+$ showed a strong dependence on the coal rank. The high-rank coals and the low-rank coals showed a moderate negative correlation with the S/Cl ratio (-0.51 and -0.59). Furthermore, the competitive reactions of S and Cl can influence the formation of NaCl, and therefore the ratio is important for the regulation of the formation of HCl and NaCl. It is assumed that S undergoes reactions with alkali metals that result in a reduced formation of alkali metal chloride. However, this is ra-

ther speculative; the formation of alkali metal sulphide may be of an intermediate character. Additionally, the occurrence of alkali metal sulphide was not predicted by the thermodynamic calculations.

Likely explanations for the observed differences are the following: Usually, much of the Na in lignite is found to be surface-bound to the coal matrix or associated with Cl; only some exists as Na-silicates [Raask, 1985; Yudovich and Ketris, 2006]. The amount of organically fixed Na decreases with increasing coal rank. Loosely bound Na usually forms volatile species during coal conversion. The Cl and the Na content of coal are correlated. In principle, the Cl content is a reliable indicator of the NaCl content of the coal. The differences in the peak areas can be explained by the mode of occurrence of Na. The lignites K2-1, K2-2, HKN-S-, HKN-S+, HKS, and HKT, as well as the hard coals K2-4, K2-5, and STN-2, have a high Na/Cl ratio, e.g. 16.2 for K2-2 and 44.9 for K2-4. It can be concluded that a significant portion of the Na did not occur in the form of NaCl. Furthermore, it is likely that a portion occurred in non-volatile form. The other coals have a relatively low Na/Cl ratio, and therefore it can be assumed that the portion of highly volatile Na is larger. These are likely explanations for the different release characteristics of $^{58}NaCl^{+}$. Furthermore, the ash-rich coals have a higher potential for the capture of Na, e.g. by aluminosilicate, which can lead to a reduced release of Na compounds. The suppression due to capture becomes increasingly significant at a kaolinite (Al_2O_3*2SiO_2*2H_2O)/Na molar ratio greater than 1.5 for a devolatilisation temperature of 1220 °C as mentioned in Section 2.3.

Additionally, the relatively low release of STN-2 can be explained by the lack of Cl, which functions as a carrier for the release of Na. Former investigations highlighted the importance of Cl during the release of alkali metals. In this context, Cl was often referred to as a carrier [Tillman et al., 2009]. Gottwald et al. [2002] reported the disproportionately high increase in alkali metal release in experiments with Cl-doped coals under fluidised bed combustion conditions. Regarding the chemical analysis in Tables 4 and 5, the amount of Cl is similar to the amount of Na for the five German hard coals. In contrast, there is a lack of Cl among the four Renish lignites and the Norwegian hard coal STN-2. The amount of Cl is about one order of magnitude smaller than the amount of Na. In conclusion, the release of Na in the form of NaCl is limited by the amount of Cl for coals that lack Cl, as shown by the experimental results. The noticeably high release of $^{39}NaO^{+}$ is an indicator that, during the experiments with steam, highly volatile NaOH is formed, as discussed in Section 5.3.

In general, the release of $^{39}K^{+}$/$^{39}NaO^{+}$ was high for the low-rank coals and low for the high-rank coals. An exception was the relatively high release from the high-rank coal K2-4. There was a difference of two orders of magnitude between the highest and

the lowest release. No significant correlation between the coal composition and the peak areas was found. Complementary explanations regarding the increase of the m/z = 39 signal were given above.

The correlation coefficients of $^{74}KCl^{+}$ and $^{56}KOH^{+}$ must be interpreted with care on account of the low signal-to-noise ratio of the signals. The peak areas were of equal quantity. In general, the release of the K species $^{56}KOH^{+}$ and $^{74}KCl^{+}$ was much smaller (two orders of magnitude) than the release of Na species, reflecting the commonly non-volatile character of K bound in coal. There was no significant trend related to the release of $^{56}KOH^{+}$ and the K content for the 17 coals under investigation. The release of the high-rank coals STD-1, STD-2, STD-3, STD-4, and STD-5 was one order of magnitude lower than the release of the low-rank coal with the highest release (K3-1). The peak areas exhibited a high positive correlation with the Cl content of the high-rank coals. For the hard coals under investigation, the peak areas of $^{56}KOH^{+}$ exhibited a high positive correlation (0.99) with the Na/Cl ratio, a high positive correlation with the Na/Si ratio (0.92), a high positive correlation with the Na/Al+Si ratio, a high positive correlation with the S/Cl ratio, and good negative correlations with the K/Si and K/Al+Si ratios (Table 8).

To aid in the interpretation of the experimental results, thermodynamic calculations were performed. The results are depicted in Figures 63 and 64.

Na-aluminosilicate is the main Na compound, from a thermodynamic point of view, when sufficient alumina and silica are available, as shown for the nine hard coals and the lignite HKT. The order of Na-containing compounds, starting with those with the highest amount, is Na-aluminosilicate > NaCl > NaOH > Na. The formation of Na-aluminosilicate was not predicted for the lignites HKN-S-, HKN-S+, and HKS. The main alkali metal species for the lignites HKN-S-, HKN-S+, and HKS were NaOH, Na, and NaCl. In most cases, NaOH was the main species.

According to the calculated predictions, K-aluminosilicate was the main K compound for all hard coals and for the lignites K3-1 and HKT. Other important K compounds were KCl, KOH, and K. For the hard coals, the amount of KCl exceeds the amount of KOH, except for STN-2. The main K compounds of the lignites K2-1, K2-2, K3-2, HKN-S-, HKN-S+, and HKS were KOH, KCl, and K. The formation of K-aluminosilicate was not predicted for these lignites.

In general, it was correctly predicted that the amount of alkali hydroxide would exceed the amount of alkali chloride for the lignites. The formation of alkali metal hydroxide was correctly predicted by thermodynamic calculations for both hard coals and lignites. However, the calculated increase was much lower than the experimental

findings. In addition, the calculations correctly predicted that the amount of NaOH and KOH formed from the lignites (except K3-1 and HKT) exceeded the amount formed from the hard coals, whereas the formation of NaCl from the hard coals was higher than that from the lignites during the experiments. This was not correctly predicted by the calculations. Aluminosilicates were found to be an efficient getter of alkali metals under gasification-like conditions at 1400 °C from a thermodynamic point of view. The differences between the experimental findings and the thermodynamic calculations are mainly kinetic in nature. Equilibrium is not reached during the batch-scale experiments.

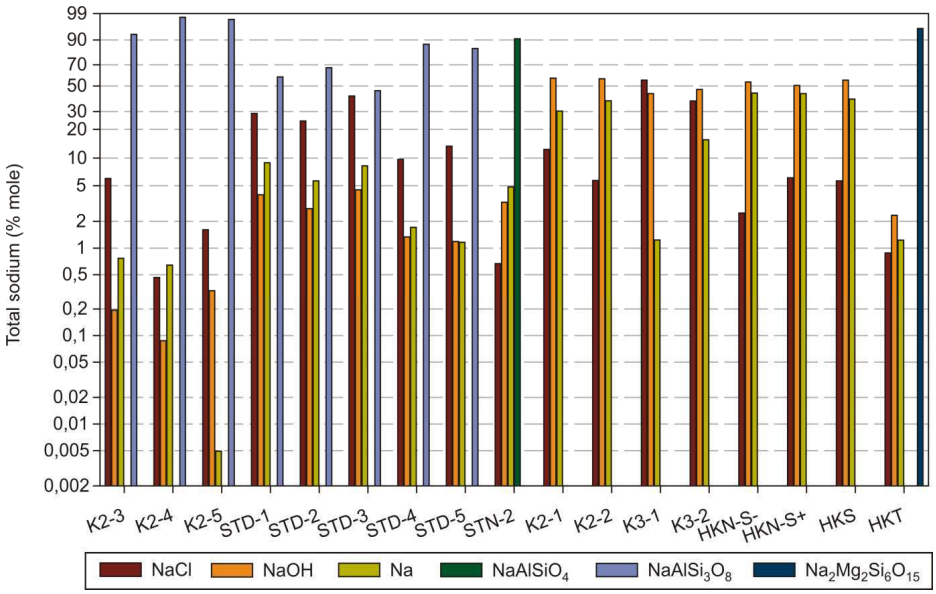

Figure 63. Thermodynamically stable compounds of Na at 1400 °C and λ = 0.5.

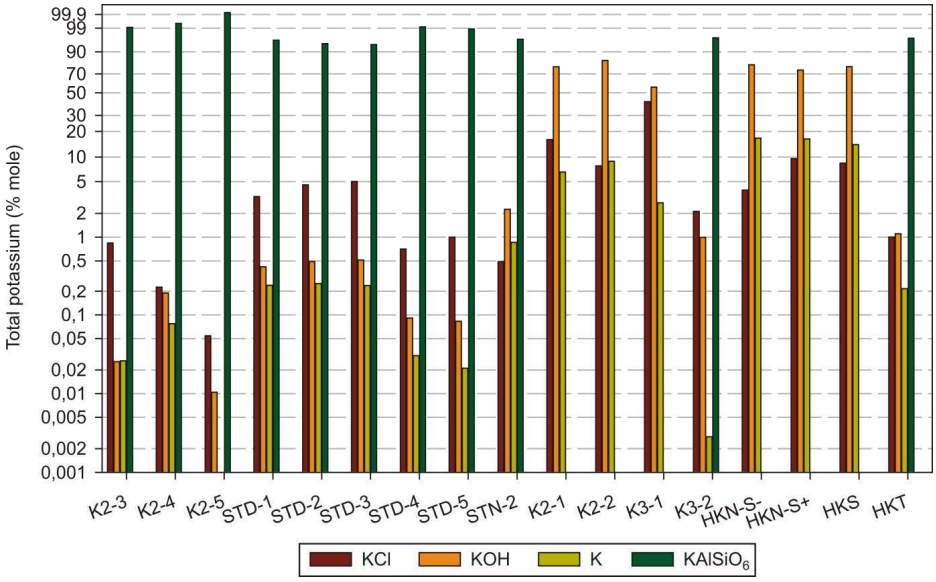

Figure 64. Thermodynamically stable compounds of K at 1400 °C and λ = 0.5.

5.5 Pressure

Regarding the release of $^{36}HCl^+$, $^{58}NaCl^+$, and $^{64}SO_2^+$, the experimental results are comparable to the results reported by Oleschko and Müller [2007a] and, specifically regarding NaCl, to the results of Reichelt et al. [2001]. Oleschko and Müller [2007a] explained the decreasing release of $^{36}HCl^+$, $^{58}NaCl^+$, and $^{64}SO_2^+$ with increasing pressure by pointing out that these species have a lower concentration in the gas phase. The increase in absolute pressure for a given partial pressure of a vapour compound, which is in equilibrium in a condensed phase, leads to a lower concentration in the gas phase. However, the influence is assumed to be rather small in the pressure range of the pressure experiments (2–6 bar). Additional explanations are now provided. In principle, there are two main mechanisms: first, the reduced formation of volatile compounds, which includes the explanation of Oleschko and Müller [2007a], and second, the enhanced capture of volatilised compounds. The investigation of Sathe et al. [2003] of the release of alkali and alkaline earth metals during devolatilisation of Victorian brown coal support the proposed classification. However, the two mechanisms occur at the same time, and the fraction of S released/captured is in variance regarding the conditions and the coal under investigation.

The influence of pressure on the release of $^{34}H_2S^+$ and $^{64}SO_2^+$ can be explained by the shift of several reactions, as partially shown in Section 2.3. The decomposition equilibrium of FeS_2 is shifted to the educts side by increasing pressure. Therefore, smaller amounts of gaseous S species were formed with increasing pressure. However, the shift is rather slight under the present experimental conditions, as shown by thermodynamic calculations and as assumed from the results of Xu and Kumagai [2003]. To describe the present results satisfactorily, further explanations are needed. A likely explanation of the release trend of $^{34}H_2S^+$ is the following: The formation of H_2S and char-bound S was described by Zevenhoven and Kilpinen [2002], as shown by way of example in the non-stoichiometric Eq. 17 and Eq. 18. Reaction 18 is suppressed under increasing pressure. Furthermore, H_2S can react with the remaining char to form stable thiophenic structures (Eq. 19). The reaction of released S with char is enhanced under increased pressure. As a result, smaller amounts of $^{34}H_2S^+$ were formed under increased pressure; this is in agreement with the present results and the results of Nichols et al. [1989].

Fuel-S $\longrightarrow$ H_2S + Char + Volatiles Eq. 18

Fuel-S $\longrightarrow$ Char-S + Volatiles Eq. 19

The released amount of the alkali metal species $^{41}K^+$/$^{41}NaO^+$, $^{58}NaCl^+$, and $^{74}KCl^+$ decreases with increasing pressure for both hard coals and lignites. A likely explanation is the following: In general, temperature and residence time have a significant influence on capture reactions. The role of the temperature was discussed in Section 5.2. The residence time of the volatilised species in the remaining coal is very important for the capture. Thus, the influence of pressure on the residence time needs to be discussed. Yang et al. [2007] investigated the influence of pressure on coal devolatilisation (up to 50 bar). They found that the majority of the volatiles evolved at 400–800 °C. The devolatilisation rate decreased and the amount of char increased with increasing pressure. Additionally, Gadiou et al. [2002] reported that increasing pressure leads to an increasing residence time of volatile products in the remaining char. In summary, the retarded mass transfer leads to the residence time of the released species increasing with increasing pressure; this effect can enhance capture reactions. On this topic, Sathe et al. [2003] reported an increased retention of Na within the coal char with increasing pressure. They explained the observation by referring to the retarded mass transfer due to increasing absolute pressure as well as to the chemical reactions responsible for the formation of volatile Na compounds.

The release of $^{36}HCl^+$ decreased for all coals under investigation. Regarding the reactions in Eq. 1 and Eq. 2 in Section 2.3, the increasing pressure caused a shift in the equilibrium to the educt side. Additionally, the retarded mass transfer out of the char could cause a reduced release of $^{36}HCl^+$ during the devolatilisation phase.

The results of thermodynamic modelling are shown in Figures 65 and 66. The most stable alkali metal compounds predicted by thermodynamic calculations are alkali metal chlorides, alkali metal hydroxides, atomic alkali metal species, and alkali metal aluminosilicates. Alkali metal aluminosilicates are by far the most abundant alkali metal compound for all hard coals and for the silica- and alumina-rich lignite HKT. For example, Na fixed in $NaAlSi_3O_8$ accounts for 72.8–80.1% of the total amount of Na in STD-1. For the lignites except K3-1 and HKT, alkali metal hydroxides are the most abundant alkali metal species, e.g. K fixed in hydroxide accounted for 80.2–86.5% of the total K in HKN-S-. The formation of alkali metal aluminosilicates and alkali metal hydroxides is, in most cases, slightly enhanced by increasing pressure. The formation of alkali metal chlorides and metallic species, in most cases, slightly decreases with increasing pressure, e.g. a decrease of 20% of KCl is predicted for STN-2 under pressure increasing from 2 to 6 bar, and a decrease of 46% of NaCl is predicted for similarly increasing pressures.

The results of the thermodynamic modelling confirm the assumption that increased pressure leads to retarded mass transfer and to enhanced capture of NaCl and KCl.

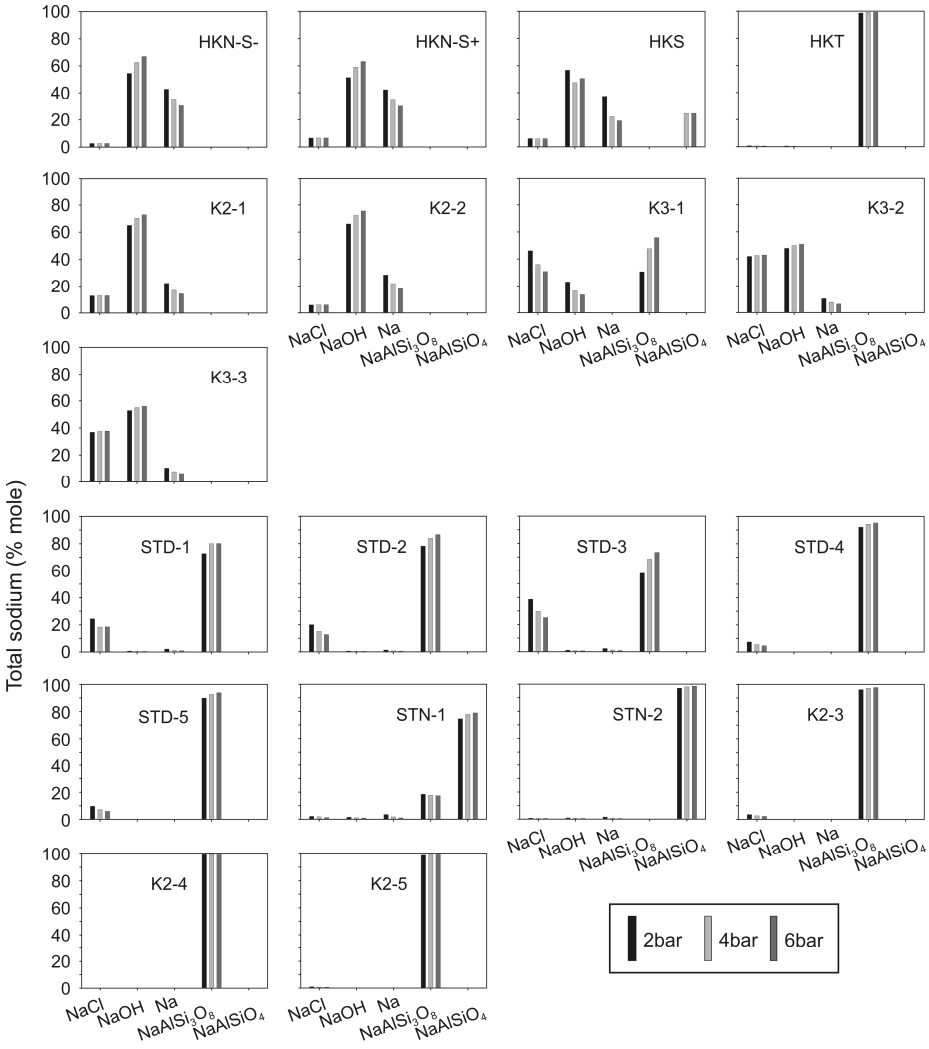

Figure 65. Thermodynamically stable compounds of Na at 1325 °C, 2–6 bar, and λ = 0.5.

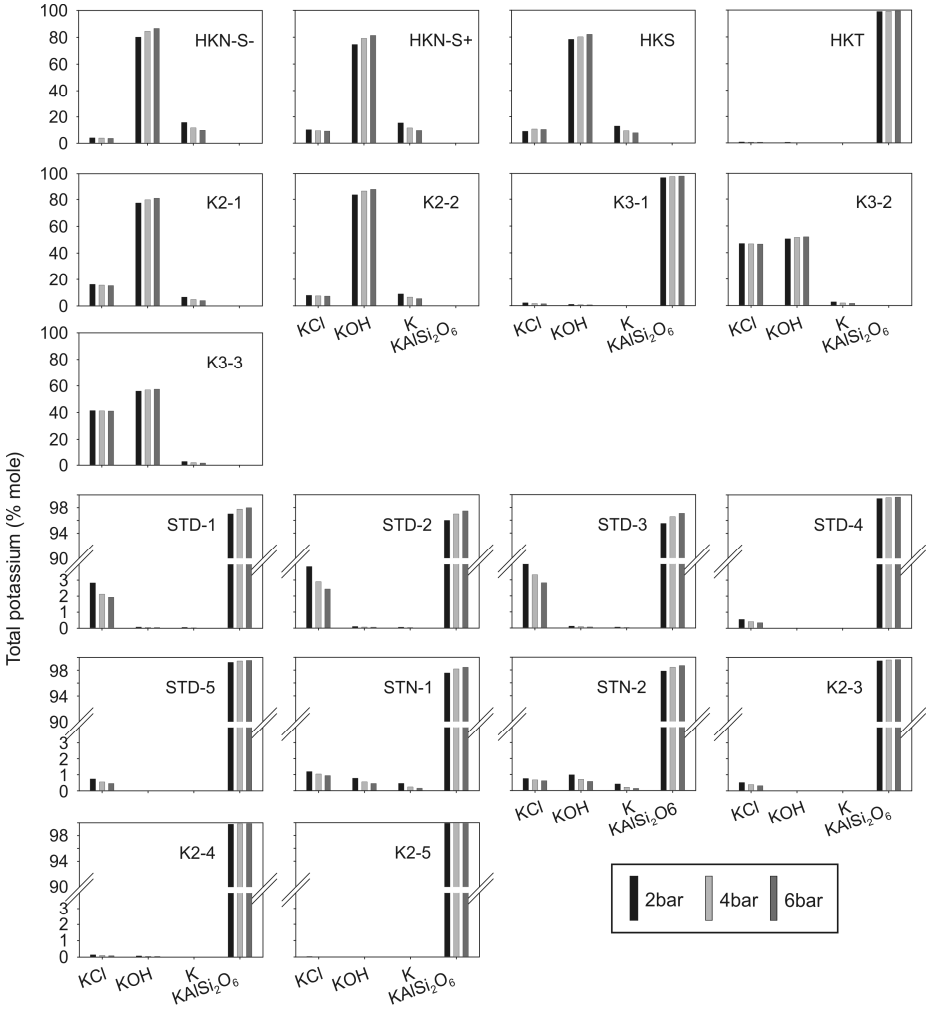

Figure 66. Thermodynamically stable compounds of K at 1325 °C, 2–6 bar, and λ = 0.5.

6 Summary and recommendations

The development of cleaner, more efficient techniques in next-generation coal power plants is becoming increasingly important, especially regarding to the discussion of the influence of CO_2 emissions on global warming. Coal-based combined-cycle power generation systems are currently under development. A promising coal utilisation process is the integrated gasification combined cycle (IGCC) process. In IGCC, a broad range of different coals can be used to produce fuel gas for gas turbines or synthesis gas for chemical applications. In addition, it offers the possibility of CO_2 sequestration. The first process step is the gasification of coal in an entrained-flow gasifier, which is operated at temperatures up to 1500 °C and pressures up to 3.0 MPa and which is able to use a wide variety of coals. The direct use of hot fuel gas for driving a gas turbine requires gas clean-up to prevent downstream parts of the gasifier from experiencing several problems, e.g. corrosion of the turbine blades and poisoning of catalysts and membranes caused by Na, K, S, and Cl compounds that are released during gasification. An increased efficiency and a decreased amount of harmful species can be achieved through hot fuel gas cleaning. This clean-up technique requires a comprehensive knowledge of the release characteristics of inorganic coal constituents. Despite research efforts during the last few decades, there are many open questions involving the release and the underlying release mechanisms, especially regarding the process conditions of high-temperature coal gasification.

The aim of this thesis was to provide enhanced knowledge of the effect of key process parameters (content of oxygen and steam, temperature, and pressure) and of the chemical constitution of several different coals on the release of inorganic species from high-temperature coal gasification. The focus was on the release of Na, K, S, and Cl species. Experiments were carried out under well-defined conditions with an emphasis on the influence of the conditions of entrained-flow gasification on the release.

The experimental setup consisted of atmospheric flow tube furnaces and a pressurised furnace. Online, in-situ analysis of the high-temperature product gas was carried out using molecular beam mass spectrometry. The rank of the investigated coals ranged from lignite to anthracite and covered a broad spectrum of different fuels with assumed qualitative and quantitative differences in the release characteristics. Additionally, experiments with model substances were performed in order to obtain more detailed information on the release mechanisms of selected species. The results of the experimental investigation were compared with thermodynamic calculations.

The experiments, as well as the equilibrium modelling, provided new information on the release of Na, K, S, and Cl species under the conditions of an entrained-flow gasifier. However, the significance of the calculations was often limited which could be caused by the non-equilibrium character of the experiments. Therefore, an advanced model including kinetics and thermodynamics of coal gasification should be invented.

Key chemical species detected by the mass spectrometer were $^{34}H_2S^+$, $^{36}HCl^+$, $^{39}K^+/^{39}NaO^+$, $^{56}KOH^+$, $^{58}NaCl^+$, $^{60}COS^+/^{60}NaCl^+$, $^{64}SO_2^+$, and $^{74}KCl^+$. The main findings are presented below.

Basic investigations on the oxygen content: Nine coals were gasified at 1400 °C in He/20% O_2 and He/7.5% O_2. The release of the inorganic species $^{34}H_2S^+$, $^{36}HCl^+$, $^{58}NaCl^+$, $^{64}SO_2^+$, and $^{74}KCl^+$ occurred mainly during devolatilisation and the char reactions phase. From a qualitative point of view, Na, K, and Cl species were unaffected by the oxygen content, whereas S formed H_2S and SO_2. Na_2SO_4 was not detected. From a quantitative point of view, several effects were found that allowed for the determination and confirmation of release mechanisms. Under the influence of a hydrogen-rich atmosphere, the dissociation of carboxylic-bound Na is enhanced. Therefore, the release of Na is likely to be enhanced during the gasification experiments. Furthermore, the capture of Na by Al-silicates is inhibited during the gasification experiments because H_2O and oxygen play an important role in the capture mechanism. These effects seem to overcome the enhanced capture capability, as described in the following: During the release process in the coal particle, the gaseous Na compounds must diffuse through a mineral-rich char matrix, and a significant fraction of the Na can react with silica. Retarded mass transfer, e.g. caused by a carbon layer or slower char conversion, should lead to a longer residence time of the released species and to an enhanced capture.

Temperature: Ten coals were gasified in He/7.5% O_2 at 1100–1700 °C. For the lignites, the release of $^{36}HCl^+$ decreased with increasing temperature, whereas the release of $^{58}NaCl^+$ increased for HKN-S-, HKN-S+, and HKS. Indications are given that the major release mechanism is the dissociation of carboxylic-bound Na species caused by reaction with hydrogen radicals. The mechanism is able to explain the increased release of $^{58}NaCl^+$ due to enhanced dissociation with increasing temperature. Additionally, higher amounts of NaCl lead to a lower amount of HCl as a result of reaction equilibrium. The divergent release of the lignite HKT is explained by the capture of Na by aluminosilicates, which seems to compensate for the enhanced release. For the hard coals, the release of $^{56}KOH^+$, $^{58}NaCl^+$, and $^{74}KCl^+$ increased with increasing temperature. The released amount of $^{36}HCl^+$ increased from 1100 to 1400 °C and decreased from 1400 to 1700 °C. The release of $^{64}SO_2^+$ decreased with increasing temperature,

whereas the amount of $^{34}H_2S^+$ increased. This is explained by a higher amount of hydrogen that occurs with increasing temperature, which enhances the formation of H_2S.

Steam: Ten coals were gasified at 1400 °C and 1 atm in a gas stream of He/7.5% O_2 with additional steam. The amount of $^{39}K^+/^{39}NaO^+$ and $^{56}KOH^+$ species increased significantly under the influence of steam. Cl and steam were identified as especially important to the release mechanism of Na and K. The present results confirm the release mechanism proposed in the literature, which includes the formation of intermediate NaOH. There were some differences found in the comparison of the experimental results and the thermodynamic calculations. The enhanced formation of alkali metal hydroxide under the influence of steam was correctly predicted. However, the calculated increase is much lower than that from the experimental findings; this is probably an effect of the non-equilibrium nature of the experiments. Aluminosilicates were found to be materials for the efficient capture of alkali metals under gasification conditions at 1400 °C from a thermodynamic point of view.

Coal rank: Seventeen coals were gasified at 1400 °C and 1 atm in a gas stream of He/7.5% O_2/2.5% H_2O. The modes of occurrence of several inorganic coal constituents were shown to have a remarkable effect on the release, e.g. the results could distinguish between thiole-bound S and thiophenic-bound S. The S content of coal is insufficient for predicting the release of $^{34}H_2S^+$. The release of $^{34}H_2S^+$ can be estimated with sufficient accuracy using the Ca/S ratio of the lignites under investigation. The release trend of the hard coals was more complex. However, the mode of occurrence of Ca seems to have a significant influence on the release of $^{34}H_2S^+$ for all coals under investigation. The S/Cl ratio seems to be important for the release of $^{34}H_2S^+$, regardless of the coal rank. This indicates the occurrence of competing reactions between S and Cl. The release of $^{58}NaCl^+$ showed a strong dependence on the coal rank. The high-rank coals and the low-rank coals exhibited a moderate negative correlation with the S/Cl ratio (-0.51 and -0.59). Furthermore, the competitive reactions of S and Cl can influence the formation of NaCl, and therefore the ratio is important for the regulation of the formation of HCl and NaCl. It is assumed that S undergoes reactions with alkali metals, resulting in a reduced formation of alkali metal chloride. The ash-rich coals have a higher potential for the capture of Na, e.g. by aluminosilicate, which can lead to a reduced release of Na compounds; this has been confirmed by the results of thermodynamic calculations. Na-aluminosilicate was the main Na compound, from a thermodynamic point of view, when sufficient alumina and silica were available. For low-ash coals, the main alkali metal species were NaOH, Na, and NaCl. In most cases, NaOH was the main species.

Pressure: Nineteen coals were gasified in He/7.5% O_2 at 2–6 bar and 1325 °C. All coals under investigation showed a decreasing release of the vapour species $^{34}H_2S^+$, $^{36}HCl^+$, $^{41}K^+/^{41}NaO^+$, $^{58}NaCl^+$, $^{64}SO_2^+$, and $^{74}KCl^+$ with increasing pressure. Likely explanations include a shift in reaction balance, retarded mass transfer, and, in consequence, an enhanced capture due to longer residence time of the volatilised compounds. In general, the thermodynamic calculations confirm the trends of decreasing alkali metal chloride release and of enhanced formation of alkali metal aluminosilicates.

Finally, the results of the study are used to formulate some important **recommendations**, from a scientific point of view, for the operation of a high-temperature gasifier. This means that several important variables—e.g. economic considerations—are excluded.

The high-temperature gasifier should work under elevated pressure on account of the extended residence time of the released species in the remaining char and the resulting enhanced capture, e.g. of alkali metals by aluminosilicates.

It is assumed that blending coals would have synergetic effects, e.g. blending clay-rich coals with Na-rich coals in order to utilise the natural capture capability of clay. However, various coal blends and the addition of additives should be investigated in more detail in order to better predict these synergetic effects.

The coals should have high aluminosilicate content on account of aluminosilicate's ability to capture alkali metals. Aluminosilicate could be used as an additive, as is already seen in the use of limestone to reduce the amount of S in combustion flue gas.

The alkali metal/Cl ratio of the coal should be high in order to minimise the amount of gaseous alkali metal chloride. This can be achieved by blending and gasification of a mixed coal.

The $Ca_{(carboxylic\ bound)}$/S ratio should be high in order to reduce the amount of released H_2S. For this reason, it could be beneficial to blend lignite of high Ca content with high-sulphur coals.

The steam content is a critical variable: first, it increases the release of alkali metal in the form of hydroxide species, and second, it decreases the amount of gaseous alkali metal species as a result of enhanced capture by aluminosilicates. However, the thermodynamic calculations showed a much lower increase.

8 Literature

AG Energiebilanzen (2010): www.ag-energiebilanzen.de, 23. Feb. 2011.

Attar, A.: Chemistry, thermodynamics and kinetics of reactions of sulphur in coal-gas reactions: A review, Fuel 1978, 57, 201-212.

Bakker, W.: High temperature corrosion in gasifiers, Materials Research 2004, 7, 53-59.

Beer, J.: High efficiency electric power generation: The environmental role, Progress in Energy and Combustion Science, 2007, 33, 107-134.

BGR – Bundesanstalt für Geowissenschaften und Rohstoffe: Energierohstoffe 2009 – Reserven, Ressourcen, Verfügbarkeit, Hannover 2009.

Blander, M., Sinha, S.: Calculations of the chemistry of coal combustion effluents, American Flame Research Committee, 1988, Pittsburgh, Pennsylvania.

Bläsing, M., Melchior, T., Müller, M.: Influence of the temperature on the release of inorganic species during high-temperature gasification of hard coal, Energy & Fuels 2010 (c), 24, 4153-4160.

Bläsing, M., Melchior, T., Müller, M.: Influence of the temperature on the release of inorganic species during high-temperature gasification of Rhenish lignite, Fuel Proc. Technology 2010 (d), 92, 511-516.

Bläsing, M., Müller, M.: Mass spectrometric investigations on the release of inorganic species during gasification and combustion of Rhenish lignite, Fuel 2010 (a), 89, 2417-2424.

Bläsing, M., Müller, M.: Mass spectrometric investigations on the release of inorganic species during gasification and combustion of German hard coals, Combustion and Flame 2010 (b), 157, 1374-1381.

Brinsmead, K.H., Kear, R.W.: Behaviour of sodium chloride during the combustion of carbon, Fuel 1956, 35, 84-93.

Brown, T.D.: Coal Gasification – Combined cycles for electricity production, Prog. Energy Combust. Sci. 1982, 8, 277-301.

Bundesministerium für Wirtschaft und Technologie: Energie in Deutschland – Trends und Hintergründe zur Energieversorgung in Deutschland, Berlin 2009.

Burdo, R.A., Morrison, G.H.: Table of atomic and molecular lines for spark source mass spectrometry of complex sample-graphite mixes, Department of Chemistry, Cornell University, Ithaca, NY, USA, Internal report 1670.

Burnham, C.W.: Part III: Silicate melts, fused satts and very concentrated solutions - The nature of multicomponent aluminosilicate melts, Physics and Chemistry of The Earth 1981, 13-14, 197-229.

Calkins, W.H.: The chemical forms of sulphur in coal: a review, Fuel 1994, 73, 475-484.

Cernic-Simic S.: A Study of factors that influence the behaviour of coal sulfur during carbonization, Fuel 1962, 41, 141-151.

Christou C., Hadjipaschalis I., Poullikkas A.: Assessment of integrated gasification combined cycle technology competitiveness. Renewable Sustainable Energy Rev 2008, 12, 2452-64.

Davidsson, K. O.; Engvall, K.; Hagstrom, M.; Korsgren, J. G.; Lönn, B.; Pettersson, J. B. C.: A surface ionization instrument for on-line measurements of alkali metal components in combustion: Instrument Description and Applications, Energy Fuels 2002, 16, 1369-1377.

Dayton, D. C., Belle-Oudry, D., Nordin, A.: Effect of coal minerals on chlorine and alkali metals released during biomass/coal cofiring, Energy & Fuels 1999, 13, 1203-1211.

Dayton, D.C., French, R.J.; Milne, T.A.: Direct observation of alkali release during biomass combustion and gasification. 1. Application of molecular beam/mass spectrometry to switchgrass combustion. Energy & Fuels 1995, 9, 855-865.

Descamps, C., Bouallou, C., Kanniche, M.: Efficiency of an integrated gasification combined cycle (IGCC) power plant including CO_2 removal, Energy 2008, 33, 874-881.

Drowart, J., Goldfinger, P.: Die Massenspektrometrie anorganischer Systeme bei hohen Temperaturen, Angewandte Chemie 1967, 79, 589-628.

Durie, R.A., Johnson, G.M., Smith, M.Y.: Gas phase reactions of sodium species with sulfur species in hydrocarbon flames, Symp. Combust. 1974, 15, 1123-1232.

Earth fact sheet, http://nssdc.gsfc.nasa.gov/planetary/factsheet/earthfact.html. abgerufen am 13.11.2010.

Eriksson, G., Hack, K.: Chemsage – A Computer program for the calculation of complex chemical equilibria, Metallurgical Transactions B 1990, 21, 1013-1023.

FAA - Gesamtverband des deutschen Steinkohlenbergbaus. 24/2006.

Formella, K., Leonhardt, P., Sulimma, A., van Heek, K.-H., Jüntgen, H.: Interaction of mineral matter in coal with potassium during gasification, Fuel 1986, 65, 1470-1472.

French, R.J., Dayton, D.C., Milne, T.A.: The direct observation of alkali sulphur species in biomass combustion and gasification, National Renewable Energy Laboratory, 1994.

Gadiou, G., Bouzidi, Y., Prado, G.: The devolatilisation of millimetre sized coal particles at high heating rate: the influence of pressure on the structure and reactivity of the char, Fuel 2002, 81, 2121-2130.

Gibb, W.H., Angus, J.G.: The release of potassium from coal during bomb combustion, J. Inst. Energy, 56, 1983, 149-157.

Glazer, M. P., Khan, N. A., de Jong, W., Spliethoff, H., Schürmann, H., Monkhouse, P.: Alkali metals in circulating fluidized bed combustion of biomass and coal: Measurements and Chemical Equilibrium Analysis, Energy & Fuels 2005, 19, 1889-1897.

Gottwald, U., Monkhouse, P., Bonn, B.: Dependence of alkali emissions in PFB combustion on coal composition, Fuel 2001, 80, 1893-1899.

Gottwald, U.; Monkhouse, P.; Wulgaris, N.; Bonn, B. In-situ study of the effect of operating conditions and additives on alkali emissions in fluidised bed combustion. Fuel Process. Technol. 2002, 75, 215-226.

Groen, J.C., Craig, J.R.: The inorganic geochemistry of coal, petroleum, and their gasification/combustion products, Fuel Processing Technology 1994, 40, 15-48.

Gryglewicz, G.: Effectiveness of high temperature devolatilisation in sulfur removal from coal, Fuel Proc. Techno. 1996, 46, 217-226.

GTW - Gas turbine world hand book, 25, 2006.

Gyo, S., Yang, J., Liu, Z.: The fate of fluorine and chlorine during thermal treatment of coals, Environ. Sci. Technol. 2006, 40, 7886-7889.

Halstead, W.D., Raask, E.: The behaviour of sulphur and chlorine compounds in pulverized-coal-fired boilers, Journal of the Institute of Fuel 1969, 344-349.

Halstead, W.D., Raask, E.: The behaviour of sulphur and chlorine compounds in pulverised coal fired boilers, Jour. Inst. Fuel 1968, 4-9.

Hansen, PFB., Andersen, K.H., Wieck-Hansen, K., Overgaard, P., Rasmussen, I., Frandsen, F.J. , Hansen, L.A., Dam-Johansen, K.: Co-firing straw and coal in a 150-MW utility boiler: in situ measurements, Fuel Processing Technology 1998, 54, 207-225.

Hastie, J.W., Bonnell, D.W., Schenck, P.K.: Development and application of very high temperature mass spectrometry. Vapor pressure determinations over liquid refractories, Pure Appl. Chem. 2000, 72, 2111–2126.

Hastie, J.W., Zmbov, K.F., Bonnel, D.W.: Transpiration mass spectrometric analysis of liquid KCl and KOH Vaporization, High Temperature Science 1984, 17, 333-364.

Helble, J.J., Srinivasachar, S., Boni, A.A., Charon, O., Modestino, A.: Measurement and modeling of vapor-phase sodium chloride formed during pulverized coal combustion, Combustion Science and Technologie 1992, 81, 192-205.

Hellhold, P.: Hochtemperaturreaktionen, Akademie-Verlag-Berlin 1983.

Herod, A. A., Hodges, N. J., Pritchard, E., Smith, C. A.: Mass spectrometric study of HCl and other volatiles from coals during mild heat treatment, Fuel 1983, 62, 1331-1336.

Higman, C.H., Van der Burgt, M.: Gasification, Gulf Professional Publishing; 2. Edition 2008.

Hodges, N. J., Richards, D. G.: The fate of chlorine, sulphur, sodium, potassium, calcium and magnesium during fluidized combustion of coal, Fuel 1989, 68, 440-445.

Howarth, O.W., Ratcliffe, G.S., Burchill, P.: Solid state nuclear magnetic resonance studies of sodium and aluminium in coal, Fuel 1987, 66, 34-39.

Huffman, G.P., Huggins, F.E., Levasseur, A.A., Durant, J.F., Lytle, F.W., Greegor, R.B., Mehta, A.: Investigation of atomic structures of calcium in ash and deposits produced during the combustion of lignite and bituminous coal, Fuel 1989, 68, 238-242.

Huffman, G.P., Huggins, F.E.: Analysis of the inorganic constituents in low-rank coals, ACS Symposium Series, 1984, 264.

Ibarra, J.V., Boneta, A.J., Moliner, R.: Release of volatile sulfur compounds during low temperature devolatilisation of coal.

IEA 2009 - International Energy Agency: World Energy Outlook , 2009.

Inaba, A.; Okada, K.: Coal utilization technology for reducing carbon dioxide emis-sion, Coal Science 1995, 1919-1922.

Joshi, M.M., Sunggyu, L.: Integrated gasification combined cycle – A review of IGCC technology, Energy Source, 1996, 18, 537-568.

Kanniche, M., Bouallou, C.: CO_2 capture study in advanced integrated gasification combined cycle, Applied Thermal Engineering 2007, 27, 2693–2702.

Khan, M.R.: Prediction of sulphur distribution in products during low temperature coal pyrolysis and gasification, Fuel 1989, 68, 1439-1449.

Kosminski, A., Ross, D.P., Agnew, J.B.: Influence of gas environment on reactions between sodium and silicon minerals during gasification of low-rank coal, Fuel Processing Technology 2006 (a), 87, 953-962.

Kosminski, A., Ross, D.P., Agnew, J.B.: Reactions between sodium and silica during gasification of a low-rank coal, Fuel Processing Technology 2006 (b), 87, 1037-1049.

Kosminski, A., Ross, D.P., Agnew, J.B.: Transformations of sodium during gasification of low-rank coal, Fuel Processing Technology 2006 (c), 87, 943-952.

Kowalski, T., Ludwig, C., Wokaun, A.: Qualitative evaluation of alkali release during the devolatilisation of biomass, Energy Fuels 2007, 21, 3017-3022.

Krishnan, G. N., Wood, B. J.: The fate of alkali species in advanced coal combustion systems, United States Department of Energy, Final Report, 1991.

Kühn, L., Plogman, H.: Reaction of catalysts with mineral matter during coal gasification, Fuel, 1983, 62, 205-208.

Kuramochi, H., Wu, W., Kawamoto, K.: Prediction of the behaviours of H_2S and HCl during gasification of selected biomass fuels by equilibrium calculation, Fuel 2005, 84, 377-387.

Li, X.T., Grace, J.R., Lim, C.J., Watkinson, A.P., Chen, H.P., Kim, J.R.: Biomass gasification in a circulating fluidized bed, Biomass Bioenergy 2004, 26, 171-193.

Lindner, E.R., Wall, T.F.: Sodium ash reactions during combustion of pulverised coal, 2007.

Lindner, H., Siebke, W., Simon, G.: Physik für Ingenieure, Fachbuchverlag Leipzig, 2006.

Lior, N.: Energy resources and use: The present situation and possible paths, to the future, Energy 2008, 33, 842-857.

Maes, I. I., Gryglewicz, G., Machnikowska, H., Yperman, J., Franco, D. V., Mullens, J., Van Poucke, L. C.: Rank dependence of organic sulphur functionalities in coal, Fuel 1997, 5, 391-395.

Manzoori, A.R., Linder, E.R., Agarwal, P.K.: Inorganic transformation during the circulating fluid bed combustion of low-rank coals with high content of sodium and sulphur, Inorganic transformations and ash deposition during combustion, 735-62.

Matsuoka, K., Yamashita, T., Kuramoto, K., Suzuki, Y., Takaya, A., Tomita, A.: Transformation of alkali and alkaline earth metals in low rank coal during gasification, Fuel 2008, 87, 885-893.

Merrick, D., Coal combustion and conversion technology, London 1984.

Miller, T.A.: Chemistry and chemical intermediates in supersonic free jet expansion, Science 1984, 223, 545-553.

Milne, T.A., Soltys, M.N.: Direct mass-spectrometric studies of the devolatilisation of carbonaceous fuels – I. A flame – Devolatilisation molecular-beam sampling technique, Journal of Analytical and Applied Devolatilisation 1983 (a), 5, 93-110.

Milne, T.A., Soltys, M.N.: Direct mass-spectrometric studies of the devolatilisation of carbonaceous fuels – II. A flame – Qualitative observations of primary and secondary processes in biomass 1983 (b), 5, 111-131.

Mondol, J.D., McIlveen-Wright, D., Rezvani, S., Huang Y., Hewitt, N.: Techno-economic evaluation of advanced IGCC lignite coal fueled power plants with CO_2 capture, Fuel 2009, 88, 2495-2506.

Monkhouse, P.: On-line diagnostic methods for metal species in industrial process gases, Progress in Energy and Combustion Science 2002, 28, 331-381.

Monkhouse, P.: On-line spectroscopic and spectrometric methods for the determination of metal species in industrial processes, Progress in Energy and Combustion Science 2011, 37, 125-171.

Müller, M., Pavone, D., Rieger, M., Abraham, R.: Hot fuel gas cleaning in IGCC at gasification temperature, Fourth International Conference on Clean Coal Technologies, Dresden, Germany May 2009.

Müller, M., Willenborg, W., Hilpert, K., Singheiser, L.: Structural dependence of alkali oxide activity in coal ash slags, in Proceedings of the VII International Conference on Molten Slags Fluxes and Salts, Cape Town, South Africa (2004) 615-618.

Müller, M., Willenborg, W., Hilpert, K., Singheiser, L.: Structural dependence of alkali oxide activity in coal ash slags, VII International Conference on Molten Slags Fluxes and Salts, The South African Institute of Mining and Metallurgy, 2004.

Müller, M., Wolf, K.J., Smeda, A., Hilpert, K.: Release of K, Cl, and S species during co-combustion of coal and straw, Energy & Fuels 2006, 20, 1444-1449.

Murakami, T., Naruse, I.: Prediction of evolution characteristics of alkali metal compounds in coal combustion/gasification from coal properties, Journal of Chemical Engineering of Japan 2001, 34, 899-905.

Murakami, T.: Fundamental evolution characteristics of alkali metal compounds in coal combustion, Kagaku Kogaku Ronbunshu 1999, 25, 389-394.

Neville, M., Sarofim, A.F.: The fate of sodium during pulverized coal combustion, Fuel, 1985, 64, 384-390.

Newby, R.A., Bannister, R.L.: Advanced hot gas cleaning systems for coal gasification processes, Transactions of the ASME 1994, 116, April 1994.

Newcomer, A., Jay, A.: Storing syngas lowers the carbon price for profitable coal gasification, Environ. Sci. Technol. 2007, 41, 7974–7979.

Nichols, K.M., Hedman, P.O., Smoot, L.D., Blackham, A.U.: Fate of coal-sulphur in a laboratory-scale coal gasifier, Fuel 1989, 68, 243-248.

Novakovic, A., Van Lith, S.C., Frandsen, F.J., Jensen, P.A., Holgersen, L.B.: Release of potassium from the systems K-Ca-Si and K-Ca-P, Energy & Fuels, 2009, 23, 3423-3428.

Nykänen, J.I.: The behaviour of alkali compounds and particles in high temperature filtration, PhD-thesis, Technical University of Helsinki, 2002.

Oader, Sheik: Natural gas substitutes from coal and oil, Elsevier, Amsterdam 1985.

Oleschko, H., Müller, M.: Influence of coal composition and operating conditions on the release of alkali species during combustion of hard coal, Energy & Fuels 2007 (a), 21, 3240-3248.

Oleschko, H., Müller, M.: Influence of coal composition on the release of Na-, K-, Cl- and S-species during the combustion of brown coal, Fuel 2007 (b), 86, 2275-2282.

Osborn, G. A.: Review of sulfur and chlorine retention in coal-fired boiler deposits, Fuel 1992, 71, 131-142.

Ota, R., Wakasugi, T., Kawamura, W., Tuchiya, B., Fukunaga, J.: Glass formation and crystallization in Li2O-Na2O-K2O-SiO2, Journal of Non-Crystalline Solids 1995, 188, 136-146.

Partanen, J., Backman, P., Backman, R., Hupa, M.: Adsorption of HCl by limestone in hot flue gases. Part I: the effects of temperature, gas atmosphere and adsorbent quality, Fuel 2005, 84, 1664-1673.

Porbatzki, D.: Freisetzung anorganischer Spezies bei der thermochemischen Umwandlung biogener Festbrennstoffe, PhD-thesis, RWTH Aachen, Aachen 2008.

Oleschko, H..: Freisetzung von Alkalien und Halogeniden bei der Kohleverbrennung, PhD-thesis, RWTH Aachen, Aachen 2007.

Questor GP Manual, March 26, 1998.

Raask, E.: Mineral impurities in coal combustion, Hemisphere Publishing Corporation, 1985.

Raask, E.: Sulphate capture in ash and boiler deposits in relation to SO_2 emission, Prog. Enery Combust. Sci. 1982, 8, 261- 276.

Reichelt, T.: Freisetzung gasförmiger Alkaliverbindungen bei atmosphärischer und druckaufgeladener Verbrennung, VDI-Verlag GmbH, Düsseldorf 2001.

Richet, P., Roskosz, M., Roux, J.: Glass formation in silicates: Insights from composition, Chemical Geology 2006, 225, 388-401.

Ryś, M.: Investigation of Thermodynamic Properties of Alkali Metals in Oxide Systems Relevant to Coal Slags, PhD-thesis, RWTH Aachen, Aachen 2007.

Sakanishi, K., Saito, I., Ishom, F., Watanabe, I., Mochida, I., Okuyama, N., Deguchi, T., Simazaki, K.: Characterization and elution behaviours of organically associated minerals in coals during acid treatment and solvent extraction, Fuel 2002, 81, 1471-1475.

Sathe, C., Hayashi, J., Li, C.Z., Chiba, T.: Release of alkali and alkaline earth metallic species during rapid devolatilisation of a Victorian brown coal at elevated pressure, Fuel 2003, 82, 1491-1497.

Scandrett, L.A.: The thermodynamics of alkali removal from coal-derived gases, J. Inst. Energy, 1984, 57, 391-397.

Schairer, J.F.: Melting relations of the common rock-forming oxides, Journal of the American Ceramic Society 1957, 40, 215-235.

Schmidt, J.: Vergasung, Deutscher Verlag für Grundstoffindustrie, Leipzig 1966.

Schürmann, H., Monkhouse, P, Unterberger, S., Hein, K.R.G.: In situ parametric study of alkali release in pulverized coal combustion: Effects of operating conditions and gas composition, Proceedings oft he Combustion Institute 2007, 31, 1913-1920.

Schürmann, H., Unterberger, S., Hein, K.R.G., Monkhouse, P., Gottwald, U.: The influence of fuel additives on the behaviour of gaseous alkali-metal compounds during pulverised coal combustion, Faraday Discuss, 2001, 119, 433-444.

Shah, A.D., Huffman, G.P., Huggins, F.E., Shah, N., Helble, J.J.: Behaviour of carboxyl-bound potassium during combustion of an ion-exchanged lignite, Fuel Processing Technology 1995, 44, 105-120.

Shemwell, B., Levendis, Y.A., Simons, G.: Laboratory study on the high-temperature capture of HCl gas by dry-injection of calcium-based sorbents, Chemosphere, 2001, 42, 785-796.

Sheth, A. C., Li, J., Rasnake, D. G.: Interactions between potassium and sulfur species in a coal-fired magnetohydrodynamics system, Air Waste Manage. Assoc. 1992, 42, 1466-1472.

Sonoyama, N., Okuno, T., Masek, O., Hosokai, S., Li, C.-Z., Hayashi, J.-I.: Interparticle desorption and re-adsorption of alkali and alkaline earth metallic species within a bed of pyrolyzing char from pulverized woody biomass, Energy & Fuels, 2006, 20, 1294-1297.

Speight, J.G.: Handbook of Coal Analysis, Wiley-Interscience, New Jersey 2005.

Spiro, C.L., Wong, J., Lytle, F.W., Greegor, R.B., Maylotte, D.H., Lamson, S.H.: Forms of potassium in coal and its combustion products, Fuel 1986, 65, 327-336.

Srinivasachar, S., Helble, J.J., Boni, A.A., Shah N., Huffman, G.P., Huggins, F.E.: Mineral behaviour during coal combustion 2. Illite transformations, Prog. Energy Combust. Sci. 16, 1990b, 293-302.

Srinivasachar, S., Helble, J.J., Boni, A.A.: Mineral behaviour during coal combustion 1. Pyrite transformations, Prog. Energy Combust. Sci. 16, 1990a, 281-292.

Steffin, C.: Freisetzung und Einbindung von Alkalien bei der Verbrennung und Vergasung von Kohle unter Druck, Shaker Verlag, Diss., 1999.

Steinberg, M., Schofield, K.: The chemistry of sodium with sulfur in flames, Prog. Energy Combust. Sci., 1990, 16, 311-317.

Stemmler, M.: Chemische Heißgasreinigung bei Biomassevergasungsprozessen, PhD-thesis, RWTH Aachen, Aachen 2010.

Strohbeen, D.T.: An investigation of the reactions leading to volatilization of inorganic sulfur during pyrolysis with vanillic acid and sodium gluconate, PhD-thesis, The Institute of Paper Chemistry, Appleton Wisconsin, 1981.

Takarada, T., Ishikawa, H., Abe, H., Nakaike, Y.: Alkali volatilization during devolatilisation and gasification of coal, Coal Science, 1995, 687-690.

Takuwa, T., Mkilaha, I.S.N., Naruse, I.: Mechanisms of fine particulates formation with alkali metal compounds during coal combustion, Fuel Vol. 85, 2006, 671-678.

Takuwa, T., Naruse, I: Emission control of sodium compounds and their formation mechanisms during coal combustion, Proceedings of the Combustion Institute 2007, 31, 2863-2870.

Thompson, D., Argent, B.B.: The mobilisation of sodium and potassium during coal combustion and gasification, Fuel 1999, 78: 1679–1689.

Tillman, D.A., Duong, D., Miller B.: Chlorine in solid fuels fired pulverized boilers – sources, forms, reactions, and consequences: a literature review, Energy & Fuels, 2009.

Tomeczek, J.; Palugniok, H. Kinetics of mineral matter transformation during coal combustion. Fuel 2002, 81, 1451−1258.

Van Eyk, P. J., Ashman, P. J., Alwahabi, Z. T., Nathan G. J.: Quantitative measurement of atomic sodium in the plume of a single burning coal particle, Combustion and Flame 2008, 155, 529-537.

Van Eyk, P.J., Wong, C.Y., Syred, N., Ung, E.P., Alwahabi, Z.T., Ashman, P.J., Nathan, G.J.: Study on atomic sodium release from pulverised coal particles in a pre-mixed natural gas flame, Fourth Australian Conference on Laser Diagnostics in Fluid Mechanics and Combustion, The University of Adelaide, South Australia, 7-9 December, 2005.

Van Krevelen, D.W.: Coal – typology, physics, chemistry, constitution, Amsterdam, Elsevier, 1993.

Vassilev, S.V., Kitano, K., Vassileva, C.A.: Some relationships between coal rank and chemical and mineral composition, Fuel 1996, 75, 1537-154

Wall, T.F.: Combustion processes for carbon capture, Proceedings of the Combustion Institute 2007, 31, 31-47.

Wang, Q., Qiu, J., Liu, Y., Zheng, C.: Effect of atmosphere and temperature on the speciation of mineral in coal combustion, Fuel Processing Technology 2004, 85, 1431-1441.

Wei, X., Huang, J., Liu, T., Fang, Y., Wang, Y.: Transformation of alkali metals during devolatilisation and gasification of a lignite, Energy & Fuels, 2008.

Wibberley, L.J., Wall, T.: Alkali-ash reactions and deposit formation in pulverized-coal-fired boilers: experimental aspects of sodium silicate formation and formation of deposits, Fuel, 1982a, 61, 87-92.

Wibberley, L.J., Wall, T.: Alkali-ash reactions and deposit formation in pulverized-coal-fired boilers: the thermodynamic aspects involving silica, sodium, sulphur and chlorine, Fuel 1982b, 61, 93-99.

Willenborg, W., Müller, M., Hilpert, K.: Alkali Removal at about 1400°C for the pressured pulverized coal combustion combined cycle., 1. Thermodynamics and Concept, Energy & Fuels, 2006, 20, 2593-2598.

Wolf K. J.: Untersuchungen zur Freisetzung und Einbindung von Alkalien bei der reduzierenden Druckwirbelschichtverbrennung, PhD-thesis, RWTH Aachen, Aachen 2003.

Wolk, R. H.; McDaniel, J.: High efficiency coal fuelled power generation, Energy Convers. Mgmt. 1992, 33, 705-712.

Wu, P., Erriksson, G., Pelton, A.D.: Optimization of the thermodynamic properties and phase diagrams of the Na_2O-SiO_2 and K_2O-SiO_2 systems, Journal of the American Ceramics Society 1993, 76, 2059-2064.

Xu, W.C., Kumagai, M.: Sulfur transformation during rapid hydrodevolatilisation of coal under pressure by using a continous free fall pyrolyszer, Fuel 2003, 82, 245-254.

Yan, J., Yang, J., Liu, Z.: SH Radical: The key intermediate in sulphur transformation during thermal processing of coal, Environ. Sci. Technol. 2005, 39, 5043-5051.

Yan, R., Gauthier, D., Flamant, G.: Volatility and chemistry of trace elements in a coal combustor, Fuel 80 2001, 2217-2226.

Yang, H., Chen, H., Ju, F., Yan, R., Zhang, S.: Influence of pressure on coal devolatilisation and char gasification, Energy & Fuels 2007, 21, 3165-3170.

Yudovich, Y.E., Ketris, M.P.: Chlorine in coal: A review, Coal Geology 2006, 67, 127-144.

Zevenhoven, R., Kilpinen, P.: Control of pollutants in flue gases and fuel gases, ebook, 2002.

9 Appendix

9.1 Setup of the MBMS

Table A. 1. Setup of the MBMS.

Ionisation:	Cathode	Emission voltage:	-50 V
		Emission current:	1.0 mA
Lens:	Optic	Ion region:	8 V
		Extractor:	-10 V
		Lens 1/3:	-370 V
		Lens 2:	9 V
		Quadrupole entrance:	-10 V
		Quadrupole exit:	-40 V
		Dynode voltage:	5000 V
		Dynode polarity:	negative
Recipient:		Front nozzle:	0.3 mm
		Skimmer:	1.0 mm
		Blende Kammer 2/3:	1.5 mm

9.2 Results in tables

9.2.1 Influence of the oxygen content

Table A. 2. Experimental results: Averaged, normalised peak areas (-).

7.5v% O_2	**m/z**	**34**	**36**	**58**	**64**	**74**
	STD-1	2.68E-03	1.34E-02	3.68E-03	3.94E-02	6.79E-05
	STD-2	9.55E-03	1.90E-02	4.73E-03	2.56E-02	9.75E-05
	STD-3	2.62E-02	2.76E-02	4.35E-03	3.90E-02	1.12E-04
	STD-4	7.65E-04	2.09E-02	4.05E-03	4.35E-02	1.39E-04
	STD-5	3.37E-03	3.62E-02	4.54E-03	6.23E-02	1.45E-04
	m/z	**34**	**36**	**39**	**58**	**64**
	HKN-S-	3.08E-02	2.75E-03	3.77E-01	3.59E-03	-
	HKN-S+	3.86E-02	5.38E-03	4.57E-01	5.71E-03	-
	HKS	2.21E-02	5.08E-03	7.40E-01	6.26E-03	-
	HKT	2.92E-02	5.70E-03	3.93E-01	1.94E-03	-
20v% O_2	**m/z**	**34**	**36**	**58**	**64**	**74**
	STD-1	0.00E+00	2.63E-02	1.28E-02	6.54E-02	4.01E-03
	STD-2	0.00E+00	4.02E-02	1.64E-02	6.16E-02	9.86E-03
	STD-3	0.00E+00	4.24E-02	1.67E-02	9.66E-02	7.61E-03
	STD-4	0.00E+00	3.22E-02	5.03E-02	6.77E-02	2.17E-02
	STD-5	0.00E+00	5.82E-02	4.15E-02	9.93E-02	1.38E-02
	m/z	**34**	**36**	**39**	**58**	**64**
	HKN-S-	0.00E+00	1.41E-03	6.88E-02	1.53E-03	1.07E-02
	HKN-S+	0.00E+00	1.88E-03	3.93E-01	2.15E-03	3.45E-02
	HKS	0.00E+00	2.91E-03	4.55E-01	2.10E-03	2.25E-02
	HKT	0.00E+00	3.62E-03	2.01E-01	6.69E-04	2.21E-02

Table A. 3. Results of thermodynamic modelling: Fugacity in atm.

Lambda 1.0		**H_2S**	**HCl**	**NaCl**	**SO_2**	**KCl**
	STD-1	0.00E+00	5.30E-05	1.35E-04	2.28E-03	1.73E-04
	STD-2	0.00E+00	6.16E-05	2.32E-04	2.42E-03	1.89E-04
	STD-3	0.00E+00	8.92E-05	2.19E-04	2.88E-03	2.64E-04
	STD-4	0.00E+00	5.99E-05	2.43E-04	3.07E-03	1.84E-04
	STD-5	0.00E+00	1.09E-04	4.19E-04	3.69E-03	3.18E-04
	HKN-S-	0.00E+00	1.08E-06	3.26E-05	8.08E-04	-
	HKN-S+	0.00E+00	2.90E-06	7.95E-05	1.98E-03	-
	HKS	6.31E-08	1.39E-05	4.85E-05	1.49E-03	-
	HKT	2.98E-06	6.11E-06	2.21E-05	2.14E-03	-
Lambda 0.5		**H_2S**	**HCl**	**NaCl**	**SO_2**	**KCl**
	STD-1	1.99E-03	4.37E-05	9.90E-05	0.00E+00	2.19E-04
	STD-2	2.09E-03	5.44E-05	1.80E-04	0.00E+00	2.49E-04
	STD-3	2.41E-03	7.45E-05	1.72E-04	0.00E+00	3.25E-04
	STD-4	2.65E-03	3.81E-05	2.74E-04	0.00E+00	2.08E-04
	STD-5	3.37E-03	7.92E-05	4.92E-04	0.00E+00	3.73E-04
	HKN-S-	6.82E-04	1.97E-06	2.96E-05	8.45E-06	-
	HKN-S+	1.65E-03	5.12E-06	7.22E-05	1.86E-05	-
	HKS	1.26E-03	1.02E-05	5.46E-05	1.45E-05	-
	HKT	1.82E-03	3.98E-06	2.34E-05	1.33E-05	-

9.2.2 Influence of the temperature

Table A. 4. Experimental results: Averaged, normalised peak areas (-).

Temperature	**1100 °C**		**1400 °C**		**1700 °C**	
m/z = 34	Mean	Variance	Mean	Variance	Mean	Variance
STD-1	1.78E-03	4.69E-04	1.23E-02	7.45E-03	5.54E-02	1.46E-02
STD-2	1.08E-03	2.38E-04	2.31E-02	7.00E-03	6.71E-02	9.25E-03
STD-3	4.33E-04	1.11E-04	3.58E-02	1.17E-02	1.12E-01	1.42E-02
STD-4	2.86E-03	1.71E-03	2.42E-03	1.48E-03	5.99E-02	1.48E-02
STD-5	8.83E-04	3.38E-04	4.48E-03	1.86E-03	5.20E-02	1.28E-02
STN-2	4.26E-03	2.89E-03	6.61E-02	1.73E-02	7.83E-02	1.64E-02
HKN-S-	2.80E-02	3.47E-03	3.08E-02	2.79E-03	1.29E-02	2.62E-03
HKN-S+	3.36E-02	8.16E-03	4.25E-02	4.94E-03	2.17E-02	2.87E-03
HKS	3.57E-02	3.63E-03	2.65E-02	1.82E-03	8.28E-03	1.95E-03
HKT	4.36E-02	1.04E-03	3.80E-02	2.37E-03	3.35E-02	4.19E-03
m/z = 36	Mean	Variance	Mean	Variance	Mean	Variance
STD-1	5.14E-02	2.57E-02	6.04E-02	3.90E-03	3.71E-02	1.47E-02
STD-2	8.39E-02	1.02E-02	9.71E-02	4.03E-03	7.03E-02	1.45E-02
STD-3	1.08E-01	9.39E-03	1.16E-01	5.30E-03	8.01E-02	1.35E-02
STD-4	6.42E-02	7.69E-03	8.56E-02	2.41E-03	4.65E-02	5.08E-03
STD-5	1.10E-01	1.25E-02	1.62E-01	4.80E-03	6.74E-02	1.80E-02
STN-2	4.74E-03	1.67E-03	9.65E-03	1.29E-03	5.04E-03	1.98E-03
HKN-S-	2.90E-03	9.29E-04	3.45E-03	7.74E-04	1.32E-03	4.19E-04
HKN-S+	6.94E-03	9.24E-04	5.59E-03	6.21E-04	1.38E-03	7.20E-04
HKS	4.67E-03	7.53E-04	3.73E-03	4.46E-04	1.88E-03	4.82E-04
HKT	6.30E-03	1.00E-03	4.66E-03	1.10E-03	4.90E-03	7.63E-04
m/z = 58	Mean	Variance	Mean	Variance	Mean	Variance
STD-1	2.88E-03	1.92E-03	3.44E-03	6.71E-04	5.29E-03	2.25E-03
STD-2	3.40E-03	1.51E-03	5.06E-03	1.32E-03	1.06E-02	1.65E-03
STD-3	5.16E-03	1.31E-03	5.62E-03	9.36E-04	1.11E-02	1.49E-03
STD-4	4.48E-03	1.72E-03	3.48E-03	1.23E-03	9.37E-03	1.69E-03
STD-5	1.00E-02	3.51E-03	4.35E-03	1.25E-03	1.02E-02	2.52E-03
STN-2	3.16E-04	2.92E-04	7.48E-04	2.04E-04	1.15E-03	2.12E-04
HKN-S-	2.77E-03	5.83E-04	3.37E-03	3.09E-04	3.29E-03	1.22E-03
HKN-S+	2.60E-03	2.93E-04	4.78E-03	6.51E-04	5.93E-03	9.72E-04
HKS	3.34E-03	6.78E-04	4.92E-03	5.59E-04	5.42E-03	4.59E-04
HKT	1.49E-03	2.60E-04	1.63E-03	3.20E-04	1.54E-03	3.92E-04

m/z = 64	Mean	Variance	Mean	Variance	Mean	Variance
STD-1	1.42E-01	7.76E-03	1.48E-01	1.87E-02	9.59E-02	2.54E-02
STD-2	1.53E-01	1.02E-02	1.30E-01	1.27E-02	6.74E-02	1.48E-02
STD-3	2.56E-01	8.99E-03	2.08E-01	2.01E-02	8.05E-02	1.40E-02
STD-4	1.85E-01	1.07E-02	1.71E-01	1.05E-02	1.29E-01	2.24E-02
STD-5	2.90E-01	9.29E-03	2.50E-01	1.37E-02	1.32E-01	4.05E-02
STN-2	2.85E-01	1.12E-02	1.81E-01	3.76E-02	8.58E-02	2.94E-02
HKN-S-	4.71E-02	6.12E-03	3.79E-02	1.18E-02	5.28E-02	4.55E-03
HKN-S+	1.25E-01	1.32E-02	9.76E-02	3.45E-03	1.20E-01	2.46E-03
HKS	6.02E-02	2.97E-02	7.31E-02	2.60E-03	9.77E-02	7.46E-03
HKT	1.13E-01	1.14E-02	1.13E-01	1.02E-02	8.94E-02	1.01E-02

m/z = 74	Mean	Variance	Mean	Variance	Mean	Variance
STD-1	4.86E-05	2.58E-05	3.21E-05	1.05E-05	7.90E-05	4.03E-05
STD-2	1.05E-05	3.81E-06	1.84E-04	1.05E-04	3.44E-04	8.89E-05
STD-3	1.20E-04	4.44E-05	6.24E-05	2.78E-05	4.81E-04	1.82E-04
STD-4	4.74E-05	2.53E-05	4.68E-05	1.48E-05	1.22E-03	1.45E-04
STD-5	1.02E-04	3.54E-05	1.61E-04	7.85E-05	2.22E-03	2.37E-04
STN-2	7.86E-06	4.69E-06	1.72E-05	1.81E-05	3.45E-05	1.94E-05

9.2.3 Influence of the steam content

Table A. 5. Experimental results: Averaged, normalised peak areas (-).

	With steam		Without steam	
m/z = 23	**Mean**	**Variance**	**Mean**	**Variance**
HKN-S-	4.06E-02	1.20E-02	0.0112	5.35E-03
HKN-S+	3.23E-02	1.48E-02	0.0101	1.54E-03
HKS	9.24E-02	5.00E-02	0.0113	4.08E-04
HKT	1.37E-02	2.20E-03	3.51E-03	5.29E-04
STD-1	7.58E-03	2.10E-03	5.11E-03	1.53E-03
STD-2	1.19E-02	2.09E-03	7.63E-03	4.58E-04
STD-3	9.67E-03	1.84E-03	7.85E-03	3.73E-04
STD-4	1.70E-02	5.49E-03	5.99E-03	5.25E-04
STD-5	2.58E-02	2.79E-03	8.02E-03	1.42E-03
STN-2	1.60E-02	5.89E-03	1.24E-03	4.92E-04
m/z = 34	**Mean**	**Variance**	**Mean**	**Variance**
HKN-S-	2.68E-02	2.39E-03	0.0308	2.79E-03
HKN-S+	4.51E-02	2.91E-03	0.0425	4.94E-03
HKS	1.62E-02	8.43E-03	0.0265	1.82E-03
HKT	2.23E-02	5.63E-03	0.038	2.37E-03
STD-1	9.59E-03	6.35E-03	1.23E-02	7.45E-03
STD-2	9.19E-03	3.94E-03	2.31E-02	7.00E-03
STD-3	9.00E-03	4.69E-03	3.58E-02	1.17E-02
STD-4	3.73E-03	1.67E-03	2.42E-03	1.48E-03
STD-5	1.01E-02	8.75E-03	4.48E-03	1.86E-03
STN-2	5.14E-02	6.25E-03	6.61E-02	1.73E-02
m/z = 36	**Mean**	**Variance**	**Mean**	**Variance**
HKN-S-	3.53E-03	4.17E-04	3.45E-03	7.74E-04
HKN-S+	4.53E-03	1.08E-03	5.59E-03	6.21E-04
HKS	2.94E-03	3.94E-04	3.73E-03	4.46E-04
HKT	4.37E-03	1.17E-03	4.66E-03	1.10E-03
STD-1	5.19E-02	4.52E-03	6.04E-02	3.90E-03
STD-2	6.51E-02	1.68E-02	9.71E-02	4.03E-03
STD-3	9.36E-02	9.91E-03	1.16E-01	5.30E-03
STD-4	6.38E-02	2.19E-02	8.56E-02	2.41E-03
STD-5	1.21E-01	1.42E-02	1.62E-01	4.80E-03
STN-2	4.06E-03	1.11E-03	9.65E-03	1.29E-03

m/z = 39	Mean	Variance	Mean	Variance
HKN-S-	3.71E-01	1.19E-01	0.0706	0.0895
HKN-S+	2.97E-01	2.22E-01	8.05E-03	4.50E-03
HKS	8.46E-01	4.25E-01	0.0181	0.0186
HKT	1.08E+00	1.59E-01	0.0157	0.0262
STD-1	2.90E-02	8.32E-03	9.69E-03	1.89E-03
STD-2	3.72E-02	2.22E-02	2.17E-02	1.00E-02
STD-3	3.19E-02	1.36E-02	1.81E-02	4.65E-03
STD-4	6.00E-02	2.23E-02	1.43E-02	2.73E-03
STD-5	7.52E-02	1.44E-02	1.89E-02	4.89E-03
STN-2	5.80E-02	1.37E-02	2.87E-03	1.12E-03

m/z = 56	Mean	Variance	Mean	Variance
HKN-S-	1.90E-03	4.85E-04	5.31E-04	3.20E-04
HKN-S+	2.49E-03	7.41E-04	5.75E-04	3.49E-04
HKS	1.40E-03	5.64E-04	6.66E-04	2.34E-04
HKT	5.94E-04	5.53E-04	4.21E-04	1.10E-04
STD-1	4.69E-04	2.88E-04	3.39E-05	2.13E-05
STD-2	4.29E-04	3.01E-04	2.24E-05	2.45E-05
STD-3	4.67E-04	1.93E-04	1.84E-05	1.56E-05
STD-4	4.13E-04	3.44E-04	3.42E-05	7.42E-05
STD-5	4.93E-04	2.17E-04	2.59E-05	4.19E-05
STN-2	3.90E-03	1.74E-03	6.03E-06	6.08E-06

m/z = 58	Mean	Variance	Mean	Variance
HKN-S-	4.68E-03	6.71E-04	3.37E-03	3.09E-04
HKN-S+	8.00E-03	1.38E-03	4.78E-03	6.51E-04
HKS	7.10E-03	1.43E-03	4.92E-03	5.59E-04
HKT	1.83E-03	5.94E-04	1.63E-03	3.20E-04
STD-1	5.48E-03	1.07E-03	3.44E-03	6.71E-04
STD-2	7.01E-03	3.49E-03	5.06E-03	1.32E-03
STD-3	6.14E-03	2.21E-03	5.62E-03	9.36E-04
STD-4	1.16E-02	4.40E-03	3.48E-03	1.23E-03
STD-5	1.80E-02	2.45E-03	4.35E-03	1.25E-03
STN-2	2.22E-03	7.33E-04	7.48E-04	2.04E-04

m/z = 60	Mean	Variance	Mean	Variance
HKN-S-	7.28E-03	3.06E-04	5.15E-03	6.17E-04
HKN-S+	1.06E-02	7.15E-04	7.34E-03	9.35E-04
HKS	6.68E-03	5.55E-04	6.10E-03	4.43E-04

HKT	4.46E-03	3.51E-04	6.60E-03	4.85E-04
STD-1	2.32E-03	1.27E-03	1.54E-03	6.81E-04
STD-2	3.24E-03	1.69E-03	3.08E-03	8.52E-04
STD-3	2.85E-03	1.14E-03	4.01E-03	1.45E-03
STD-4	3.64E-03	1.45E-03	9.63E-04	9.06E-04
STD-5	6.59E-03	1.13E-03	1.82E-03	2.74E-04
STN-2	6.25E-03	1.08E-03	4.02E-03	1.72E-03

m/z = 64	**Mean**	**Variance**	**Mean**	**Variance**
HKN-S-	5.35E-02	2.95E-03	0.0379	0.0118
HKN-S+	9.83E-02	1.06E-02	0.0976	3.45E-03
HKS	1.13E-01	9.80E-03	0.0731	2.60E-03
HKT	1.63E-01	7.70E-03	0.113	0.0102
STD-1	2.02E-01	2.84E-02	1.48E-01	1.87E-02
STD-2	1.72E-01	3.03E-02	1.30E-01	1.27E-02
STD-3	2.90E-01	2.34E-02	2.08E-01	2.01E-02
STD-4	2.09E-01	4.12E-02	1.71E-01	1.05E-02
STD-5	3.19E-01	1.89E-02	2.50E-01	1.37E-02
STN-2	2.70E-01	4.38E-02	1.81E-01	3.76E-02

m/z = 74	**Mean**	**Variance**	**Mean**	**Variance**
HKN-S-	1.35E-04	7.95E-05	1.28E-04	3.90E-05
HKN-S+	2.12E-04	7.85E-05	1.82E-04	8.47E-05
HKS	1.62E-04	3.66E-05	1.32E-04	4.02E-05
HKT	1.29E-04	4.32E-05	3.59E-05	6.27E-05
STD-1	1.74E-04	2.11E-04	3.21E-05	1.05E-05
STD-2	2.71E-04	1.96E-04	1.84E-04	1.05E-04
STD-3	3.76E-04	1.19E-04	6.24E-05	2.78E-05
STD-4	3.31E-04	1.75E-04	4.68E-05	1.48E-05
STD-5	5.43E-04	1.21E-04	1.61E-04	7.85E-05
STN-2	1.18E-04	9.97E-05	1.72E-05	1.81E-05

Table A. 6. Results of thermodynamic modelling: Mole fraction.

Na-species		NaCl	NaOH	Na	$NaAlSi_3O_8$	$NaAlSiO_4$	$Na_2Mg_2Si_6O_{15}$
STD-1	Without H_2O	9.26E-04	4.27E-05	2.19E-04	1.12E-03	0.00E+00	0.00E+00
	With H_2O	6.60E-04	9.16E-05	2.06E-04	1.35E-03	0.00E+00	0.00E+00
STD-2	Without H_2O	1.24E-03	5.28E-05	2.21E-04	2.31E-03	0.00E+00	0.00E+00
	With H_2O	9.29E-04	1.06E-04	2.17E-04	2.58E-03	0.00E+00	0.00E+00
STD-3	Without H_2O	1.45E-03	6.00E-05	2.09E-04	1.41E-03	0.00E+00	0.00E+00
	With H_2O	1.29E-03	1.41E-04	2.59E-04	1.44E-03	0.00E+00	0.00E+00
STD-4	Without H_2O	8.98E-04	4.50E-05	1.05E-04	5.91E-03	0.00E+00	0.00E+00
	With H_2O	6.75E-04	9.29E-05	1.19E-04	6.07E-03	0.00E+00	0.00E+00
STD-5	Without H_2O	1.41E-03	5.04E-05	7.99E-05	6.73E-03	0.00E+00	0.00E+00
	With H_2O	1.11E-03	9.82E-05	9.61E-05	6.96E-03	0.00E+00	0.00E+00
STN-2	Without H_2O	1.62E-04	4.26E-04	1.11E-03	0.00E+00	2.00E-02	0.00E+00
	With H_2O	1.45E-04	7.11E-04	1.05E-03	9.58E-05	1.97E-02	0.00E+00
HKN-S-	Without H_2O	2.46E-04	4.21E-03	5.10E-03	0.00E+00	0.00E+00	0.00E+00
	With H_2O	2.37E-04	5.14E-03	4.19E-03	0.00E+00	0.00E+00	0.00E+00
HKN-S+	Without H_2O	6.05E-04	3.94E-03	5.02E-03	0.00E+00	0.00E+00	0.00E+00
	With H_2O	5.84E-04	4.83E-03	4.15E-03	0.00E+00	0.00E+00	0.00E+00
HKS	Without H_2O	5.60E-04	4.46E-03	4.54E-03	0.00E+00	0.00E+00	0.00E+00
	With H_2O	5.41E-04	5.30E-03	3.72E-03	0.00E+00	0.00E+00	0.00E+00
HKT	Without H_2O	1.05E-04	1.23E-04	9.55E-05	0.00E+00	0.00E+00	9.68E-03
	With H_2O	8.81E-05	2.34E-04	1.23E-04	0.00E+00	0.00E+00	9.56E-03

K-species		KCl	KOH	K	$KAlSi_2O_6$
STD-1	Without H_2O	1.86E-04	8.04E-06	1.06E-05	3.89E-03
	With H_2O	1.33E-04	1.73E-05	1.00E-05	3.93E-03
STD-2	Without H_2O	2.50E-04	9.94E-06	1.08E-05	3.82E-03
	With H_2O	1.87E-04	2.00E-05	1.05E-05	3.87E-03
STD-3	Without H_2O	2.70E-04	1.04E-05	9.42E-06	4.06E-03
	With H_2O	2.18E-04	2.23E-05	1.06E-05	4.10E-03
STD-4	Without H_2O	1.81E-04	8.47E-06	5.10E-06	1.90E-02
	With H_2O	1.36E-04	1.75E-05	5.81E-06	1.90E-02
STD-5	Without H_2O	2.83E-04	9.50E-06	3.89E-06	2.20E-02
	With H_2O	2.23E-04	1.85E-05	4.68E-06	2.20E-02
STN-2	Without H_2O	3.15E-05	7.73E-05	5.22E-05	4.19E-03
	With H_2O	2.13E-05	9.78E-05	3.75E-05	4.19E-03
HKN-S-	Without H_2O	2.32E-05	3.72E-04	1.16E-04	0.00E+00
	With H_2O	2.00E-05	4.06E-04	8.55E-05	0.00E+00
HKN-S+	Without H_2O	6.46E-05	3.94E-04	1.30E-04	0.00E+00
	With H_2O	5.62E-05	4.35E-04	9.66E-05	0.00E+00
HKS	Without H_2O	5.89E-05	4.39E-04	1.16E-04	0.00E+00
	With H_2O	5.18E-05	4.76E-04	8.62E-05	0.00E+00
HKT	Without H_2O	2.18E-05	2.41E-05	4.81E-06	2.10E-03
	With H_2O	1.83E-05	4.56E-05	6.20E-06	2.10E-03

9.2.4 Influence of the coal rank

Table A. 7. Coal Rank: Averaged, normalised peak areas (-).

m/z	34		36		39		56	
	Mean	Variance	Mean	Variance	Mean	Variance	Mean	Variance
K2-3	2.44E-03	6.22E-04	4.45E-02	5.31E-03	1.12E-02	1.35E-03	6.15E-04	2.88E-04
K2-4	5.71E-02	9.10E-03	4.43E-03	6.78E-04	3.56E-01	2.21E-01	1.98E-03	5.06E-04
K2-5	8.32E-02	5.65E-03	1.40E-02	4.45E-03	6.77E-02	3.02E-02	5.22E-04	4.02E-04
STD-1	9.59E-03	6.35E-03	5.19E-02	4.52E-03	3.19E-02	1.04E-02	4.69E-04	2.88E-04
STD-2	9.19E-03	3.94E-03	6.51E-02	1.68E-02	1.63E-01	6.10E-02	4.29E-04	3.01E-04
STD-3	9.00E-03	4.69E-03	9.36E-02	9.91E-03	3.72E-02	1.71E-02	4.67E-04	1.93E-04
STD-4	3.73E-03	1.67E-03	6.38E-02	2.19E-02	1.43E-01	7.25E-02	4.13E-04	3.44E-04
STD-5	1.01E-02	8.75E-03	1.21E-01	1.42E-02	2.90E-02	7.20E-03	4.93E-04	2.17E-04
STN-2	5.14E-02	6.25E-03	4.06E-03	1.11E-03	7.52E-02	1.71E-02	3.90E-03	1.74E-03
K2-1	1.36E-02	3.28E-03	4.06E-03	2.95E-03	8.24E-01	1.08E-01	1.90E-03	1.34E-03
K2-2	3.03E-02	2.62E-03	3.86E-03	1.12E-03	2.20E-01	3.75E-02	3.01E-03	9.13E-04
K3-1	7.04E-02	1.13E-02	4.65E-03	1.20E-03	6.21E-01	8.28E-02	4.20E-03	5.14E-04
K3-2	1.29E-02	3.51E-03	2.47E-03	9.42E-04	2.47E-01	2.49E-02	1.56E-03	4.14E-04
HKN-S-	2.68E-02	1.20E-03	3.53E-03	8.33E-04	3.71E-01	7.11E-02	1.90E-03	4.85E-04
HKN-S+	4.51E-02	1.46E-03	4.53E-03	2.15E-03	2.97E-01	1.33E-01	2.49E-03	7.41E-04
HKS	7.74E-03	4.22E-03	2.94E-03	7.87E-04	8.46E-01	2.55E-01	1.40E-03	5.64E-04
HKT	2.23E-02	2.82E-03	4.37E-03	2.33E-03	1.08E+00	9.54E-02	5.94E-04	5.53E-04

m/z	58		60		74	
	Mean	Variance	Mean	Variance	Mean	Variance
K2-3	2.11E-02	3.03E-03	6.80E-03	8.40E-04	2.48E-04	1.84E-04
K2-4	2.40E-03	8.07E-04	8.48E-03	3.32E-03	1.04E-04	3.06E-05
K2-5	4.51E-03	5.11E-04	1.30E-02	8.08E-04	1.77E-04	4.71E-05
STD-1	5.48E-03	1.07E-03	2.32E-03	1.27E-03	1.74E-04	1.05E-04
STD-2	7.01E-03	3.49E-03	3.24E-03	1.69E-03	2.71E-04	9.80E-05
STD-3	6.14E-03	2.21E-03	2.85E-03	1.14E-03	3.76E-04	5.95E-05
STD-4	1.16E-02	4.40E-03	3.64E-03	1.45E-03	3.31E-04	8.75E-05
STD-5	1.80E-02	2.45E-03	6.59E-03	1.13E-03	5.43E-04	6.05E-05
STN-2	2.22E-03	7.33E-04	6.25E-03	1.08E-03	1.18E-04	4.99E-05
K2-1	4.59E-03	1.28E-03	5.12E-03	1.31E-03	9.50E-05	2.35E-05
K2-2	7.81E-03	1.70E-03	7.68E-03	1.43E-03	1.43E-04	4.08E-05
K3-1	3.43E-03	4.96E-04	1.21E-02	2.11E-03	1.52E-04	5.90E-05
K3-2	4.22E-03	8.78E-04	5.08E-03	8.10E-04	4.29E-04	1.09E-04
HKN-S-	4.68E-03	6.71E-04	7.28E-03	6.11E-04	1.35E-04	7.95E-05
HKN-S+	8.00E-03	1.38E-03	1.06E-02	1.43E-03	2.12E-04	7.85E-05
HKS	7.10E-03	1.43E-03	6.68E-03	1.11E-03	1.62E-04	3.66E-05
HKT	1.83E-03	5.94E-04	4.46E-03	7.02E-04	1.29E-04	4.32E-05

Table A. 8. Results of thermodynamic modelling: Mole fraction.

Na-sepcies	NaCl	NaOH	Na	$NaAlSiO_4$	NaAlSiO3O8	$Na_2Mg_2Si_6O_{15}$
K2-3	6.00E+00	1.94E-01	7.68E-01	0.00E+00	9.30E+01	0.00E+00
K2-4	4.66E-01	8.75E-02	6.42E-01	0.00E+00	9.85E+01	0.00E+00
K2-5	1.61E+00	3.30E-01	4.92E-03	0.00E+00	9.81E+01	0.00E+00
STD-1	2.86E+01	3.97E+00	8.92E+00	0.00E+00	5.84E+01	0.00E+00
STD-2	2.43E+01	2.78E+00	5.66E+00	0.00E+00	6.73E+01	0.00E+00
STD-3	4.13E+01	4.50E+00	8.27E+00	0.00E+00	4.59E+01	0.00E+00
STD-4	9.70E+00	1.34E+00	1.72E+00	0.00E+00	8.72E+01	0.00E+00
STD-5	1.34E+01	1.19E+00	1.16E+00	0.00E+00	8.42E+01	0.00E+00
STN-2	6.68E-01	3.27E+00	4.85E+00	9.08E+01	0.00E+00	0.00E+00
K2-1	1.24E+01	5.74E+01	3.02E+01	0.00E+00	0.00E+00	0.00E+00
K2-2	5.71E+00	5.67E+01	3.75E+01	0.00E+00	0.00E+00	0.00E+00
K3-1	5.54E+01	4.33E+01	1.24E+00	0.00E+00	0.00E+00	0.00E+00
K3-2	3.74E+01	4.69E+01	1.56E+01	0.00E+00	0.00E+00	0.00E+00
HKN-S-	2.48E+00	5.37E+01	4.38E+01	0.00E+00	0.00E+00	0.00E+00
HKN-S+	6.11E+00	5.05E+01	4.33E+01	0.00E+00	0.00E+00	0.00E+00
HKS	5.65E+00	5.54E+01	3.89E+01	0.00E+00	0.00E+00	0.00E+00
HKT	8.81E-01	2.34E+00	1.23E+00	0.00E+00	0.00E+00	9.56E+01

K-species	KCl	KOH	K	$KAlSiO_6$
K2-3	8.43E-01	2.55E-02	2.61E-02	9.91E+01
K2-4	2.32E-01	1.89E-01	7.73E-02	9.95E+01
K2-5	5.43E-02	1.04E-02	4.01E-05	9.99E+01
STD-1	3.25E+00	4.22E-01	2.45E-01	9.61E+01
STD-2	4.57E+00	4.90E-01	2.58E-01	9.47E+01
STD-3	5.02E+00	5.12E-01	2.43E-01	9.42E+01
STD-4	7.08E-01	9.13E-02	3.03E-02	9.92E+01
STD-5	1.00E+00	8.31E-02	2.10E-02	9.89E+01
STN-2	4.90E-01	2.25E+00	8.62E-01	9.64E+01
K2-1	1.61E+01	7.73E+01	6.56E+00	0.00E+00
K2-2	7.79E+00	8.33E+01	8.88E+00	0.00E+00
K3-1	4.14E+01	5.59E+01	2.71E+00	0.00E+00
K3-2	2.12E+00	9.93E-01	2.83E-03	9.69E+01
HKN-S-	3.92E+00	7.94E+01	1.67E+01	0.00E+00
HKN-S+	9.56E+00	7.40E+01	1.64E+01	0.00E+00
HKS	8.44E+00	7.75E+01	1.40E+01	0.00E+00
HKT	1.00E+00	1.11E+00	2.21E-01	9.68E+01

9.2.5 Influence of the pressure

Table A. 9. Experimental results: Averaged, normalised peak areas (-).

m/z = 34	2 bar		4 bar		6 bar	
	Mean	Variance	Mean	Variance	Mean	Variance
HKN-S-	6.30E-02	1.31E-02	3.20E-02	1.20E-02	2.07E-02	5.45E-03
HKN-S+	1.56E-01	2.34E-02	8.23E-02	1.46E-02	7.38E-02	7.30E-03
HKS	9.21E-02	1.11E-02	5.49E-02	1.10E-02	3.41E-02	6.05E-03
HKT	1.19E-01	1.80E-02	8.59E-02	1.99E-02	5.63E-02	1.87E-02
K2-1	4.47E-02	9.75E-03	3.15E-02	8.50E-03	2.95E-02	2.43E-03
K2-2	1.12E-01	2.23E-02	5.89E-02	2.39E-02	3.95E-02	9.05E-03
K3-1	2.35E-01	5.80E-02	1.79E-01	4.14E-02	1.17E-01	3.45E-02
K3-2	1.22E-01	4.38E-03	3.54E-02	1.14E-02	2.42E-02	5.30E-03
K3-3	1.55E-01	2.34E-02	4.25E-02	6.75E-03	2.98E-02	1.76E-03
STD-1	1.22E-01	4.38E-02	5.17E-02	1.77E-02	2.69E-02	4.98E-03
STD-2	1.70E-01	6.45E-02	1.06E-01	2.42E-02	7.22E-02	1.87E-02
STD-3	3.18E-01	7.40E-02	1.59E-01	5.55E-02	1.10E-01	2.47E-02
STD-4	1.73E-01	1.49E-02	7.10E-02	2.16E-02	1.86E-02	1.75E-03
STD-5	2.79E-01	3.97E-02	1.61E-01	2.90E-02	2.35E-02	3.66E-03
STN-1	2.53E-01	5.95E-02	1.31E-01	2.62E-02	7.75E-02	1.34E-02
STN-2	3.16E-01	7.25E-02	2.16E-01	5.70E-02	1.27E-01	3.72E-02
K2-3	5.63E-02	2.00E-02	2.57E-02	9.90E-03	2.44E-02	6.05E-03
K2-4	1.71E-01	3.67E-02	1.12E-01	3.79E-02	7.51E-02	1.79E-02
K2-5	2.08E-01	2.45E-02	7.07E-02	1.26E-02	2.66E-02	4.22E-03

m/z = 36	2 bar		4 bar		6 bar	
	Mean	Variance	Mean	Variance	Mean	Variance
HKN-S-	5.10E-03	1.41E-03	2.82E-03	9.15E-04	2.59E-03	7.65E-04
HKN-S+	1.07E-02	5.05E-04	9.25E-03	1.24E-03	5.40E-03	1.55E-03
HKS	1.10E-02	2.23E-03	6.39E-03	5.50E-04	5.73E-03	1.15E-03
HKT	7.56E-03	7.15E-04	6.19E-03	1.40E-03	2.69E-03	1.50E-03
K2-1	6.30E-03	5.50E-04	4.62E-03	7.75E-04	3.88E-03	9.95E-04
K2-2	9.21E-03	2.65E-04	5.19E-03	1.03E-03	3.89E-03	1.12E-03
K3-1	1.03E-02	1.57E-03	9.75E-03	1.19E-03	8.81E-03	2.42E-03
K3-2	7.70E-03	6.20E-04	4.67E-03	7.85E-04	4.04E-03	1.17E-03
K3-3	1.04E-02	1.46E-03	5.56E-03	1.10E-03	3.88E-03	1.08E-03
STD-1	2.47E-02	3.61E-03	1.72E-02	2.44E-03	6.63E-03	7.54E-04
STD-2	3.63E-02	6.55E-03	2.04E-02	3.17E-03	1.71E-02	6.70E-03
STD-3	4.34E-02	1.10E-02	4.19E-02	2.55E-03	2.50E-02	4.21E-03
STD-4	3.57E-02	1.02E-03	2.16E-02	2.91E-03	1.30E-02	1.03E-03
STD-5	7.26E-02	5.75E-03	4.02E-02	6.80E-04	1.87E-02	4.89E-03
STN-1	1.22E-02	1.52E-03	8.02E-03	1.50E-03	4.14E-03	1.11E-03
STN-2	1.92E-02	3.55E-03	9.28E-03	2.57E-03	6.73E-03	1.78E-03
K2-3	3.28E-02	5.10E-03	2.61E-02	3.70E-03	1.48E-02	3.97E-03

K2-4	8.24E-03	1.92E-03	7.04E-03	5.75E-04	5.34E-03	2.81E-04
K2-5	2.31E-02	3.43E-03	1.09E-02	6.65E-04	3.34E-03	7.70E-04

m/z = 39	**2 bar**		**4 bar**		**6 bar**	
	Mean	Variance	Mean	Variance	Mean	Variance
HKN-S-	9.11E-03	1.87E-03	5.03E-03	1.61E-03	1.66E-03	7.90E-05
HKN-S+	1.75E-02	3.20E-04	1.09E-02	1.27E-03	5.66E-03	1.38E-03
HKS	1.74E-02	1.34E-03	6.48E-03	5.13E-04	5.80E-03	5.03E-04
HKT	8.12E-03	1.26E-03	5.91E-03	4.35E-04	1.92E-03	1.33E-03
K2-1	1.15E-02	2.22E-03	6.30E-03	1.19E-03	6.03E-03	3.80E-04
K2-2	1.20E-02	8.88E-04	9.16E-03	1.60E-03	8.83E-03	5.93E-04
K3-1	7.21E-03	4.95E-04	6.02E-03	1.76E-03	4.31E-03	1.26E-03
K3-2	6.85E-03	8.93E-04	6.85E-03	8.93E-04	2.97E-03	1.60E-03
K3-3	8.84E-03	2.43E-03	7.67E-03	3.78E-04	4.22E-03	5.88E-04
STD-1	1.90E-02	4.68E-04	4.59E-03	7.65E-04	2.76E-03	6.99E-04
STD-2	1.57E-02	6.63E-04	1.01E-02	5.60E-04	6.79E-03	1.54E-03
STD-3	2.57E-02	1.26E-03	9.20E-03	5.48E-04	8.18E-03	9.33E-04
STD-4	1.78E-02	2.53E-03	1.33E-02	1.41E-03	1.64E-03	1.34E-04
STD-5	1.22E-02	2.02E-03	8.02E-03	5.10E-04	1.08E-03	6.48E-04
STN-1	2.52E-02	2.40E-03	1.23E-02	9.93E-04	6.93E-03	5.35E-04
STN-2	2.34E-02	3.13E-03	8.31E-03	8.23E-04	4.32E-03	1.09E-03
K2-3	6.10E-03	8.63E-04	5.64E-03	9.10E-04	4.50E-03	3.60E-04
K2-4	2.13E-02	1.60E-03	5.79E-03	5.78E-04	4.67E-03	1.17E-03
K2-5	5.74E-03	2.05E-03	3.85E-03	1.29E-03	3.10E-03	9.25E-04

m/z = 58	**2 bar**		**4 bar**		**6 bar**	
	Mean	Variance	Mean	Variance	Mean	Variance
HKN-S-	1.39E-03	2.89E-04	8.86E-04	2.85E-04	5.06E-04	7.75E-05
HKN-S+	2.12E-03	3.78E-04	1.02E-03	1.68E-04	7.57E-04	1.89E-04
HKS	1.99E-03	2.99E-04	1.05E-03	1.92E-04	3.11E-04	1.16E-04
HKT	1.30E-03	2.31E-04	8.08E-04	1.91E-04	2.78E-04	2.80E-05
K2-1	1.47E-03	3.54E-04	1.03E-03	2.82E-04	4.32E-04	8.70E-05
K2-2	1.63E-03	1.50E-04	9.99E-04	5.45E-04	3.21E-04	3.91E-04
K3-1	1.73E-03	3.69E-04	8.74E-04	2.87E-04	4.96E-04	7.20E-05
K3-2	1.96E-03	6.15E-04	1.15E-03	1.21E-04	5.12E-05	8.75E-05
K3-3	2.08E-03	1.98E-05	5.34E-04	2.16E-04	2.94E-04	9.95E-05
STD-1	4.02E-03	8.70E-04	6.17E-04	2.49E-04	4.50E-04	3.24E-04
STD-2	5.39E-03	9.00E-04	1.17E-03	2.18E-04	1.17E-03	1.82E-04
STD-3	7.09E-03	1.57E-03	6.70E-04	1.59E-04	5.09E-04	1.63E-04
STD-4	2.98E-03	6.10E-04	1.52E-03	1.23E-04	2.40E-04	9.05E-05
STD-5	4.96E-03	6.10E-04	1.19E-03	1.93E-04	2.54E-04	8.25E-05
STN-1	5.05E-03	1.78E-03	1.36E-03	3.83E-04	5.04E-04	1.31E-04
STN-2	1.03E-02	2.44E-03	1.16E-03	4.14E-05	4.50E-04	1.36E-04
K2-3	5.00E-04	6.05E-05	3.75E-04	3.75E-04	4.14E-04	1.59E-04

K2-4	3.13E-03	9.10E-05	1.55E-03	2.71E-04	7.56E-04	1.48E-04
K2-5	1.41E-03	3.52E-04	3.64E-04	2.53E-04	2.88E-04	1.37E-04

m/z = 64	**2 bar**		**4 bar**		**6 bar**	
	Mean	Variance	Mean	Variance	Mean	Variance
HKN-S-	1.59E-01	4.25E-02	9.36E-02	9.45E-03	4.98E-02	1.11E-02
HKN-S+	2.08E-01	3.16E-02	1.02E-01	1.71E-02	8.02E-02	1.07E-02
HKS	1.62E-01	3.93E-02	1.13E-01	1.63E-02	5.35E-02	1.17E-02
HKT	2.57E-01	6.10E-02	1.18E-01	1.94E-02	9.77E-02	1.94E-02
K2-1	1.69E-01	4.40E-02	7.76E-02	1.38E-02	7.39E-02	5.50E-03
K2-2	2.47E-01	5.55E-02	9.19E-02	1.09E-02	7.97E-02	1.59E-02
K3-1	2.56E-01	3.54E-02	1.10E-01	2.55E-02	7.35E-02	5.10E-03
K3-2	4.61E-01	1.54E-01	1.97E-01	2.14E-02	1.27E-01	2.01E-02
K3-3	2.35E-01	6.10E-02	1.09E-01	9.00E-03	5.41E-02	9.30E-03
STD-1	3.59E-01	7.65E-02	1.70E-01	3.85E-02	1.35E-01	1.73E-02
STD-2	4.29E-01	1.20E-01	1.78E-01	2.73E-02	1.43E-01	1.57E-02
STD-3	5.12E-01	8.40E-02	2.76E-01	2.71E-02	2.01E-01	4.40E-02
STD-4	3.93E-01	4.95E-02	2.38E-01	1.65E-02	1.38E-01	1.42E-02
STD-5	6.02E-01	1.03E-01	2.91E-01	4.13E-02	2.05E-01	2.06E-02
STN-1	2.84E-01	6.00E-02	1.62E-01	2.48E-02	1.04E-01	1.86E-02
STN-2	5.61E-01	1.05E-01	2.18E-01	2.32E-02	1.26E-01	2.25E-02
K2-3	2.81E-01	3.67E-02	7.98E-02	2.01E-03	4.51E-02	7.45E-03
K2-4	2.92E-01	5.20E-02	1.54E-01	1.46E-02	8.92E-02	2.29E-02
K2-5	6.02E-01	9.40E-02	2.06E-01	1.84E-02	6.96E-02	6.60E-03

m/z = 74	**2 bar**		**4 bar**		**6 bar**	
	Mean	Variance	Mean	Variance	Mean	Variance
HKN-S-	4.32E-03	1.84E-03	9.02E-04	5.35E-04	9.02E-04	4.24E-04
HKN-S+	6.58E-03	2.08E-03	2.29E-03	9.65E-04	1.79E-03	5.05E-04
HKS	8.71E-03	1.35E-03	3.63E-03	1.11E-03	3.52E-03	1.95E-03
HKT	4.34E-03	8.70E-04	2.11E-03	4.28E-04	7.65E-04	2.52E-04
K2-1	4.06E-03	8.80E-04	2.22E-03	1.02E-03	1.19E-03	6.25E-04
K2-2	7.40E-03	2.21E-03	2.06E-03	4.71E-04	1.68E-03	7.00E-04
K3-1	1.03E-02	1.03E-03	2.18E-03	2.74E-04	6.72E-04	2.53E-04
K3-2	1.05E-02	1.28E-03	1.76E-03	5.20E-04	6.19E-04	1.70E-04
K3-3	1.06E-02	2.49E-03	1.64E-03	9.75E-04	1.91E-03	6.15E-04
STD-1	3.71E-03	8.90E-04	1.83E-03	8.00E-04	3.55E-04	3.47E-05
STD-2	6.43E-03	2.49E-03	2.21E-03	2.49E-04	1.41E-03	5.60E-04
STD-3	7.66E-03	1.42E-03	1.55E-03	4.31E-04	6.13E-04	1.99E-04
STD-4	3.91E-03	4.31E-04	1.76E-03	5.35E-04	4.84E-04	2.92E-04
STD-5	4.00E-03	8.10E-04	1.31E-03	2.47E-04	1.39E-04	6.50E-05
STN-1	8.93E-03	2.18E-03	3.81E-03	1.14E-03	1.24E-03	1.00E-03
STN-2	6.83E-03	1.68E-03	1.65E-03	6.30E-04	1.02E-03	5.70E-04
K2-3	2.53E-04	1.84E-04	6.59E-05	4.38E-05	5.82E-05	4.06E-05

K2-4	4.17E-03	5.40E-04	2.73E-03	1.01E-03	1.58E-03	1.23E-04
K2-5	2.51E-03	4.08E-04	3.79E-04	4.65E-05	8.21E-05	6.90E-05

Table A. 10. Results of thermodynamic modelling: Mole fraction.

Na-species	p in bar	NaCl	NaOH	Na	$NaAlSi_3O_8$	$NaAlSiO_4$
STD-1	2	5.61E-04	1.64E-05	4.98E-05	1.68E-03	0.00E+00
	4	4.23E-04	1.16E-05	2.49E-05	1.85E-03	0.00E+00
	6	4.26E-04	1.16E-05	2.05E-05	1.85E-03	0.00E+00
STD-2	2	7.64E-04	2.06E-05	5.11E-05	2.99E-03	0.00E+00
	4	5.76E-04	1.46E-05	2.55E-05	3.21E-03	0.00E+00
	6	4.84E-04	1.19E-05	1.70E-05	3.31E-03	0.00E+00
STD-3	2	1.21E-03	3.40E-05	7.25E-05	1.81E-03	0.00E+00
	4	9.28E-04	2.41E-05	3.62E-05	2.14E-03	0.00E+00
	6	7.87E-04	1.96E-05	2.41E-05	2.30E-03	0.00E+00
STD-4	2	5.13E-04	1.78E-05	2.06E-05	6.41E-03	0.00E+00
	4	3.80E-04	1.26E-05	1.03E-05	6.56E-03	0.00E+00
	6	3.18E-04	1.03E-05	6.87E-06	6.62E-03	0.00E+00
STD-5	2	8.01E-04	1.96E-05	1.57E-05	7.43E-03	0.00E+00
	4	5.92E-04	1.39E-05	7.83E-06	7.65E-03	0.00E+00
	6	4.93E-04	1.13E-05	5.21E-06	7.75E-03	0.00E+00
STN-1	2	2.31E-04	1.61E-04	3.75E-04	2.00E-03	8.11E-03
	4	2.00E-04	1.14E-04	1.87E-04	1.92E-03	8.45E-03
	6	1.25E-04	9.26E-05	1.02E-04	1.89E-03	8.59E-03
STN-2	2	1.41E-04	1.96E-04	3.32E-04	0.00E+00	2.11E-02
	4	1.24E-04	1.38E-04	1.66E-04	0.00E+00	2.13E-02
	6	1.14E-04	1.13E-04	1.10E-04	0.00E+00	2.14E-02
K2-3	2	4.69E-04	9.43E-06	2.44E-05	1.25E-02	0.00E+00
	4	3.48E-04	6.67E-06	1.22E-05	1.27E-02	0.00E+00
	6	2.90E-04	5.44E-06	8.13E-06	1.27E-02	0.00E+00
K2-4	2	3.82E-05	2.11E-05	2.16E-05	1.38E-02	0.00E+00
	4	2.82E-05	1.49E-05	1.08E-05	1.39E-02	0.00E+00
	6	2.35E-05	1.22E-05	7.19E-06	1.39E-02	0.00E+00
K2-5	2	7.62E-05	1.03E-05	6.15E-08	8.18E-03	0.00E+00
	4	5.57E-05	7.29E-06	2.59E-08	8.20E-03	0.00E+00
	6	4.62E-05	5.95E-06	1.56E-08	8.21E-03	0.00E+00
HKN-S-	2	2.53E-04	5.22E-03	4.09E-03	0.00E+00	0.00E+00
	4	2.55E-04	5.98E-03	3.32E-03	0.00E+00	0.00E+00
	6	2.57E-04	6.40E-03	2.90E-03	0.00E+00	0.00E+00
HKN-S+	2	6.24E-04	4.90E-03	4.04E-03	0.00E+00	0.00E+00
	4	6.31E-04	5.64E-03	3.28E-03	0.00E+00	0.00E+00
	6	6.34E-04	6.05E-03	2.87E-03	0.00E+00	0.00E+00
HKS	2	5.76E-04	5.42E-03	3.57E-03	0.00E+00	0.00E+00

	4	5.62E-04	4.54E-03	2.11E-03	0.00E+00	2.35E-03
	6	5.65E-04	4.82E-03	1.83E-03	0.00E+00	2.35E-03
HKT	2	6.92E-05	4.80E-05	2.40E-05	9.86E-03	0.00E+00
	4	5.32E-05	3.39E-05	1.19E-05	9.91E-03	0.00E+00
	6	4.51E-05	2.77E-05	7.95E-06	9.92E-03	0.00E+00
K2-1	2	8.87E-04	4.53E-03	1.54E-03	0.00E+00	0.00E+00
	4	8.91E-04	4.89E-03	1.18E-03	0.00E+00	0.00E+00
	6	8.93E-04	5.07E-03	9.95E-04	0.00E+00	0.00E+00
K2-2	2	9.83E-04	1.12E-02	4.78E-03	0.00E+00	0.00E+00
	4	9.86E-04	1.23E-02	3.70E-03	0.00E+00	0.00E+00
	6	9.88E-04	1.28E-02	3.15E-03	0.00E+00	0.00E+00
K3-1	2	1.60E-04	8.00E-05	9.18E-07	1.06E-04	0.00E+00
	4	1.25E-04	5.66E-05	3.86E-07	1.66E-04	0.00E+00
	6	1.07E-04	4.62E-05	2.35E-07	1.94E-04	0.00E+00
K3-2	2	3.09E-04	3.54E-04	7.64E-05	0.00E+00	0.00E+00
	4	3.14E-04	3.69E-04	5.63E-05	0.00E+00	0.00E+00
	6	3.17E-04	3.76E-04	4.68E-05	0.00E+00	0.00E+00
K3-3	2	2.72E-04	3.91E-04	7.62E-05	0.00E+00	0.00E+00
	4	2.77E-04	4.07E-04	5.61E-05	0.00E+00	0.00E+00
	6	2.79E-04	4.14E-04	4.66E-05	0.00E+00	0.00E+00

K-species		**KCl**	**KOH**	**K**	**$KAlSi_2O_6$**
STD-1	2	1.16E-04	3.16E-06	2.40E-06	3.97E-03
	4	8.70E-05	2.24E-06	1.20E-06	4.00E-03
	6	7.90E-05	2.03E-06	8.88E-07	4.01E-03
STD-2	2	1.57E-04	3.99E-06	2.46E-06	3.93E-03
	4	1.18E-04	2.82E-06	1.23E-06	3.97E-03
	6	9.96E-05	2.31E-06	8.20E-07	3.99E-03
STD-3	2	1.88E-04	4.98E-06	2.64E-06	4.15E-03
	4	1.44E-04	3.52E-06	1.32E-06	4.20E-03
	6	1.22E-04	2.87E-06	8.79E-07	4.22E-03
STD-4	2	1.05E-04	3.44E-06	9.95E-07	1.91E-02
	4	7.83E-05	2.43E-06	4.97E-07	1.91E-02
	6	6.54E-05	1.99E-06	3.31E-07	1.91E-02
STD-5	2	1.65E-04	3.80E-06	7.57E-07	2.21E-02
	4	1.22E-04	2.69E-06	3.77E-07	2.21E-02
	6	1.01E-04	2.19E-06	2.51E-07	2.21E-02
STN-1	2	3.36E-05	2.19E-05	1.27E-05	2.75E-03
	4	2.91E-05	1.55E-05	6.36E-06	2.76E-03
	6	2.64E-05	1.27E-05	4.24E-06	2.77E-03
STN-2	2	3.26E-05	4.27E-05	1.80E-05	4.25E-03
	4	2.88E-05	3.02E-05	9.01E-06	4.28E-03
	6	2.65E-05	2.47E-05	6.01E-06	4.29E-03

K2-3	2	9.64E-05	1.82E-06	1.18E-06	1.86E-02
	4	7.15E-05	1.29E-06	5.88E-07	1.86E-02
	6	5.97E-05	1.05E-06	3.92E-07	1.86E-02
K2-4	2	7.86E-06	4.08E-06	1.04E-06	5.61E-03
	4	5.81E-06	2.89E-06	5.20E-07	5.62E-03
	6	4.84E-06	2.36E-06	3.46E-07	5.62E-03
K2-5	2	1.57E-05	1.99E-06	2.97E-09	4.93E-02
	4	1.15E-05	1.41E-06	1.25E-09	4.93E-02
	6	9.51E-06	1.15E-06	7.51E-10	4.94E-02
HKN-S-	2	2.12E-05	4.10E-04	8.02E-05	0.00E+00
	4	1.96E-05	4.32E-04	5.97E-05	0.00E+00
	6	1.89E-05	4.43E-04	4.99E-05	0.00E+00
HKN-S+	2	5.95E-05	4.39E-04	9.00E-05	0.00E+00
	4	5.54E-05	4.65E-04	6.75E-05	0.00E+00
	6	5.33E-05	4.78E-04	5.66E-05	0.00E+00
HKS	2	5.43E-05	4.81E-04	7.88E-05	0.00E+00
	4	6.48E-05	4.92E-04	5.70E-05	0.00E+00
	6	6.28E-05	5.03E-04	4.75E-05	0.00E+00
HKT	2	1.43E-05	9.28E-06	2.87E-07	2.15E-03
	4	1.09E-05	6.56E-06	5.76E-07	2.16E-03
	6	9.29E-06	5.36E-06	3.83E-07	2.16E-03
K2-1	2	5.77E-05	2.77E-04	2.35E-05	0.00E+00
	4	5.54E-05	2.86E-04	1.71E-05	0.00E+00
	6	5.43E-05	2.90E-04	1.42E-05	0.00E+00
K2-2	2	4.18E-05	4.48E-04	4.77E-05	0.00E+00
	4	3.96E-05	4.63E-04	3.48E-05	0.00E+00
	6	3.85E-05	4.70E-04	2.88E-05	0.00E+00
K3-1	2	1.69E-04	2.29E-04	1.11E-05	0.00E+00
	4	1.68E-04	2.33E-04	7.99E-06	0.00E+00
	6	1.68E-04	2.35E-04	6.58E-06	0.00E+00
K3-2	2	3.30E-05	1.55E-05	4.42E-08	1.51E-03
	4	2.57E-05	1.10E-05	1.86E-08	1.52E-03
	6	2.20E-05	8.95E-06	1.13E-08	1.53E-03
K3-3	2	1.68E-04	1.80E-04	9.70E-06	0.00E+00
	4	1.67E-04	1.84E-04	7.00E-06	0.00E+00
	6	1.67E-04	1.86E-04	5.76E-06	0.00E+00

1. **Einsatz von multispektralen Satellitenbilddaten in der Wasserhaushalts- und Stoffstrommodellierung – dargestellt am Beispiel des Rureinzugsgebietes**
   von C. Montzka (2008), XX, 238 Seiten
   ISBN: 978-3-89336-508-1

2. **Ozone Production in the Atmosphere Simulation Chamber SAPHIR**
   by C. A. Richter (2008), XIV, 147 pages
   ISBN: 978-3-89336-513-5

3. **Entwicklung neuer Schutz- und Kontaktierungsschichten für Hochtemperatur-Brennstoffzellen**
   von T. Kiefer (2008), 138 Seiten
   ISBN: 978-3-89336-514-2

4. **Optimierung der Reflektivität keramischer Wärmedämmschichten aus Yttrium-teilstabilisiertem Zirkoniumdioxid für den Einsatz auf metallischen Komponenten in Gasturbinen**
   von A. Stuke (2008), X, 201 Seiten
   ISBN: 978-3-89336-515-9

5. **Lichtstreuende Oberflächen, Schichten und Schichtsysteme zur Verbesserung der Lichteinkopplung in Silizium-Dünnschichtsolarzellen**
   von M. Berginski (2008), XV, 171 Seiten
   ISBN: 978-3-89336-516-6

6. **Politikszenarien für den Klimaschutz IV – Szenarien bis 2030**
   hrsg.von P. Markewitz, F. Chr. Matthes (2008), 376 Seiten
   ISBN 978-3-89336-518-0

7. **Untersuchungen zum Verschmutzungsverhalten rheinischer Braunkohlen in Kohledampferzeugern**
   von A. Schlüter (2008), 164 Seiten
   ISBN 978-3-89336-524-1

8. **Inorganic Microporous Membranes for Gas Separation in Fossil Fuel Power Plants**
   by G. van der Donk (2008), VI, 120 pages
   ISBN: 978-3-89336-525-8

9. **Sinterung von Zirkoniumdioxid-Elektrolyten im Mehrlagenverbund der oxidkeramischen Brennstoffzelle (SOFC)**
   von R. Mücke (2008), VI, 165 Seiten
   ISBN: 978-3-89336-529-6

10. **Safety Considerations on Liquid Hydrogen**
    by K. Verfondern (2008), VIII, 167 pages
    ISBN: 978-3-89336-530-2

11. **Kerosinreformierung für Luftfahrtanwendungen**
von R. C. Samsun (2008), VII, 218 Seiten
ISBN: 978-3-89336-531-9

12. **Der 4. Deutsche Wasserstoff Congress 2008 – Tagungsband**
hrsg. von D. Stolten, B. Emonts, Th. Grube (2008), 269 Seiten
ISBN: 978-3-89336-533-3

13. **Organic matter in Late Devonian sediments as an indicator for environmental changes**
by M. Kloppisch (2008), XII, 188 pages
ISBN: 978-3-89336-534-0

14. **Entschwefelung von Mitteldestillaten für die Anwendung in mobilen Brennstoffzellen-Systemen**
von J. Latz (2008), XII, 215 Seiten
ISBN: 978-3-89336-535-7

15. **RED-IMPACT**
Impact of Partitioning, Transmutation and Waste Reduction Technologies on the Final Nuclear Waste Disposal
SYNTHESIS REPORT
ed. by W. von Lensa, R. Nabbi, M. Rossbach (2008), 178 pages
ISBN 978-3-89336-538-8

16. **Ferritic Steel Interconnectors and their Interactions with Ni Base Anodes in Solid Oxide Fuel Cells (SOFC)**
by J. H. Froitzheim (2008), 169 pages
ISBN: 978-3-89336-540-1

17. **Integrated Modelling of Nutrients in Selected River Basins of Turkey**
Results of a bilateral German-Turkish Research Project
project coord. M. Karpuzcu, F. Wendland (2008), XVI, 183 pages
ISBN: 978-3-89336-541-8

18. **Isotopengeochemische Studien zur klimatischen Ausprägung der Jüngeren Dryas in terrestrischen Archiven Eurasiens**
von J. Parplies (2008), XI, 155 Seiten, Anh.
ISBN: 978-3-89336-542-5

19. **Untersuchungen zur Klimavariabilität auf dem Tibetischen Plateau - Ein Beitrag auf der Basis stabiler Kohlenstoff- und Sauerstoffisotope in Jahrringen von Bäumen waldgrenznaher Standorte**
von J. Griessinger (2008), XIII, 172 Seiten
ISBN: 978-3-89336-544-9

20. **Neutron-Irradiation + Helium Hardening & Embrittlement Modeling of 9%Cr-Steels in an Engineering Perspective (HELENA)**
by R. Chaouadi (2008), VIII, 139 pages
ISBN: 978-3-89336-545-6

21. **in Bearbeitung**

22. **Verbundvorhaben APAWAGS (AOEV und Wassergenerierung) – Teilprojekt: Brennstoffreformierung – Schlussbericht**
von R. Peters, R. C. Samsun, J. Pasel, Z. Porš, D. Stolten (2008), VI, 106 Seiten
ISBN: 978-3-89336-547-0

23. **FREEVAL**
Evaluation of a Fire Radiative Power Product derived from Meteosat 8/9 and Identification of Operational User Needs
Final Report
project coord. M. Schultz, M. Wooster (2008), 139 pages
ISBN: 978-3-89336-549-4

24. **Untersuchungen zum Alkaliverhalten unter Oxycoal-Bedingungen**
von C. Weber (2008), VII, 143, XII Seiten
ISBN: 978-3-89336-551-7

25. **Grundlegende Untersuchungen zur Freisetzung von Spurstoffen, Heißgaschemie, Korrosionsbeständigkeit keramischer Werkstoffe und Alkalirückhaltung in der Druckkohlenstaubfeuerung**
von M. Müller (2008), 207 Seiten
ISBN: 978-3-89336-552-4

26. **Analytik von ozoninduzierten phenolischen Sekundärmetaboliten in *Nicotiana tabacum* L. cv Bel W3 mittels LC-MS**
von I. Koch (2008), III, V, 153 Seiten
ISBN 978-3-89336-553-1

27. **IEF-3 Report 2009. Grundlagenforschung für die Anwendung**
(2009), ca. 230 Seiten
ISBN: 978-3-89336-554-8

28. **Influence of Composition and Processing in the Oxidation Behavior of MCrAlY-Coatings for TBC Applications**
by J. Toscano (2009), 168 pages
ISBN: 978-3-89336-556-2

29. **Modellgestützte Analyse signifikanter Phosphorbelastungen in hessischen Oberflächengewässern aus diffusen und punktuellen Quellen**
von B. Tetzlaff (2009), 149 Seiten
ISBN: 978-3-89336-557-9

30. **Nickelreaktivlot / Oxidkeramik – Fügungen als elektrisch isolierende Dichtungskonzepte für Hochtemperatur-Brennstoffzellen-Stacks**
von S. Zügner (2009), 136 Seiten
ISBN: 978-3-89336-558-6

31. **Langzeitbeobachtung der Dosisbelastung der Bevölkerung in radioaktiv kontaminierten Gebieten Weißrusslands – Korma-Studie**
von H. Dederichs, J. Pillath, B. Heuel-Fabianek, P. Hill, R. Lennartz (2009), Getr. Pag.
ISBN: 978-3-89336-532-3

32. **Herstellung von Hochtemperatur-Brennstoffzellen über physikalische Gasphasenabscheidung**
von N. Jordán Escalona (2009), 148 Seiten
ISBN: 978-3-89336-532-3

33. **Real-time Digital Control of Plasma Position and Shape on the TEXTOR Tokamak**
by M. Mitri (2009), IV, 128 pages
ISBN: 978-3-89336-567-8

34. **Freisetzung und Einbindung von Alkalimetallverbindungen in kohlebefeuerten Kombikraftwerken**
von M. Müller (2009), 155 Seiten
ISBN: 978-3-89336-568-5

35. **Kosten von Brennstoffzellensystemen auf Massenbasis in Abhängigkeit von der Absatzmenge**
von J. Werhahn (2009), 242 Seiten
ISBN: 978-3-89336-569-2

36. **Einfluss von Reoxidationszyklen auf die Betriebsfestigkeit von anodengestützten Festoxid-Brennstoffzellen**
von M. Ettler (2009), 138 Seiten
ISBN: 978-3-89336-570-8

37. **Großflächige Plasmaabscheidung von mikrokristallinem Silizium für mikromorphe Dünnschichtsolarmodule**
von T. Kilper (2009), XVII, 154 Seiten
ISBN: 978-3-89336-572-2

38. **Generalized detailed balance theory of solar cells**
by T. Kirchartz (2009), IV, 198 pages
ISBN: 978-3-89336-573-9

39. **The Influence of the Dynamic Ergodic Divertor on the Radial Electric Field at the Tokamak TEXTOR**
von J. W. Coenen (2009), xii, 122, XXVI pages
ISBN: 978-3-89336-574-6

40. **Sicherheitstechnik im Wandel Nuklearer Systeme**
von K. Nünighoff (2009), viii, 215 Seiten
ISBN: 978-3-89336-578-4

41. **Pulvermetallurgie hochporöser NiTi-Legierungen für Implanat- und Dämpfungsanwendungen**
von M. Köhl (2009), XVII, 199 Seiten
ISBN: 978-3-89336-580-7

42. **Einfluss der Bondcoatzusammensetzung und Herstellungsparameter auf die Lebensdauer von Wärmedämmschichten bei zyklischer Temperaturbelastung**
von M. Subanovic (2009), 188, VI Seiten
ISBN: 978-3-89336-582-1

43. **Oxygen Permeation and Thermo-Chemical Stability of Oxygen Permeation Membrane Materials for the Oxyfuel Process**
by A. J. Ellett (2009), 176 pages
ISBN: 978-3-89336-581-4

44. **Korrosion von polykristallinem Aluminiumoxid (PCA) durch Metalljodidschmelzen sowie deren Benetzungseigenschaften**
von S. C. Fischer (2009), 148 Seiten
ISBN: 978-3-89336-584-5

45. **IEF-3 Report 2009. Basic Research for Applications**
(2009), 217 Seiten
ISBN: 978-3-89336-585-2

46. **Verbundvorhaben ELBASYS (Elektrische Basissysteme in einem CFK-Rumpf) - Teilprojekt: Brennstoffzellenabgase zur Tankinertisierung - Schlussbericht**
von R. Peters, J. Latz, J. Pasel, R. C. Samsun, D. Stolten
(2009), xi, 202 Seiten
ISBN: 978-3-89336-587-6

47. **Aging of ^{14}C-labeled Atrazine Residues in Soil: Location, Characterization and Biological Accessibility**
by N. D. Jablonowski (2009), IX, 104 pages
ISBN: 978-3-89336-588-3

48. **Entwicklung eines energetischen Sanierungsmodells für den europäischen Wohngebäudesektor unter dem Aspekt der Erstellung von Szenarien für Energie- und CO_2 - Einsparpotenziale bis 2030**
von P. Hansen (2009), XXII, 281 Seiten
ISBN: 978-3-89336-590-6

49. **Reduktion der Chromfreisetzung aus metallischen Interkonnektoren für Hochtemperaturbrennstofzellen durch Schutzschichtsysteme**
von R. Trebbels (2009), iii, 135 Seiten
ISBN: 978-3-89336-591-3

50. **Bruchmechanische Untersuchung von Metall / Keramik-Verbundsystemen für die Anwendung in der Hochtemperaturbrennstoffzelle**
von B. Kuhn (2009), 118 Seiten
ISBN: 978-3-89336-592-0

51. **Wasserstoff-Emissionen und ihre Auswirkungen auf den arktischen Ozonverlust**
Risikoanalyse einer globalen Wasserstoffwirtschaft
von T. Feck (2009), 180 Seiten
ISBN: 978-3-89336-593-7

52. **Development of a new Online Method for Compound Specific Measurements of Organic Aerosols**
by T. Hohaus (2009), 156 pages
ISBN: 978-3-89336-596-8

53. **Entwicklung einer FPGA basierten Ansteuerungselektronik für Justageeinheiten im Michelson Interferometer**
von H. Nöldgen (2009), 121 Seiten
ISBN: 978-3-89336-599-9

54. **Observation – and model – based study of the extratropical UT/LS**
by A. Kunz (2010), xii, 120, xii pages
ISBN: 978-3-89336-603-3

55. **Herstellung polykristalliner Szintillatoren für die Positronen-Emissions-Tomographie (PET)**
von S. K. Karim (2010), VIII, 154 Seiten
ISBN: 978-3-89336-610-1

56. **Kombination eines Gebäudekondensators mit H2-Rekombinatorelementen in Leichwasserreaktoren**
von S. Kelm (2010), vii, 119 Seiten
ISBN: 978-3-89336-611-8

57. **Plant Leaf Motion Estimation Using A 5D Affine Optical Flow Model**
by T. Schuchert (2010), X, 143 pages
ISBN: 978-3-89336-613-2

58. **Tracer-tracer relations as a tool for research on polar ozone loss**
by R. Müller (2010), 116 pages
ISBN: 978-3-89336-614-9

59. **Sorption of polycyclic aromatic hydrocarbon (PAH) to Yangtze River sediments and their components**
by J. Zhang (2010), X, 109 pages
ISBN: 978-3-89336-616-3

60. **Weltweite Innovationen bei der Entwicklung von CCS-Technologien und Möglichkeiten der Nutzung und des Recyclings von CO_2**
Studie im Auftrag des BMWi
von W. Kuckshinrichs et al. (2010), X, 139 Seiten
ISBN: 978-3-89336-617-0

61. **Herstellung und Charakterisierung von sauerstoffionenleitenden Dünnschichtmembranstrukturen**
von M. Betz (2010), XII, 112 Seiten
ISBN: 978-3-89336-618-7

62. **Politikszenarien für den Klimaschutz V – auf dem Weg zum Strukturwandel, Treibhausgas-Emissionsszenarien bis zum Jahr 2030**
hrsg. von P. Hansen, F. Chr. Matthes (2010), 276 Seiten
ISBN: 978-3-89336-619-4

63. **Charakterisierung Biogener Sekundärer Organischer Aerosole mit Statistischen Methoden**
von C. Spindler (2010), iv, 163 Seiten
ISBN: 978-3-89336-622-4

64. **Stabile Algorithmen für die Magnetotomographie an Brennstoffzellen**
von M. Wannert (2010), ix, 119 Seiten
ISBN: 978-3-89336-623-1

65. **Sauerstofftransport und Degradationsverhalten von Hochtemperaturmembranen für CO2-freie Kraftwerke**
von D. Schlehuber (2010), VII, 139 Seiten
ISBN: 978-3-89336-630-9

66. **Entwicklung und Herstellung von foliengegossenen, anodengestützten Festoxidbrennstoffzellen**
von W. Schafbauer (2010), VI, 164 Seiten
ISBN: 978-3-89336-631-6

67. **Disposal strategy of proton irradiated mercury from high power spallation sources**
by S. Chiriki (2010), xiv, 124 pages
ISBN: 978-3-89336-632-3

68. **Oxides with polyatomic anions considered as new electrolyte materials for solid oxide fuel cells (SOFCs)**
by O. H. Bin Hassan (2010), vii, 121 pages
ISBN: 978-3-89336-633-0

69. **Von der Komponente zum Stack: Entwicklung und Auslegung von HT-PEFC-Stacks der 5 kW-Klasse**
von A. Bendzulla (2010), IX, 203 Seiten
ISBN: 978-3-89336-634-7

70. **Satellitengestützte Schwerewellenmessungen in der Atmosphäre und Perspektiven einer zukünftigen ESA Mission (PREMIER)**
von S. Höfer (2010), 81 Seiten
ISBN: 978-3-89336-637-8

71. **Untersuchungen der Verhältnisse stabiler Kohlenstoffisotope in atmosphärisch relevanten VOC in Simulations- und Feldexperimenten**
von H. Spahn (2010), IV, 210 Seiten
ISBN: 978-3-89336-638-5

72. **Entwicklung und Charakterisierung eines metallischen Substrats für nanostrukturierte keramische Gastrennmembranen**
von K. Brands (2010), vii, 137 Seiten
ISBN: 978-3-89336-640-8

73. **Hybridisierung und Regelung eines mobilen Direktmethanol-Brennstoffzellen-Systems**
von J. Chr. Wilhelm (2010), 220 Seiten
ISBN: 978-3-89336-642-2

74. **Charakterisierung perowskitischer Hochtemperaturmembranen zur Sauerstoffbereitstellung für fossil gefeuerte Kraftwerksprozesse**
von S.A. Möbius (2010) III, 208 Seiten
ISBN: 978-3-89336-643-9

75. **Characterization of natural porous media by NMR and MRI techniques: High and low magnetic field studies for estimation of hydraulic properties**
by L.-R. Stingaciu (2010), 96 pages
ISBN: 978-3-89336-645-3

76. **Hydrological Characterization of a Forest Soil Using Electrical Resistivity Tomography**
by Chr. Oberdörster (2010), XXI, 151 pages
ISBN: 978-3-89336-647-7

77. **Ableitung von atomarem Sauerstoff und Wasserstoff aus Satellitendaten und deren Abhängigkeit vom solaren Zyklus**
von C. Lehmann (2010), 127 Seiten
ISBN: 978-3-89336-649-1

78. **18th World Hydrogen Energy Conference 2010 – WHEC2010 Proceedings**
Speeches and Plenary Talks
ed. by D. Stolten, B. Emonts (2010)
ISBN: 978-3-89336-658-3

78-1. **18th World Hydrogen Energy Conference 2010 – WHEC2010 Proceedings**
Parallel Sessions Book 1:
Fuel Cell Basics / Fuel Infrastructures
ed. by D. Stolten, T. Grube (2010), ca. 460 pages
ISBN: 978-3-89336-651-4

78-2. **18th World Hydrogen Energy Conference 2010 – WHEC2010 Proceedings**
Parallel Sessions Book 2:
Hydrogen Production Technologies – Part 1
ed. by D. Stolten, T. Grube (2010), ca. 400 pages
ISBN: 978-3-89336-652-1

78-3. **18th World Hydrogen Energy Conference 2010 – WHEC2010 Proceedings**
Parallel Sessions Book 3:
Hydrogen Production Technologies – Part 2
ed. by D. Stolten, T. Grube (2010), ca. 640 pages
ISBN: 978-3-89336-653-8

78-4. **18th World Hydrogen Energy Conference 2010 – WHEC2010 Proceedings**
Parallel Sessions Book 4:
Storage Systems / Policy Perspectives, Initiatives and Cooperations
ed. by D. Stolten, T. Grube (2010), ca. 500 pages
ISBN: 978-3-89336-654-5

78-5. **18th World Hydrogen Energy Conference 2010 – WHEC2010 Proceedings**
Parallel Sessions Book 5:
Stategic Analysis / Safety Issues / Existing and Emerging Markets
ed. by D. Stolten, T. Grube (2010), ca. 530 pages
ISBN: 978-3-89336-655-2

78-6. **18th World Hydrogen Energy Conference 2010 – WHEC2010 Proceedings**
Parallel Sessions Book 6:
Stationary Applications / Transportation Applications
ed. by D. Stolten, T. Grube (2010), ca. 330 pages
ISBN: 978-3-89336-656-9

78 Set (complete book series)

18th World Hydrogen Energy Conference 2010 – WHEC2010 Proceedings
ed. by D. Stolten, T. Grube, B. Emonts (2010)
ISBN: 978-3-89336-657-6

79. **Ultrafast voltex core dynamics investigated by finite-element micromagnetic simulations**
by S. Gliga (2010), vi, 144 pages
ISBN: 978-3-89336-660-6

80. **Herstellung und Charakterisierung von keramik- und metallgestützten Membranschichten für die CO_2-Abtrennung in fossilen Kraftwerken**
von F. Hauler (2010), XVIII, 178 Seiten
ISBN: 978-3-89336-662-0

81. **Experiments and numerical studies on transport of sulfadiazine in soil columns**
by M. Unold (2010), xvi, 115 pages
ISBN: 978-3-89336-663-7

82. **Prompt-Gamma-Neutronen-Aktivierungs-Analyse zur zerstörungsfreien Charakterisierung radioaktiver Abfälle**
von J.P.H. Kettler (2010), iv, 205 Seiten
ISBN: 978-3-89336-665-1

83. **Transportparameter dünner geträgerter Kathodenschichten der oxidkeramischen Brennstoffzelle**
von C. Wedershoven (2010), vi, 137 Seiten
ISBN: 978-3-89336-666-8

84. **Charakterisierung der Quellverteilung von Feinstaub und Stickoxiden in ländlichem und städtischem Gebiet**
von S. Urban (2010), vi, 211 Seiten
ISBN: 978-3-89336-669-9

85. **Optics of Nanostructured Thin-Film Silicon Solar Cells**
by C. Haase (2010), 150 pages
ISBN: 978-3-89336-671-2

86. **Entwicklung einer Isolationsschicht für einen Leichtbau-SOFC-Stack**
von R. Berhane (2010), X, 162 Seiten
ISBN: 978-3-89336-672-9

87. **Hydrogen recycling and transport in the helical divertor of TEXTOR**
by M. Clever (2010), x, 172 pages
ISBN: 978-3-89336-673-6

88. **Räumlich differenzierte Quantifizierung der N- und P-Einträge in Grundwasser und Oberflächengewässer in Nordrhein-Westfalen unter besonderer Berücksichtigung diffuser landwirtschaftlicher Quellen**
von F. Wendland et. al. (2010), xii, 216 Seiten
ISBN: 978-3-89336-674-3

89. **Oxidationskinetik innovativer Kohlenstoffmaterialien hinsichtlich schwerer Lufteinbruchstörfälle in HTR´s und Graphitentsorgung oder Aufarbeitung**
von B. Schlögl (2010), ix, 117 Seiten
ISBN: 978-3-89336-676-7

90. **Chemische Heißgasreinigung bei Biomassenvergasungsprozessen**
von M. Stemmler (2010), xv, 196 Seiten
ISBN: 978-3-89336-678-1

91. **Untersuchung und Optimierung der Serienverschaltung von Silizium-Dünnschicht-Solarmodulen**
von S. Haas (2010), ii, 202 Seiten
ISBN: 978-3-89336-680-4

92. **Non-invasive monitoring of water and solute fluxes in a cropped soil**
by S. Garré (2010), xxiv, 133 pages
ISBN: 978-3-89336-681-1

93. **Improved hydrogen sorption kinetics in wet ball milled Mg hydrides**
by L. Meng (2011), II, 119 pages
ISBN: 978-3-89336-687-3

94. **Materials for Advanced Power Engineering 2010**
ed. by J. Lecomte-Beckers, Q. Contrepois, T. Beck and B. Kuhn
(2010), 1327 pages
ISBN: 978-3-89336-685-9

95. **2D cross-hole MMR – Survey design and sensitivity analysis for cross-hole applications of the magnetometric resistivity**
by D. Fielitz (2011), xvi, 123 pages
ISBN: 978-3-89336-689-7

96. **Untersuchungen zur Oberflächenspannung von Kohleschlacken unter Vergasungsbedingungen**
von T. Melchior (2011), xvii, 270 Seiten
ISBN: 978-3-89336-690-3

97. **Secondary Organic Aerosols: Chemical Aging, Hygroscopicity, and Cloud Droplet Activation**
by A. Buchholz (2011), xiv, 134 pages
ISBN: 978-3-89336-691-0

98. **Chrom-bezogene Degradation von Festoxid-Brennstoffzellen**
von A. Neumann (2011), xvi, 218 Seiten
ISBN: 978-3-89336-692-7

99. **Amorphous and microcrystalline silicon applied in very thin tandem solar cells**
by S. Schicho (2011), XII, 190 pages
ISBN: 978-3-89336-693-4

100. **Sol-gel and nano-suspension electrolyte layers for high performance solid oxide fuel cells**
by F. Han (2011), iv, 131 pages
ISBN: 978-3-89336-694-1

101. **Impact of different vertical transport representations on simulating processes in the tropical tropopause layer (TTL)**
by F. Plöger (2011), vi, 104 pages
ISBN: 978-3-89336-695-8

102. **Untersuchung optischer Nanostrukturen für die Photovoltaik mit Nahfeldmikroskopie**
von T. Beckers (2011), xiii, 128 Seiten
ISBN: 978-3-89336-696-5

103. **Impact of contamination on hydrogenated amorphous silicon thin films & solar cells**
by J. Wördenweber (2011), XIV, 138 pages
ISBN: 978-3-89336-697-2

104. **Water and Organic Nitrate Detection in an AMS: Laboratory Characterization and Application to Ambient Measurements**
by A. Mensah (2011), XI, 111 pages
ISBN: 978-3-89336-698-9

105. **Entwicklung eines neuen Konzepts zur Steuerung der thermischen Ausdehnung von glaskeramischen Verbundwerkstoffen mit angepasster Fließfähigkeit am Beispiel der Hochtemperatur-Brennstoffzelle**
von E. Wanko (2011), xi, 134 Seiten
ISBN: 978-3-89336-705-4

106. **Tomographic reconstruction of atmospheric volumes from infrared limb-imager measurements**
by J. Ungermann (2011), xiv, 153 pages
ISBN: 978-3-89336-708-5

107. **Synthese und Identifizierung von substituierten Mg-Al-Cl Doppelhydroxidverbindungen mit Schwerpunkt IR-Spektroskopie**
von B. Hansen (2011), XII, 121 Seiten
ISBN: 978-3-89336-709-2

108. **Analysis of spatial soil moisture dynamics using wireless sensor networks**
by U. Rosenbaum (2011), xxii, 120 pages
ISBN: 978-3-89336-710-8

109. **Optimierung von APS-ZrO2-Wärmedämmschichten durch Variation der Kriechfestigkeit und der Grenzflächenrauhigkeit**
von M. E. Schweda (2011), 168 Seiten
ISBN: 978-3-89336-711-5

110. **Sorption of a branched nonylphenol isomer and perfluorooctanoic acid on geosorbents and carbon nanotubes**
by C. Li (2011), X, 102 pages
ISBN: 978-3-89336-716-0

111. **Electron Transport in the Plasma Edge with Rotating Resonant Magnetic Perturbations at the TEXTOR Tokamak**
by H. Stoschus (2011), iv, 113 pages
ISBN: 978-3-89336-718-4

112. **Diffusion and Flow Investigations in Natural Porous Media by Nuclear Magnetic Resonance**
by N. Spindler (2011), viii, 144 pages
ISBN: 978-3-89336-719-1

113. **Entwicklung und Erprobung des Hygrometer for Atmospheric Investigations**
von T. Klostermann (2011), IV, 118 Seiten
ISBN: 978-3-89336-723-8

114. **Application of functional gene arrays for monitoring influences of plant/seasons on bacterial functions and community structures in constructed wetlands (Bitterfeld, Germany)**
by J. Ning (2011), xiv, 157 pages
ISBN: 978-3-89336-724-5

115. **Wasseraustrag aus den Kathodenkanälen von Direkt-Methanol-Brennstoffzellen**
von A. Schröder (2011), VII, 228 Seiten
ISBN: 978-3-89336-727-6

116. **CITYZEN Climate Impact Studies**
ed. by M. Schultz (2011), 45 pages
ISBN: 978-3-89336-729-0

117. **Software Tools zum interoperablen Austausch und zur Visualisierung von Geodatensätzen über das Internet**
von M. Schultz, M. Decker, S. Lührs (2011), iv, 156 Seiten
ISBN: 978-3-89336-730-6

118. **Optimierung eines Leichtbaudesigns für ein SOFC-Brennstoffzellenstack**
von T. Nguyen-Xuan (2011), III, 154 Seiten
ISBN: 978-3-89336-732-0

119. **Institute of Energy and Climate Research IEK-6:**
Nuclear Waste Management & Reactor Safety Report 2009/2010
Material Science for Nuclear Waste Management
ed. by M. Klinkenberg, S. Neumeier, D. Bosbach (2011), 242 pages
ISBN: 978-3-89336-735-1

120. **Fate of the Antibiotic Sulfadiazine in Yangtze River Sediments: Transformation, Sorption and Transport**
by N. Meng (2011), XII, 111 pages
ISBN: 978-3-89336-736-8

121. **Thermodynamische Eigenschaften gasförmiger und kondensierter Verbindungen für Hochtemperaturanwendungen**
von T. Markus (2011), II, 131 Seiten
ISBN: 978-3-89336-728-3

122. **Ein neues LIF-Instrument für flugzeug- und bodengebundene Messungen von OH- und HO_2-Radikalen in der Troposphäre**
von S. Broch (2011), IV, 160 Seiten
ISBN: 978-3-89336-742-9

123. **Processes in the Yangtze River System - Experiences and Perspectives**
Workshop-Proceedings
ed. by S. Küpper, G. Subklew, R.-D. Wilken (2011), 83 pages
ISBN: 978-3-89336-744-3

124. **Thermo-Mechanical Properties of Mixed Ion-Electron Conducting Membrane Materials**
by B. Huang (2011), 130 pages
ISBN: 978-3-89336-746-7

125. **Growth, Etching, and Stability of Sputtered ZnO:Al for Thin-Film Silicon Solar Cells**
by J. I. Owen (2011), xv, 192 pages
ISBN: 978-3-89336-749-8

126. **Entwicklung geträgerter $Ba_{0,5}Sr_{0,5}Co_{0,8}Fe_{0,2}O_{3-\delta}$ Sauerstoff-Permeationsmembranen**
von F. Schulze-Küppers (2011), ii, 119 Seiten
ISBN: 978-3-89336-752-8

127. **Development of the 2-Component-Injection Moulding for Metal Powders**
by A. P. Cysne Barbosa (2011), XIV, 150 pages
ISBN: 978-3-89336-753-5

128. **Performance of Tungsten-Based Materials and Components under ITER and DEMO Relevant Steady-State Thermal Loads**
by G. H. Ritz (2011), X, 128 pages
ISBN: 978-3-89336-755-9

129. **Experimentelle Bestimmung und numerische Simulation von Viskositäten in Schlackesystemen unter Vergasungsbedingungen**
von T. Nentwig (2011), 156 Seiten
ISBN: 978-3-89336-756-6

130. **Development of Thin Film Oxygen Transport Membranes on Metallic Supports**
by Y. Xing (2012), iv, 117 pages
ISBN: 978-3-89336-765-8

131. **Release of Inorganic Trace Elements from High-Temperature Gasification of Coal**
by M. Bläsing (2012), XVIII, 145 pages
ISBN: 978-3-89336-772-6

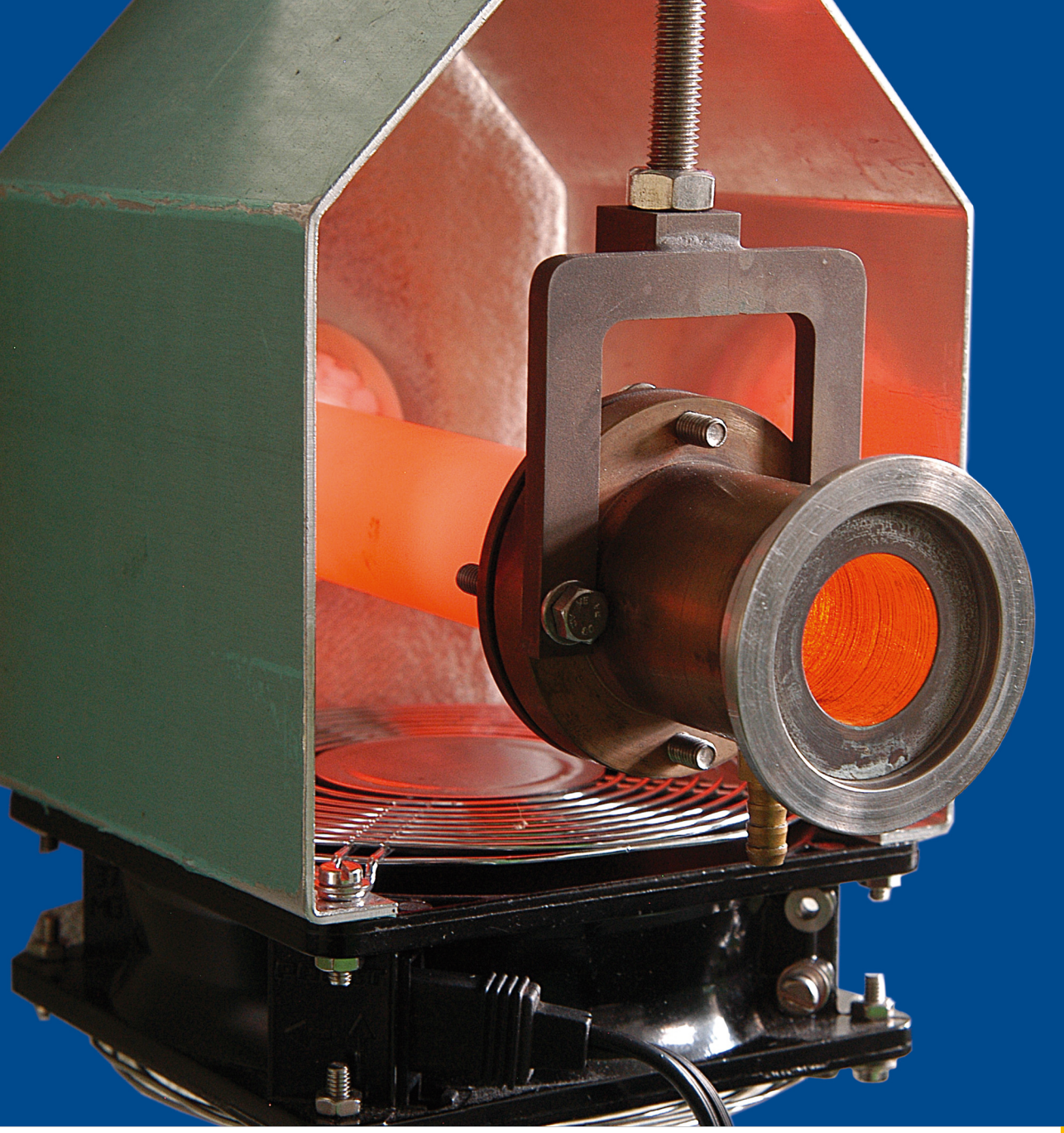

Energie & Umwelt / Energy & Environment
Band / Volume 131
ISBN 978-3-89336-772-6

JÜLICH
FORSCHUNGSZENTRUM